Ida Synnøve Bukkholm

Electric steam methane reforming

Economical and environmental implications of replacing methane with electricity for heating in a steam methane reformer

Master's thesis in Chemical Engineering
Supervisor: Hanna Knuutila
Co-supervisor: Andressa Nakao, Lucas Braakhuis, Rosetta Steeneveldt, Ida Mortensen Bernhardsen
June 2021

Master's thesis

NTNU
Norwegian University of Science and Technology
Faculty of Natural Sciences
Department of Energy and Process Engineering

NTNU
Kunnskap for en bedre verden

Ida Synnøve Bukkholm

Electric steam methane reforming

Economical and environmental implications of replacing methane with electricity for heating in a steam methane reformer

Master's thesis in Chemical Engineering
Supervisor: Hanna Knuutila
Co-supervisor: Andressa Nakao, Lucas Braakhuis, Rosetta Steeneveldt, Ida Mortensen Bernhardsen
June 2021

Norwegian University of Science and Technology
Faculty of Natural Sciences
Department of Energy and Process Engineering

NTNU
Norwegian University of
Science and Technology

Abstract

Green energy has gained traction as a result of a growing focus on sustainability, and it is being investigated like never before. Because fossil fuels are intrinsically harmful to the environment, they must be replaced. Hydrogen is a viable substitute since it is the most abundant element in the universe and has a high gravimetric energy.

This work focused on the hydrogen production method of steam methane reforming (SMR) with amine-based carbon capture. The heating in the primary reformer, supplied by the combustion of natural gas had the opportunity to be improved. That improvement was to replace the combustion of natural gas with electrical heating. The conventional SMR was compared to the electrically heated SMR in terms of operational and capital costs, levelized cost of hydrogen, and CO_2 emissions. Both technologies were simulated in Aspen Hysys.

The operational cost of electrical SMR was found to be 0.13 USD/kg H_2 cheaper than conventional SMR. Calculations of the capital investments showed that because of the lower operational costs, the capital expenditures could be higher based on the levelized cost of hydrogen.

Based on the simulations, it was found that the main CO_2 emissions in conventional SMR with carbon capture stem from the heating of the primary reformer. By switching to an electrically heated SMR with renewable electricity, emissions were found to be reduced by 77%. The importance of renewable electricity was also demonstrated.

In summary, by electrically heating the primary reformer in SMR there can be improvements in both costs, and emissions. The electrically heated SMR can be a useful technology in the energy transition towards a hydrogen economy.

Sammendrag

Grønn energi har fått en trekkraft som et resultat av økt fokus på bærekraft, og det blir forsket på mer enn noen gang før. Ettersom fossile brennstoff er skadelig for miljøet, er det på tide at de byttes ut. Hydrogen er en god erstatning, som det vanligste elementet i universet og med sin høye gravimetriske energi.

Dette arbeidet fokuserte på hydrogenproduksjonsmetoden for dampmetanreformering (SMR) med aminbasert karbonfangst. Oppvarmingen av hovedreformeren viste rom for forbedring, da varmen ble tilført fra forbrenning av naturgass. En idé er å bruke elektrisk varme istedenfor. Elektrisk SMR ble sammenlignet med konvensjonell SMR i drifts- og kapitalkostnader, nullpunktspris og CO_2-utslipp. Begge teknologiene ble simulert i Aspen Hysys.

Driftskostnadene til elektrisk SMR ble funnet til å være 0,13 USD / kg H_2 billigere enn konvensjonell SMR. Beregninger av kapitalinvesteringene viste at på grunn av de lavere driftskostnadene, kunne investeringene være høyere basert på de nullpunktsprisen.

Basert på simuleringene ble det funnet at hovedutslippene av CO_2 i konvensjonell SMR med karbonfangst stammer fra oppvarmingen av hovedreformeren. Ved å bytte til en elektrisk oppvarmet SMR med fornybar elektrisitet, ble utslippene funnet å være redusert 77 %. Viktigheten av fornybar elektrisitet ble også demonstrert.

Oppsummert ser man at ved å varme opp hovedreformeren i SMR elektrisk kan man få ned både kostnader og utslipp. Elektrisk SMR kan være en nyttig teknologi i overgangen mot en hydrogenøkonomi.

Acknowledgements

The work with this master thesis has been carried out at the Department of Chemical Engineering at the Norwegian University of Science and Technology during the spring of 2021. This thesis was written in collaboration with Equinor, who proposed the subject.

First, I would like to thank my supervisor, Dr. Hanna K. Knuutila for her support, expertise, and valuable guidance through each stage of the process. I am grateful for the contributions and questions from Rossetta Steeneveldt and Ida Bernhardsen at Equinor, and for allowing me to make my own choices in regards to the research.

I also wish to express my gratitude to Andressa Nakao and Lucas Braakhuis for their help in all things literature reviews, resources, calculations, and simulations.

Contents

Abstract

Sammendrag

Acknowledgements

1 Introduction **1**
- 1.1 Outline of Thesis 2

2 Background **3**
- 2.1 State of Climate Changes 3
  - 2.1.1 The Energy Transition 4
- 2.2 Hydrogen 4
- 2.3 Steam Methane Reforming (SMR) 6
  - 2.3.1 Overview of the SMR Process 6
- 2.4 Carbon Capture Technologies 9
  - 2.4.1 Adsorption 9
  - 2.4.2 Membrane Separation 9
  - 2.4.3 Cryogenic Separation 9
  - 2.4.4 Chemical Absorption 10
    - Absorption Column 11
    - Stripping Column 12
- 2.5 Limitations of Steam Methane Reforming 12
  - 2.5.1 Carbon Tax 13
- 2.6 Introduction to Electrification 13
  - 2.6.1 Electrical Steam Methane Reforming 14
    - Choice of Electricity 15
- 2.7 Challenges with Electrification 17
  - 2.7.1 Electrical Power Tax 17

3 Methodology **19**
- 3.1 Simulation 19
  - 3.1.1 Base Case 19
  - 3.1.2 Electric SMR 23
- 3.2 Cost Estimations 24
  - 3.2.1 CAPEX 24
    - Size Estimations of Vessels 25
    - SMR, PSA, and Pre-reformer 26
    - Absorption and Stripping Column 27

Shift Reactors 28
Heat Exchangers 28
Electric SMR 29
3.2.2 OPEX 30
3.2.3 LCOH 32
3.3 Analyses of CO_2 Emissions 33

4 Results and Discussion 35
4.1 Process Simulations 35
4.1.1 Simulation of Base Case 35
4.1.2 Simulation of Electric SMR 39
4.2 Comparison of Conventional and Electric SMR 40
4.3 Cost Estimations 42
4.3.1 CAPEX 42
4.3.2 OPEX 45
4.3.3 OPEX Prediction 2021-2030 48
4.3.4 OPEX Prediction for 2030 51
4.3.5 Sensitivity Analyses 53
SMR 53
Electric SMR 54
Comparing Sensitivity Analyses 55
4.3.6 Comparison of the LCOH 57
4.4 CO_2 Emissions 58
4.4.1 Direct Emissions 59
4.4.2 Life Cycle Emissions 60
4.5 Benefits and Challenges with Electric SMR 61

5 Conclusions and Future Work 65

Bibliography 67

A Simulation i
A.1 Conventional SMR (Hysys figure) iii
A.2 Electric SMR (Hysys figure) v
A.3 Simulation values (El. SMR) vi
A.4 Specifics of each unit operation viii
A.4.1 Pre-reformer viii
A.4.2 SMR viii
Furnace viii
A.4.3 Shift reactors ix
A.4.4 Heat exchangers before capture plant x
A.4.5 Carbon capture plant x
Absorber x
A.4.6 Flash drums in capture plant x
A.4.7 Cross heat exchanger xi
A.4.8 Stripper xi
A.4.9 PSA xi
A.5 Scenarios xii

A.5.1 Ideal SMR xii
A.5.2 Electric SMR with reduced tax xii
A.5.3 Ideal electrical SMR xii

B Calculations **xiii**
B.1 Sizing calculations xiii
B.1.1 Height of vertical vessels xiii
B.1.2 Sizing of horizontal vessels xiii
B.1.3 Diameter of the absorber xiii
B.1.4 Shift reactors xiv
B.1.5 Heat exchangers xv
Choice of heat exchanger type xv
B.2 Currency conversions xv
B.3 Equations and calculations xv

C Supplementary results/Case studies **xvii**
C.1 Case studies xvii
C.1.1 Steam requirements xvii
C.1.2 Furnace case studies xviii
Conventional SMR xviii
Electrical SMR xix
C.2 OPEX xx
C.3 CAPEX xxi
C.3.1 Breakdown of capital costs for each unit in the simulation . xxi
Heat exchangers xxii
Vessels xxii
Packing xxii

D Python and Matlab scripts **xxiii**
D.1 Sizing of horizontal vessels xxiii

List of Figures

1.1 Papers published in Science Direct with the given keywords in the title. 1

2.1 Global annual temperature 3
2.2 An illustration of the space of the storage required for different fuels with the same amount of energy (not to scale). Reproduced from [15]. 5
2.3 A simple block diagram of an SMR plant, where feedstock enters the primary reformer (SMR) before being sent into shift reactors and then purified in a pressure swing adsorber (PSA). 6
2.4 An illustration of the primary reformer, SMR. It consists of many small reformer tubes which are heated by burners, in this case located from the top (top-fired). Inside the reformer tubes methane is converted to hydrogen which exits at the bottom. Reproduced from [27]. 7
2.5 The process of amine scrubbing, with an absorber capturing CO_2 with amines, which is subsequently released in the desorber. Reproduced from [50]. 10
2.6 An illustration of the difference between conventional SMR(A) and electric SMR(B). Reproduced and adapted from [67]. 14
2.7 Cost and life cycle emissions of renewable production sources of electricity. 16
2.8 Comparison of the average energy prices and taxes for natural gas and electricity in EU. 18

3.1 Flow sheet diagram of the conventional SMR process. 20
3.2 Flow sheet diagram over the electric SMR process. 24
3.3 Average prices of natural gas from the internal gas price at Equinor from 2015 to the first quarter of 2021 [99]. 31

4.1 Reboiler duty as a function of the L/G ratio with a constant capture rate. 37
4.2 Rich and lean loading as a function of the L/G ratio with a constant capture rate. 38
4.3 Temperature in the amine-rich (blue) and amine-lean (red) flows in the system as a function of the L/G ratio. 39
4.4 Breakdown of OPEX for both conventional and electric SMR, in terms of the proportional costs and absolute costs. 46
4.5 OPEX estimates for the different scenarios. 48
4.6 Change in the predicted OPEX from 2021 to 2030. 50

4.7 Breakdown of estimated OPEX for both conventional and electric SMR, in terms of the proportional costs and absolute costs in 2030. . 51
4.8 OPEX estimates for the different scenarios predicted fro 2030. . . . 52
4.9 Sensitivity analyses for the OPEX estimates for conventional SMR for 2021 (A) and 2030 (B). 54
4.10 Sensitivity analyses for the OPEX estimates for electric SMR for 2021 (A) and 2030 (B). 55
4.11 Comparison of the sensitivity analyses for 2021 estimate. 56
4.12 Comparison of the sensitivity analyses for 2030 prediction. 57
4.13 Comparison of the direct emissions for conventional and electric SMR. 60
4.14 Lifecycle emissions (including the albedo effect) for the case of electric SMR based on the source of electricity. 61

C.1 Conversion of hydrogen as a function of the S/C ratio. xvii
C.2 Mass flow of the heavier hydrocarbons exiting the pre-reformer as a function of the S/C carbon. xviii
C.3 The mass flow of CO as a function of the inlet mass flow of fuel into the furnace varying with the air factor. xix
C.4 The temperature of the cooled flue gas after supplying heat to the SMR as a function of the inlet mass flow of fuel into the furnace varying with the air factor. xx
C.5 Temperature of the flue gas exiting the furnace as a function of the mass flow of fuel and AF. xxi

List of Tables

2.1 Comparison of the set-up of conventional and electric SMR. The set-up for electric SMR is based on the lab work by Wismann [16]. . . . 15

3.1 Base criteria for simulations. 20
3.2 Composition of the natural gas used as feedstock and fuel in the simulation [23]. The conditions given are the inlet conditions of the natural gas as feedstock after desulphurization. 21
3.3 Assumptions used for the OPEX calculations. 24
3.4 The length-to-diameter (L/D) ratio based on the pressure in the unit [73]. 26
3.5 Values used to compute the cost of the pre-reformer, SMR, and PSA in Equation 3.10 [92][95]. 27
3.6 Variables considered in the OPEX calculations. 30
3.7 Variables considered in the OPEX calculations for the 2030 estimate. 32

4.1 Comparison of literature values and simulation results from Aspen Hysys. Literature values were collected from the IEAGHG Technical Review (2017) and are based on an SMR plant with CCS [25]. . . . 36
4.2 Values from the Aspen Hysys simulation of conventional SMR. . . . 41
4.3 Results from the absorber and stripper in the Aspen Hysys simulation. 42
4.4 CAPEX for the base case (conventional SMR). 42
4.5 Overview of the CAPEX breakdown. 43
4.6 Variation of the F_{SMR} to evaluate the total CAPEX for electric SMR. The CAPEX per kg H_2 is for a years worth of hydrogen production. 44
4.7 The levelized cost of hydrogen (LCOH) for conventional and electric SMR. 58

A.1 Values from the Hysys simulation of conventional SMR. vii
A.2 Specifications of the pre-reformer in the simulation. viii
A.3 Specifications of the SMR in the simulation. viii
A.4 Specifications of the furnace used to heat the SMR reactor in the simulation. ix
A.5 Specifications of the HTSR and LTSR in the simulation. ix
A.6 Specifications of the heat exchangers before the capture plant. . . . x
A.7 Specifications of the absorber in the capture plant. x
A.8 Specifications of the flash drums in the capture plant. xi
A.9 Specifications of the cross heat exchanger in the capture plant. . . . xi
A.10 Specifications of the stripper in the capture plant. xi
A.11 Specifications of the PSA in the simulation. xi

B.1 Specific values for the size estimations in the model for the shift reactors. xiv
B.2 Currency conversions used in the thesis. xv
B.3 Assumptions used in the computation of the pressure factor for vessels, $F_{P,vessel}$ [92]. xvi
B.4 Overview of the material factor, F_M based on the materials for the tubes and shells in a heat exchanger [92]. xvi
B.5 The factors used for the different units to compute the bare module factor, F_{BM} [92]. xvi

C.1 Comparison of OPEX costs for the base case (SMR) and the case of electric SMR (el SMR). xx
C.2 Comparison of OPEX costs for 2030 for the base case (SMR) and the case of electric SMR (el SMR). xxi
C.3 Cost and size estimation of each heat exchanger in the simulation. . xxii
C.4 Cost and size estimates of each vessel in the simulation. xxii
C.5 Packing costs for the absorber and the stripper, based on cost estimates from Turton et al 2009 [92]. xxii

List of Abbreviations

AF	**A**ir **F**actor
CAPEX	**Ca**pital **Ex**penditures
CCS	**C**arbon **C**apture and **S**torage
CEPCI	**C**hemical **E**ngineering **P**lant **C**ost **I**ndex
CRF	**C**apital **R**ecovery **F**actor
CS	**C**arbon **S**teel
CW	**C**ooling **W**ater
EIA	**E**nergy **I**nformation **A**dministration
GHG	**G**reen**h**ouse **G**ases
HCI	**H**ydrogen **C**leanness **I**ndex
HPP	**H**ydrogen **P**roduction **P**athway
HTSR	**H**igh **T**emperature **S**hift **R**eactor
IEA	**I**nternational **E**nergy **A**gency
IEAGHG	**IEA** **G**reen**h**ouse **G**as R&D Programme
IPCC	**I**ntergovernmental **P**anel on **C**limate **C**hange
IRENA	**I**nternational **R**enewable **En**ergy **A**gency
L/D	**L**ength-to-**D**iameter
L/G	**L**iquid-to-**G**as
LCC	**L**ife **C**ycle **C**ost
LCOE	**L**evelized **C**ost **O**f **E**nergy
LCOH	**L**evelized **C**ost **O**f **H**ydrogen
LHV	**L**ower **H**eating **V**alue
LNG	**L**iquefied **N**atural **G**as
LTSR	**L**ow **T**emperature **S**hift **R**eactor
MDEA	**M**ethyl**die**thanol**a**mine
MEA	**M**ono**e**thanol**a**mine
NG	**N**atural **G**as
NREL	**N**ational **R**enewable **E**nergy **L**aboratory
OPEX	**Op**erating **Ex**penditures
PFR	**P**lug **F**low **R**eactor
PSA	**P**ressure **S**wing **A**dsorption
PZ	**P**ipera**z**ine
S/C	**S**team-to-**C**arbon
SMR	**S**team **M**ethane **R**eforming
SS	**S**tainless **S**teel
TG	**T**ail **G**as
WGS	**W**ater **G**as **S**hift

List of Symbols

α	Loading
η	Efficiency
ϕ_v	Volumetric flow
ρ	Density
a	Cost adjustment factor
A	Area
C_{BM}	Bare module cost
C_O	Base cost
C_p^0	Purchase cost
C_{TM}	Total module cost
c	Concentration
D_c	Diameter of column
D_v	Diameter of vessel
E_0	Activation energy
E_{H_2}	Mass of hydrogen
F_{BM}	Bare module factor
F_M	Material factor
F_p	Pressure factor
F_{SMR}	Cost factor for SMR
F	Capacity
H_t	Total height
h_v	Height of liquid in vessel
H_v	Height of vessel
i	Nominal discount rate
I	Size parameter
k_0	Rate constant
K_{eq}	Equilibrium constant
k	Constants
n	Mole
n	Assumed lifetime
P	power
Q	Heat
r_i	Reaction rate for component i
S	Surface area
U	Overall heat transfer coefficient
V_l	Volumetric flow rate of liquid
v_s	Settling velocity
V_v	Volumetric flow rate of vapor
V	Volume

y_i	Mole fraction of component i
z	Length

Chapter 1

Introduction

Climate change is one of our generation's most substantial challenges [1]. Despite a 5.8% in global CO_2 emissions in the unique year of 2020, they are expected to rise by 4.8% in 2021, reversing most of the drop from the year before [2]. The number of countries pledged to reach net-zero emissions by 2050 are increasing, but so are CO_2 emissions [1].

In addition to an expected increase in CO_2 emissions as a result of an increasing demand for coal, the demand for electricity, natural gas, and renewables are forecast to grow 4.5%, 3.2%, and 8% respectively. This growth in demand is due to developing economies and an emerging market [2]. Hydrogen has also experienced a growth spurt, with production increasing more than threefold since 1975 [3].

First used in the 1860s, hydrogen was used as fuel in the first internal combustion engine, and is not a new energy source [3]. Hydrogen has gained tremendous momentum in the past years, and taking advantage of that will be crucial for the current energy transition. An example of the momentum both climate change and hydrogen have gained throughout the years can be illustrated by the number of papers published with these key terms (Figure 1.1). Hydrogen research has increased significantly in the past years, which can be connected to the current energy transition [4].

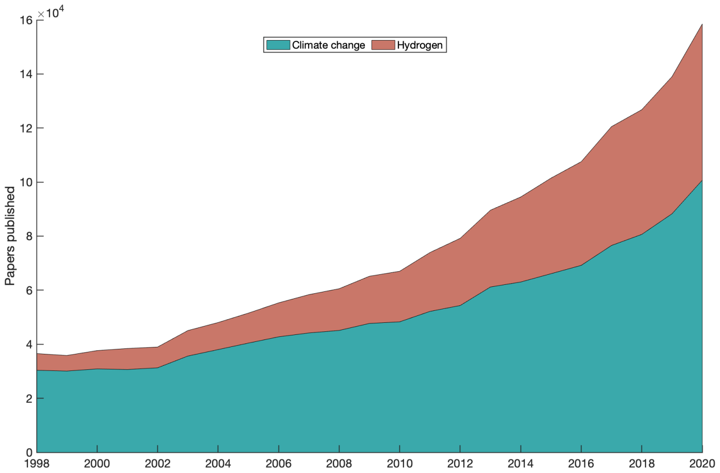

FIGURE 1.1: Papers published in Science Direct with the given keywords in the title.

The majority of hydrogen is produced by steam methane reforming (SMR), which uses steam and methane to produce hydrogen. This reaction requires significant heat, which is supplied by the combustion of natural gas.

Combustion of fossil fuels to generate heat and electricity accounts for almost half of all carbon dioxide emissions globally [5]. These emissions could be reduced by producing heat and electricity from sustainable sources. This is also the case of SMR where the natural gas furnace is replaced by electrical heating. This is called electrically heated SMR, and will also be referred to as electric SMR. Electric SMR provides reduced emissions as well as increased flexibility within operation of the plant, while cost is more disputed.

The main objective of this thesis is to compare conventional and electrically heated SMR, with respect to costs and CO_2 emissions of the two processes. The motivation behind investigation of the emissions is as discussed rooted in the problems with global warming. Investigating the costs of the electrical steam methane reforming technology, and figuring out if this technology would be viable in today's economic terrain was deemed of high importance. If a technology is not economically competitive, it is highly unlikely that it will be employed.

1.1 Outline of Thesis

Chapter 2 starts with a background that further addresses today's state of climate changes, and the energy transition before moving on to a section on hydrogen and hydrogen production. Conventional SMR is introduced, along with the carbon capture technology relevant for the plant. Electric SMR is introduced and discussed.

Chapter 3 details methodology and introduces the simulations that were done, as well as the calculations for CO_2 emissions and cost estimations for both technologies.

The Results and Discussion in Chapter 4 address the CO_2 emissions and costs from the two technologies. An additional section on the other alleged benefits of the electric SMR has been added.

Concluding remarks and ideas for future work are found in Chapter 5.

Chapter 2

Background

2.1 State of Climate Changes

Each year from 2014 to 2020 has a spot in the top seven rankings on highest global temperatures, with 2020 coming in an alarming second place [6]. This increase in annual global temperature has been closely monitored by NASA, and is illustrated in Figure 2.1a and 2.1b [7].

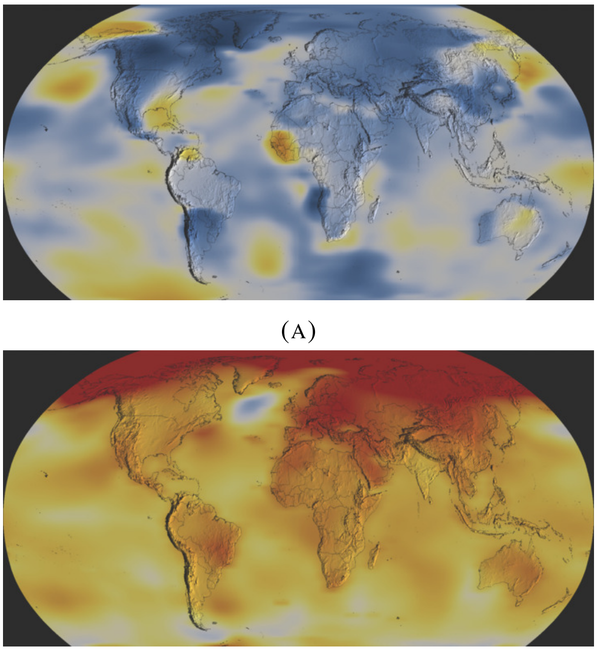

(A)

(B)

FIGURE 2.1: The figure shows the global temperature change from 1884 to 2020. (A) shows a visual representation of the global annual temperature in 1884.
(B) shows a visual representation of the global annual temperature in 2020. Reproduced from [7].

The increase in global annual temperatures is linked to the use of fossil fuels, producing around 80% of the world's energy consumption [8]. Fossil fuels have created opportunities for economic growth for the past 200 years [9]. Transportation, in particular, was revolutionized by fossil fuels, with the inventions of the car, plane, and engine-powered train, which have contributed to great improvement in the human lifestyle [10]. On the other hand, our current knowledge on the environmental impact of fossil fuels shows that the arguments of reliability and cost-efficiency are not strong enough to justify continued use. There is a clear need to transition to more sustainable energy sources.

2.1.1 The Energy Transition

The energy transition is the road to the global energy sector going completely renewable by 2050 [11]. To accomplish this goal, CO_2 emissions need to decrease by an annual average of 3.8% [11]. In this thesis, emissions will refer to CO_2 emissions, unless stated otherwise. Considering all emissions from the energy sector, including both direct and indirect electrification, the total emissions need to decrease by 90% [11]. It is not only necessary for the climate, but it is also a highly profitable investment in the long run.

Studies by the International Renewable Energy Agency (IRENA) have found that an investment of USD 19 trillion leading up to 2050 would reach a scenario where half of the energy demand is supplied by electricity and it would cumulatively ensure a payback between USD 50-142 trillion [11]. This payback stems from a reduction in both environmental and health externalities [11]. By reducing emissions even further to achieve net-zero emissions, a higher investment is necessary. However, as 2050 approaches, the urgent need for renewable energy might become even more obvious, thus triggering the investment for reaching net-zero emissions. There are several key technologies, including green hydrogen and electrification based on renewable sources for the energy transition to take place. These technologies are the motivation for this thesis

2.2 Hydrogen

As the most abundant element in the universe, hydrogen is a versatile element with a bright future [12][13]. The abundance of hydrogen, however, does not mean that it is easily accessible as an energy source. The majority of hydrogen exists in compounds and molecules and must be liberated before utilization. For this reason, hydrogen is referred to as an energy carrier rather than an energy source. Hydrogen is a strong contender to be the energy carrier of the future due to its high gravimetric energy density. Gravimetric energy density denotes how much energy a substance contains relative to its mass, and hydrogen's is the highest of all known substances [14].

Hydrogen has potential for usage in several different industries. In the transportation industry it can be used as fuel, while it can be used as heating in buildings, as well as it can be used in the energy industry [13]. The opportunity of using hydrogen in a variety of large sectors has given rise to the idea of a hydrogen economy, where hydrogen is used as the primary energy carrier and is the future for clean energy [3][13].

With today's momentum, the hydrogen economy has shown significant growth potential across a wide scope of technologies [11]. Currently, however, the most important obstacle to the hydrogen economy is storage [13]. As mentioned before, hydrogen has a very high gravimetric density. However, its volumetric energy density is very low compared to that of other energy sources [15] [16]. An illustration of this can be seen in Figure 2.2.

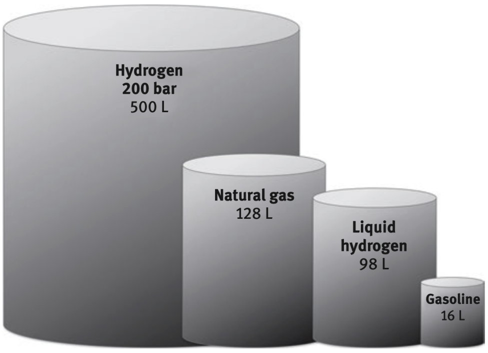

FIGURE 2.2: An illustration of the space of the storage required for different fuels with the same amount of energy (not to scale). Reproduced from [15].

Another aspect is emissions from the hydrogen industry. Although hydrogen at its end-use point is a completely carbon-emissions free energy carrier, the total emissions depend on the production method. There are three main categories of hydrogen based on the production method: gray, blue, and green.

Gray and blue hydrogen are both produced from fossil fuels such as coal or natural gas, but blue hydrogen includes carbon capture and storage (CCS). This reduces emissions, making it a more sustainable production method [17]. Finally, green hydrogen is the production of hydrogen using solely renewable sources, a typical example of this is producing hydrogen from electrolysis of water [18].

Often, green hydrogen is presented as the holy grail of hydrogen production. However, it can be argued that this depends on context and readiness. For the transport sector, green hydrogen is expected to be used as fuel already by 2030 [19]. This expectation is due to consumer pressure to decarbonize the transport sector, as well as the possibility of producing green hydrogen on-site, removing the need for transport [19]. However, using green hydrogen for heating purposes might be a less efficient use of resources. Since many countries such as the U.S and Australia use gas for heating, repurposing that to a gas-to-hydrogen infrastructure, producing blue hydrogen for decarbonization purposes should be doable. However, when available, electricity should be used directly for heating instead of being rerouted for the production of green hydrogen which then can be used to produce heat [19].

Another problem with green hydrogen is that hydrogen from electrolysis still has not been implemented in large-scale industry. One of the main arguments is its high cost; it requires four times as much energy input as hydrogen from natural gas [16]. Hence, most hydrogen is produced from natural gas and the hydrogen industry has been estimated by the International Energy Agency (IEA) to emit around 830 million tonnes of carbon dioxide annually [3]. Because of this, one study introduced a hydrogen cleanliness index (HCI) coding model to gain better insight into the carbon emissions for the different pathways [20]. This index considers the greenhouse gas (GHG) emissions for the entire life cycle, which will be affected by the cleanness of the feedstock and its input energy, and other materials and equipment used [20]. As before, hydrogen production methods, also known as the hydrogen production pathways (HPP), are categorized into the usual green, blue, and gray categories. However, two additional features are added in this new index: the percentage of cleanness within the category and a depth level number [20]. The depth level number state what emissions have been accounted for in the calculation of cleanness, so a depth level of 1 states that only direct emissions were estimated, while level 2 also include the indirect emissions and so on, up to a level of 4 [20]. This is useful to show the ranges within and differentiate better between production methods within the same category of blue, gray, and green hydrogen. In this manner, HCI supplies a better way to measure improvement within hydrogen production methods.

2.3 Steam Methane Reforming (SMR)

2.3.1 Overview of the SMR Process

Steam methane reforming is considered to be the most cost-efficient industrial-scale hydrogen production method and is the main method of hydrogen production [21][22]. The SMR process is based on converting natural gas, mainly methane, into hydrogen through the following reaction,

$$CH_4 + H_2O \rightarrow CO + 3H_2 \qquad \Delta H_f^\circ = 206\,\mathrm{kJ/mole} \tag{2.1}$$

A general overview of the process can be seen in Figure 2.3.

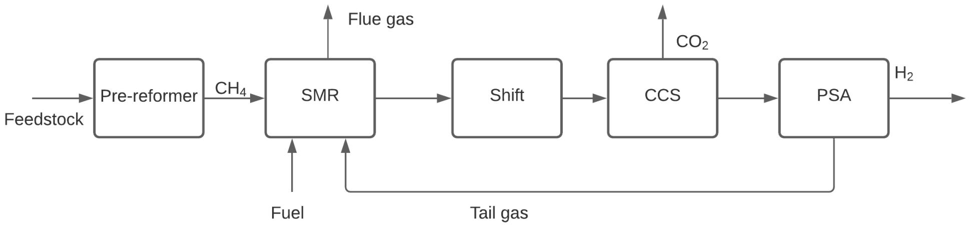

FIGURE 2.3: A simple block diagram of an SMR plant, where feedstock enters the primary reformer (SMR) before being sent into shift reactors and then purified in a pressure swing adsorber (PSA).

Pre-treatment of the natural gas is not included in the figure. Pre-treatment is often necessary due to the small amounts of sulphur that are present in natural gas. Sulphur is removed by conversion to solid H_2S before it can be removed as solid waste [23]. The desulphurization process is typically carried out under high pressures of around 25-70 bar [24]. As the natural gas not only consists of methane but also heavier hydrocarbons, these need to be converted to methane, which occurs in a pre-reformer.

The pre-reformer is an adiabatic reformer, and in it, the following reactions take place with a nickel-catalyst at around 350 to 550°C [25]:

$$C_nH_m + nH_2O \rightleftharpoons nCO + (n + \frac{m}{2})H_2 \tag{2.2}$$

$$CO + 3H_2 \rightleftharpoons CH_4 + H_2O \qquad \Delta H_f^\circ = -206\,kJ/mole \tag{2.3}$$

Following the pre-reformer is the primary reformer, also known as the SMR, where Reaction 2.1 takes place. The reaction is highly endothermic and hence requires sufficient heating. Temperatures around 700-1000°C are necessary, and to supply heat, burners that combust natural gas are placed throughout the reformer surrounding the reformer tubes [26]. To ensure safe heating, the natural gas burners are placed far apart to heat the reformer tubes throughout the reactor. An illustration of the reformer can be seen in Figure 2.4.

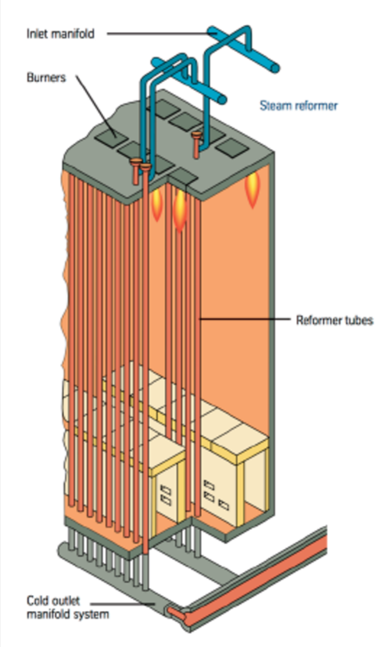

FIGURE 2.4: An illustration of the primary reformer, SMR. It consists of many small reformer tubes which are heated by burners, in this case located from the top (top-fired). Inside the reformer tubes methane is converted to hydrogen which exits at the bottom. Reproduced from [27].

In a typical reformer, there are usually over 100 tubes around 10-14 m long, with a diameter of around 8-15 cm [16] [27]. Both steam and methane enter these reformer tubes are heated by the combustion of natural gas. To reach the highest conversion, a steam-to-carbon (S/C) ratio of around 3 mol/mol has been stated as favorable although this is dependent on system parameters such as the catalyst and temperature [28] [29] [30].

All the burners that surround the reformer tubes are usually collectively referred to as the furnace. The furnace burns fuel with excess air. Air-factor (AF) is used as a measurement of the ratio between the mass flows of air and fuel,

$$AF = \frac{m_{air}}{m_{fuel}}. \tag{2.4}$$

The AF is important because this ratio affects the temperature as well as the CO and CO_2 emissions of the furnace. For example, increasing the mass flow of fuel, thus decreasing the air factor, would lead to an increase in temperature of the flue gas exiting the furnace as the efficiency of the furnace is increased. This increased efficiency stems from faster transfer of thermal energy across the furnace [31]. This effect will of course stop if the mass flow of air is decreased past the minimum value for combustion to occur.

After conversion of methane to carbon monoxide and hydrogen, it is necessary to remove the carbon monoxide in the gas mixture. In the Shift block of Figure 2.3, CO is converted to CO_2 through the water gas shift (WGS) reaction,

$$\mathrm{CO} + \mathrm{H_2O} \rightarrow \mathrm{CO_2} + \mathrm{H_2} \qquad \Delta H_\mathrm{f}^\circ = -41.1\,\mathrm{kJ/mole} \tag{2.5}$$

The WGS reaction is slightly exothermic and will favor lower temperatures [32]. However, it has been recommended to use two WGS reactors in series to maximize conversion of carbon monoxide in industrial applications [33] [34]. The first WGS reactor, the high temperature shift reactor (HTSR), is set to a higher temperature and will be limited by the equilibrium of the reaction. The second reactor, the low temperature shift reactor (LTSR), is below 250°C to shift the limitation to the kinetics rather than the equilibrium [35]. It is possible to use either isothermal or adiabatic shift reactors, but a study comparing the two showed better results for isothermal shift reactors in terms of catalyst volume, operating costs and reactor size [36]. A common type of catalyst for shift reactors is an iron catalyst, Fe_2O_3, with different additions to the catalyst [37].

As can be seen in Figure 2.3, pressure swing adsorption (PSA) follows the shift reactors. However, this applies to production of gray hydrogen. For the production of blue hydrogen, it is possible to add a carbon capture plant prior to the PSA, which will be discussed further in Section 2.4. In the PSA, hydrogen is purified and recovered by taking advantage of the fact that different gases adsorb to different solids when subjected to higher pressures [38]. In state-of-the-art PSA, around 70-90% of hydrogen can be recovered with a purity of 99.999% [39]. There are five main steps in the PSA process; (i) adsorption, (ii) regeneration, (iii) pressure equalization, (iv) depressurization, and (v) pressurization. These five steps proceed through a cycle repeated for each bed in the PSA plant. There are often several beds in one PSA plant to ensure continuous hydrogen production [38].

After the PSA, hydrogen is ready to be stored or utilized. A mixture of gases not used in further processing is also produced, known as tail gas. To ensure the most energy-efficient plant, this tail gas can be used as fuel in the furnace.

2.4 Carbon Capture Technologies

As mentioned in the previous chapter, CCS can be implemented to ensure that blue hydrogen is produced from the SMR plant rather than gray hydrogen. Some of the main technologies for carbon capture are adsorption, membranes, cryogenic separation, and absorption. The following section briefly discusses adsorption, membrane separation, and cryogenic separation before taking a deeper look into chemical absorption.

2.4.1 Adsorption

Adsorption is the process by which a substance accumulates on a surface of a volume. This differs from absorption, where the substance diffuses through the same volume. It is possible to use either physical solvents, chemical solvents, or a hybrid of these in the process.

Adsorption is often preferred at lower CO_2 concentrations of 4-8 vol%, because using conventional amine processes will result in high energy penalties [40]. The process of capturing carbon dioxide by adsorption is in general based on two technologies that are viable for industrial purposes; Pressure or Vacuum Swing Adsorption (PSA/VSA) and Temperature Swing Adsorption (TSA) [41]. TSA requires more time to regenerate the sorbent, leading to higher cycle times. For this reason, TSA is less desirable than PSA [42]. However, these current adsorption technologies are more suitable for small-scale carbon capture plants [43].

2.4.2 Membrane Separation

There are many ways to utilize membranes for separation in fluids. These membrane processes can be split into chemical processes and physical processes [44]. In pre-combustion, where CO_2 capture occurs prior to the combustion of fuels, membrane separation can be either H_2 permeable or CO_2 permeable. In general, metallic membranes are preferred for carbon capture although there are several available membranes suitable for separation [45][46]. Advantages of using membranes for the H_2/CO_2 separation include the simplicity of the technology, how easy it is to up-scale the separation, and its low capital and operating cost [46][44]. Additionally, it does not require extra columns for regeneration or solvent storage [46]. The main drawbacks of membrane technology are that the membranes generally have a low lifetime, as well as low selectivity and flux [44].

2.4.3 Cryogenic Separation

Cryogenic separation separates the CO_2 by condensation at temperatures around -55°C [43]. Typically used in oxy-fuel combustion processes that use pure oxygen rather than air for combustion, cryogenic separation is suitable for high CO_2 concentrations [45]. An obvious drawback of this technology is the cost of refrigeration [43].

2.4.4 Chemical Absorption

Absorption can be either physical or chemical. Physical absorption is based on Henry's law stating that the concentration of CO_2 is proportional to its partial pressure in the gas [47][48]. In this work, however, chemical absorption was chosen to capture the CO_2 and will be discussed in greater detail. Chemical absorption was chosen as it is the most commonly-used technology for carbon capture. Chemical absorption are reactions between a chemical absorbent or solvent and the absorbed substance, in this case CO_2. The concept of chemical absorption is based on an absorption column, in which there is a chemical reaction between the solvent and the CO_2 which leaves the column as a rich liquid, which then enters the desorption tower, also known as the stripper to separate the solvent and the CO_2. This type of separation has a high selectivity, thus allowing for production of a relatively clean CO_2 stream. Because of these features, chemical absorption is highly suited for CO_2 capture in industrial exhaust gases [43]. The set-up of chemical absorption is shown in Figure 2.5. A more detailed description of the two columns can be found in the following sections.

The placement of the carbon capture plant, as seen in Figure 2.3, was designed to allow for retrofitting of previously built SMR plants [45]. This also provides modularity allowing for future replacements of unit operations. However, this modular design comes at a cost; overall carbon capture is reduced to a maximum of 60% [49]. This is due to increased emissions from the furnace, which emits CO_2 in the flue gas that is not sent into the CCS plant (as shown in Figure 2.3). By adding CO_2 capture after the furnace, the overall carbon capture can be 90% or above, although this might prove to be expensive [49].

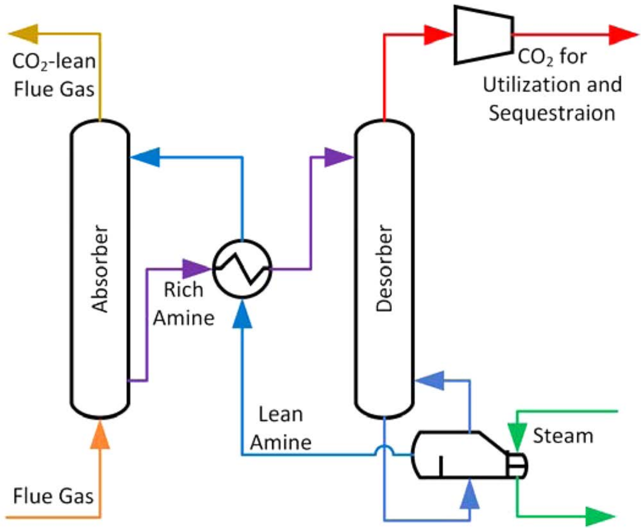

FIGURE 2.5: The process of amine scrubbing, with an absorber capturing CO_2 with amines, which is subsequently released in the desorber. Reproduced from [50].

Absorption Column

In the absorption column, there are two inlets. The flue gas enters the bottom of the column, while the liquid solvent enters at the top of the column. Throughout the column, the CO_2 gaseous molecules bind to the liquid solvent which then exits the column from the bottom. The resulting flue gas stripped from carbon dioxide exits from the top of the column and can be utilized further in the plant [50]. In this plant, the CO_2-lean Flue Gas in Figure 2.5 will be the flue gas with a high H_2-content that proceeds through the PSA to be purified from the tail gas.

Choice of Solvent

There are three possible types of solvents: chemical solvents, physical solvents, and a hybrid of these [51]. Chemical solvents are the most developed, commercially advanced technique, and have proved to be more selective than physical solvents [52][53]. Among chemical solvents, amines have proved to be the most cost-effective solvent [50]. Based on this, chemical absorption using amines is used in this thesis.

Amines can be classified into three main categories: primary, secondary, and tertiary [48]. These categories are based on the number of hydrogen attached to the nitrogen [54]. Hence, a primary amine will have two hydrogens, secondary has one while tertiary has none [54]. In general, primary and secondary amines have fast reaction kinetics with CO_2. Compared to primary and secondary amines, tertiary amines generally have slower kinetics, although their capacity is better [55]. The general chemical equations for amine carbon capture are as follows [56],

$$2R^1{-}NH_2 + CO_2 \rightleftharpoons R^1{-}NH_3{}^+ + R^1{-}NH{-}COO^- \tag{2.6}$$

$$R^1{-}NH_2 + CO_2 + H_2O \rightleftharpoons R^1{-}NH_3{}^+ + H{-}CO_3{}^- \tag{2.7}$$

for primary amines. As can be seen, two moles of amines are required per mole of CO_2. Reaction 2.7 occurs when unstable carbamates hydrolyze [56].

Secondary amines also form carbamates, and still only half a mole of CO_2 is absorbed per mole of amine, as seen in Equation 2.8 [57]:

$$2R^1R^2{-}NH + CO_2 \rightleftharpoons R^1R^2{-}NH_2{}^+ + R^1R^2{-}N{-}COO^- \tag{2.8}$$

Tertiary amines form bicarbonate through the following reaction [57]:

$$R^1R^2R^3{-}N + CO_2 + H_2O \rightleftharpoons R^1R^2R^3{-}NH^+ + HCO_3{}^- \tag{2.9}$$

Hence, tertiary amines only need one mole of amines per mole of CO_2.

In the regenerator, these reactions are reversed. For an absorber at high pressure, the absorption reactions can be reversed by combining pressure reduction with heating, resulting in the possible removal of CO_2 from the top of the stripper to be stored, utilized, or transported [47]. The stripper will be described in more detail in the following section.

The primary amine monoethanolamine (MEA) is the most studied amine in chemical absorption. It has been shown to have a high affinity for CO_2 at lower temperatures [50]. However, it does require a lot of energy to regenerate and reverse the reactions in the stripper [48].

Tertiary amines, such as methyldiethanolamine (MDEA), are less energy demanding in the regeneration process, compared to primary amines. However, as mentioned, the kinetics of the reaction between a tertiary amine and CO_2 are fairly slow. This can be overcome by creating a blend. Tertiary amines that suit the operating conditions, such as MDEA in high pressure applications, can be blended with a suitable rate promoter to greatly improve the capture plant's efficiency. A typical blend is MDEA with piperazine (PZ) as the rate promoter [58]. PZ has the ability to capture two CO_2 molecules per molecule of PZ, and combined with its fast kinetics, has proven to be a very good solvent [59]. A blend of MDEA and PZ was chosen for the capture plant in this thesis.

The amount of CO_2 absorbed is often described by CO_2 loading. For an MDEA and PZ blend, the loading, α, is defined as:

$$\alpha = \frac{mol_{\mathrm{CO_2}}}{mol_{solvent}} = \frac{mol_{\mathrm{CO_2}}}{2 \cdot mol_{PZ} + mol_{MDEA}}. \tag{2.10}$$

The rich loading is found from the stream from the bottom of the absorber as the MDEA and PZ solution will be almost satiated with carbon dioxide. The lean loading is found from the stream exiting the bottom of the stripper, containing mainly regenerated solvent solution.

Stripping Column

The stripper is a reversal of the reactions that occur in the absorber. Because of this, the reactions occurring in the stripper are optimized under operating conditions that facilitate a higher temperature, and a lower pressure. The reboiler in the stripper generates heat in the column, and this heat is further used in the cross heat exchanger to heat up the rich amine stream. Regeneration is an important part of the carbon capture plant because of its energy intensity; it is the most energy-intensive part of the entire capture plant and estimates how demanding it is to regenerate the solvent [60]. The reboiler duty will vary depending on the solvent [61]. As mentioned previously, MEA has a relatively energy-intensive regeneration process, and studies have proved that typical reboiler duties for capture plants with this solvent are in the range of 3.5 - 4.8 MJ/kg CO_2 [61] [62] [63].

2.5 Limitations of Steam Methane Reforming

Now that the method of SMR with carbon capture has been explained and assessed, some of its limitations should be discussed. Although this is the most widely used method for hydrogen production today, SMR faces a few key challenges. These challenges are rarely mentioned in existing literature and should be addressed in future research.

An important area for improvement is the energy demand of the primary reformer. Due to the endothermic reaction (Reaction 2.1), a high temperature is needed to ensure a sufficient inward flux [16]. High temperatures are often a cause of concern in industrial applications, as they increase the cost of equipment and materials. Sturdier materials are required, so that the tubes are not as prone to hot spots and heat insulation [16][64]. The high energy requirement also stems from the high steam demand of the process, a high steam-to-carbon ratio is necessary to minimize the risk of coke formation [65]. Coking is the formation of carbon filaments, which reduces activity of the nickel catalyst [65][66]. A clear indicator of the less-than-optimal catalyst utilization can be seen in the very steep temperature profile. By reducing the slope of the thermal gradient across the catalyst, the catalyst utilization could be improved. This steep gradient is a result of poor thermal conductivity as well as the strongly endothermic reaction [67].

The steep thermal gradient also affects the start-up time of the reformer. This is caused by the need for controlled heating of the tubes. Slow and controlled heating of the tubes is important for several factors, such as prevention of hot spots and controlling material expansion [16]. This causes the start-up times of steam methane reformers to be up to several days [68].

The burners are well distributed with a safe distance to the reformer tubes, leading to a very large reformer volume, and contributing to a high capital cost.

Another important limitation is the CO_2 emissions from the steam methane reformer. Despite its popularity in hydrogen production, carbon dioxide emissions are high for this type of production method. Increasingly, these emissions bear an economic cost; carbon taxes.

2.5.1 Carbon Tax

The carbon tax is the most important and efficient policy the Norwegian government has to ensure lower emissions of greenhouse gases [69]. The carbon tax varies significantly depending on governments and policies in different countries; Sweden has the highest carbon tax in the world of around 150 USD/ton CO_2, while the US does not have a specific carbon tax at all [70] [71]. In this thesis, the carbon tax is based on the Norwegian carbon tax, and the results from this analysis will differ from country to country. The Norwegian carbon tax is currently at 588 kr/ton CO_2 [72]. An increase in the carbon tax might prove to be expensive for conventional SMR, because of the relatively low overall carbon capture.

2.6 Introduction to Electrification

The cost of electricity varies greatly depending on the production method, location, and whether the electricity can be generated on-site. Overall thermal efficiencies are often in the range of 70-80% in cogeneration plants that have included a heat recovery steam generator [73]. This is a great step up compared to a conventional power station where the efficiencies are more often in the range of 30-40% for electricity production. The low efficiencies in conventional power stations are affected by the efficiency of the turbine and the condenser [73][74].

Along with the high thermal efficiencies, electricity is particularly useful because it generally increases process efficiencies. This is mainly because the conversion of useful heat from electricity is almost 100% [4][75].

2.6.1 Electrical Steam Methane Reforming

In electric SMR the primary reformer in an SMR plant is altered so that the burners can be removed. This works by using electric heating rather than combustion heating. There are two methods of heating that can be used: resistance based heating and inductive heating. In this thesis, the focus will be on resistance based heating, as this seemed to be the best option for a large-scale plant suggested by Wismann (2019) [16]. The principle of resistance based heating is heat transfer through heat loss when a current passes through a material. Resistance based heating is commonly used in lab-scale furnaces. [16]

Using resistance based heating will require two copper sockets to be placed at each end of the tube. When connected to an electric power source the electricity will provide heating from the resistance along the walls of the tube. An illustration of the concept along with a comparative illustration of conventional SMR can be seen in Figure 2.6.

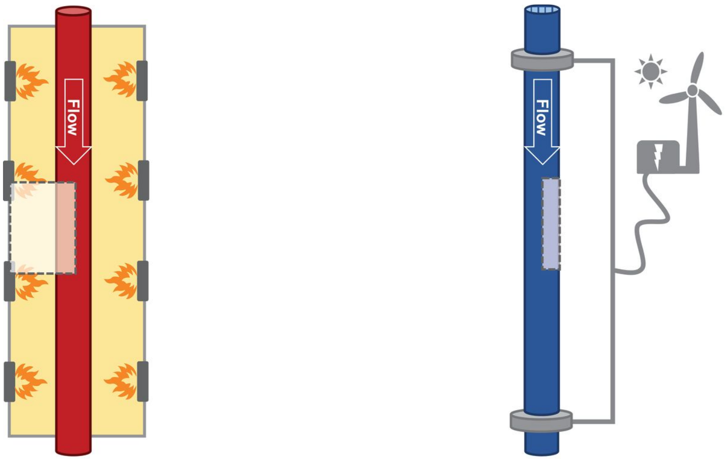

(A) Conventional SMR (B) Electric SMR

FIGURE 2.6: An illustration of the difference between conventional SMR(A) and electric SMR(B). Reproduced and adapted from [67].

Electric SMR has only been performed in one laboratory-scale experiment [16], and there is limited theoretical research. A short intro is now given to discuss whether this is feasible in a large-scale plant or not. Heating the steam methane reformer electrically in a large-scale plant would mean that it is necessary to place copper sockets on each tube [16]. The catalyst is nickel-based as in the conventional reformer, but it is inserted on top of a zirconia washcoat that covers the inside of the tubes. In a conventional steam methane reformer, the catalyst is also often nickel-based, however, the nickel catalyst is usually supported on alumina pellets filling the entire tube [65].

TABLE 2.1: Comparison of the set-up of conventional and electric SMR. The set-up for electric SMR is based on the lab work by Wismann [16].

SMR	El SMR
Furnace	Electric heating
Nickel catalyst on alumina pellets	Wall coated nickel catalyst on zirconia washcoat
	Copper sockets on ends of reformer tubes
	Insulation

The effectiveness of catalyst pellets decreases for larger pellets due to the decrease in surface area [76], but smaller pellets increase the pressure drop in the reformer [77]. Thermal expansion is also an issue and may cause catalyst pellets to break into smaller pellets and sometimes powder [77].

The alleged benefits of electric SMR are first and foremost reduced emissions and reduction of the reformer volume from removal of the furnace. It has been suggested that this could reduce the furnace volume from 3200 m^3 to 3.6 m^3 for a 100,000 Nm^3 H_2/h plant, assuming that the reactor could be scaled to an industrial size. This small a reactor could reduce both capital expenditures of the plant and the area required for it. [16]

As mentioned during the discussion of the limitations of conventional SMR, the steep temperature profile in the reformer tubes challenges the start-up time as well as utilization of the catalyst. Even though the most common catalyst is based on pellets, there have been studies performed using wall-coated catalysts. The thesis of Wismann focused on a wall coated catalyst in the electrically heated SMR to avoid the steep temperature gradient in conventional SMR [16]. By having such a small section of catalyst within the tube, the heat can be distributed better inside the tube due to reduced resistance throughout the tube. Further elaboration on the benefits of electric SMR can be found in Section 4.5.

As the heating of electric SMR is dependent on electricity rather than the combustion of natural gas, the source of electricity is an important consideration. Considering the emissions and cost of different sources of electricity it is important to evaluate the options available for the application based on cost and location.

Choice of Electricity

The viability of electric SMR is highly dependent on location of the plant, as this influences the electricity sources that are available. The relative prices of these electricity sources are also important.

In Norway, as of March 2021, 90% of electricity production was produced from hydro power, and 99% of electricity production was renewable [78]. In the US, however, around 60% of electricity was generated from fossil fuels, while 20% was produced from nuclear sources and the remaining 20% was produced by renewables in 2020 [79]. As a result, the average CO_2 emissions from electricity production in the US is 417 gCO2e/kWh [80], in comparison to an estimated 17 gCO2e/kWh for Norway in 2019 [81].

Figure 2.7 provides an overview of the different renewable electricity sources' costs and emissions. Costs were found from a report by the Intergovernmental Panel on Climate Change [82], while the emissions were found in a report from IRENA [83]. These reports are both international, and as mentioned above, the costs and emissions will vary depending on location. Hence, the emissions and costs of electricity produced by hydro power in Norway were added to the figure as well. In Norway electricity produced by hydro power has been estimated to emit around 3.3 gCO2e/kWh, which is fairly close to the international minimum at 2 gCO2e/kWh [82][84]. However, the international median for CO_2 emissions from electricity produced by hydro power is at 24 gCO2e/kWh [82].

As the electricity used in electric SMR should be produced as environmentally and economically friendly as possible, one would prefer an electricity source such as hydro power or onshore wind. There are several sources of emissions in electricity production, and many of them are dependent on the climate and resources available at the location of the production site.

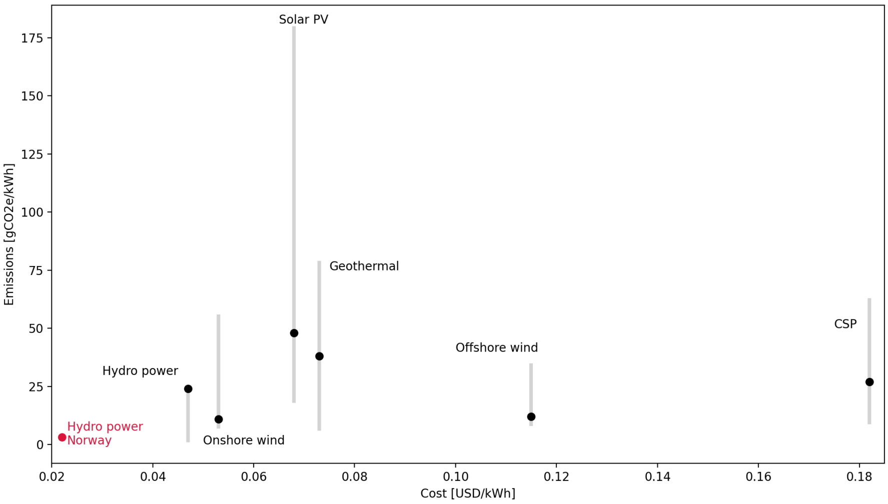

FIGURE 2.7: An overview of the international medians of cost and life cycle emissions of renewable production sources of electricity [82] [83]. The middle dot indicates the median emissions, while the lines extending vertically indicate the range of emissions for the given source. The red dot is specifically for electricity produced from hydro power in Norway [84][78]. The maximum emissions for hydro power internationally were not included.

This figure does not include the variations within the cost estimates of each renewable energy source, although these might be significant between production countries. It does not include the maximum emissions for hydro power because it was very high making it impossible to see the ranges of emissions for the other electricity sources [82].

2.7 Challenges with Electrification

Electrification is an important tool for decarbonization of the energy sector. However, there are still some challenges to overcome for electrification to be a reliable energy source. A comprehensive study by DNV from 2020 stated that there are two main issues; volume and timing. These issues are connected, as the electrification of industry will lead to an increased demand, which renewable sources won't be able to cover [4]. There is also a problem with variability for renewable energy sources.

Intermittency can be dealt with either by using storage in the production chain, or by using switching to a dispatchable fossil-based electricity source when needed [4] [85]. Using intermittent renewable electricity may mean that low costs are only available during certain hours during the day [86]. However, as renewable electricity sources are not dispatchable, this also means that sometimes an electricity surplus will be generated [85]. This surplus electricity needs to be used, and as the interconnection of transmission systems through different countries improves, there is greater opportunity to use this surplus electricity [85]. Currently, an electricity interconnector between Norway, the UK, and Germany is being commissioned and due to be completed in 2021/2022 which will provide a unified electric network between the three countries [87].

Electrifying an entire plant and changing its infrastructure is an expensive alteration. Hence, it is often more economically sustainable to replace industrial equipment at the end of its useful life. Switching to electrical equipment, or hybrid equipment, would be a good alternative when a new plant is being set up or when old equipment is due to be replaced [88]. For that reason, keeping track of predictions and trends of electricity prices, fuels, and governmental taxes and policies will be a useful tool in assessing the potential to electrify the plant in question.

2.7.1 Electrical Power Tax

The Norwegian Tax Administration reports an electrical power tax of 0.17 kr/kWh, and this value is used for this thesis (and listed in Table 3.6). However, it should be possible for an electric SMR plant to apply for a reduced electrical power tax, on the basis that the process is used for production of an energy product [72]. This tax deduction would mean that the electric SMR would be granted an electrical power tax of 0.00546 kr/kWh, which is a very significant decrease.

DNV has shown in their study from 2020 that average European taxes for electricity are significantly higher than for natural gas [4]. This is shown in Figure 2.8 where all aspects of electricity costs are higher than those of natural gas, including taxes. In Norway, on a per kWh basis, the cost of electricity is approximately 1.5 times the cost of natural gas while the European average is 3 times [4].

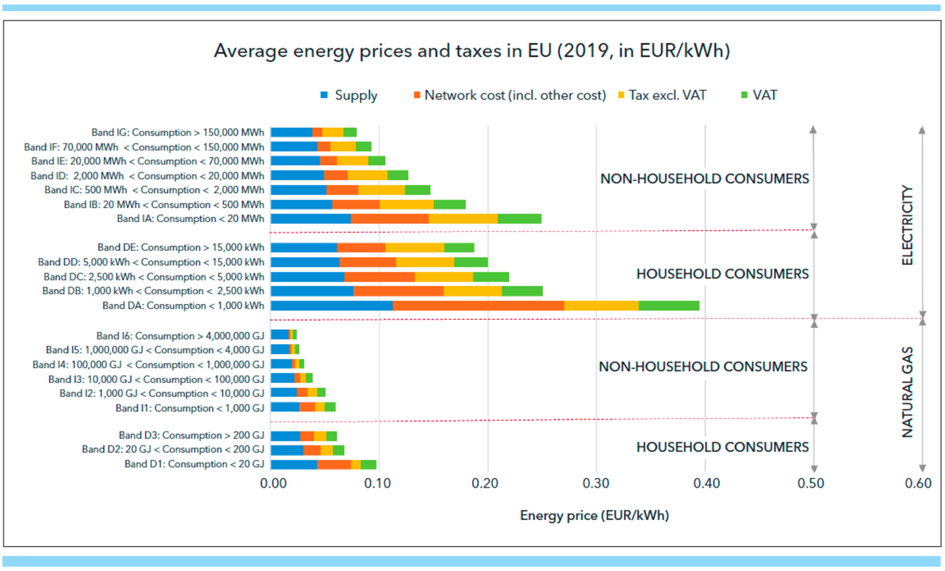

Figure 14 - Average energy prices per kWh in Europe for different consumption bands and consumer groups[24]

FIGURE 2.8: Comparison of the average energy prices and taxes of natural gas and electricity in EU from DNV [4]. Relevant for this thesis is the non-household consumer costs where it can be seen that each aspect taken into account is more expensive for electricity.

Chapter 3

Methodology

The main purpose of this thesis is to evaluate the cost and emissions of two different hydrogen production plants with implemented CO_2 capture: a conventional steam methane reformer (SMR) and an electrically heated SMR. This chapter discusses the methodology applied to this thesis.

The conventional SMR was defined as the base case. Both the base case and the electric SMR case were simulated in Aspen Hysys V9. The base case simulation was started during an autumn project at NTNU, but further improved upon throughout this thesis.

For this study: (i) steam export was not included in the simulation, even though it might improve the efficiency of the model, (ii) further processing of the produced H_2 nor CO_2 were included in the thesis and (iii) storage options of H_2 nor the CO_2 were not considered for either case. Steam export can be included by using heat from the furnace to a steam generator [89]. This has been shown to increase the thermal efficiency of the process, and the steam can be sold to customers [90].

The simulations were then used as a basis for equipment sizing and cost estimation enabling a comparison of both cases. Capital expenditures (CAPEX) and operating expenditures (OPEX) were calculated for both conventional and electric SMR, and sensitivity analyses were computed for the OPEX calculations. CO_2 emissions for both cases were also investigated. Finally, a study was run to examine how the electricity source would affect the emissions of the electric SMR.

3.1 Simulation

3.1.1 Base Case

The simulations were performed in Aspen Hysys. More information regarding the specific reactor types and their operational conditions and features can be found in Appendix A, along with a print screen of the simulation as it looks in Aspen Hysys. The base case is a conventional SMR plant with amine-based carbon capture implemented. It was simulated using the Peng-Robinson equation of state, as this is the most enhanced cubic equation of state available in Aspen Hysys. The carbon capture plant used a property package specifically for chemical solvents to get MDEA and PZ.

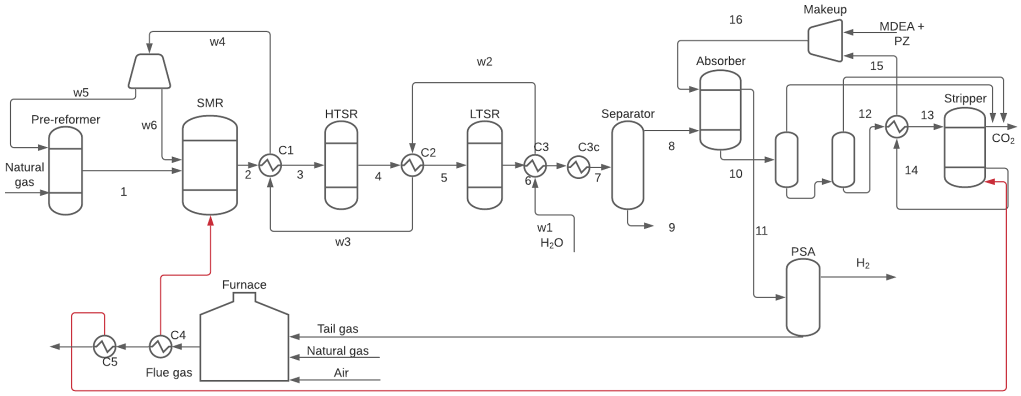
Makeup
16
MDEA +
PZ
w4
w2
15
Absorber
w5
SMR
Pre-reformer
w6
HTSR
LTSR
Separator
Stripper
12
13
CO$_2$
C1
C2
C3
C3c
8
Natural
gas
2
3
4
5
6
7
10
14
1
w3
w1
H$_2$O
9
11
PSA
H$_2$
Furnace
Tail gas
Natural gas
Air
C4
C5
Flue gas

FIGURE 3.1: Flow sheet diagram of the conventional SMR process.
Red lines indicate heat flows.

A typical SMR plant consists of a pre-reformer, a primary reformer (the SMR), two shift reactors, a carbon capture plant, and a PSA, all of which are included for both cases. A flow sheet of the plant is shown in Figure 3.1. An overview of the criteria and main points in the simulation can be found in Table 3.1. A short description will follow for the basis of each unit operation. All operational conditions for the unit operations can be found in 4.2.

TABLE 3.1: Base criteria for simulations. The energy is based on the lower heating value (LHV).

Feedstock basis	Natural gas
Amount of feedstock	$4.1 \cdot 10^4$ kg/h
Feedstock energy (LHV)	$5.35 \cdot 10^5$ kW
Desulphurization	Not included in simulation
Type of CO_2 capture	Amine-based carbon capture
Capture rate	95%
Solvent	35 wt% MDEA and 5 wt% PZ
H_2 produced	$1.5 \cdot 10^4$ kg/h
Energy produced (LHV)	$5.15 \cdot 10^5$ kW

The composition of the natural gas used as feedstock and fuel can be found in Table 3.2.

Pre-reformer and SMR

As the natural gas was assumed to be desulphurized before entering the pre-reformer, it was set at a high pressure. The natural gas was expanded to 25 bar and heated to 400°C before entering the pre-reformer to convert the heavier hydrocarbons to methane (Reaction 2.2). Steam is required in both the pre-reformer and the SMR, and water was pumped up to 25 bar and heated to 250°C. Different amounts of steam are required in each of the reformers. Case studies were done for both reformers to find the optimal amount of steam. The case study for the pre-reformer focused on

TABLE 3.2: Composition of the natural gas used as feedstock and fuel in the simulation [23]. The conditions given are the inlet conditions of the natural gas as feedstock after desulphurization.

Compound	Mole%
Methane	85.30
Ethane	7.05
Propane	2.73
i-Butane	0.55
n-Butane	0.94
i-Pentane	0.27
n-Pentane	0.27
n-Hexane	0.18
n-Heptane	0.13
n-Octane	0.04
Carbon dioxide	2.21
Nitrogen	0.33
Temperature	50°C
Pressure	50 bar
Flow	$4.1 \cdot 10^4$ kg/h

finding the minimal steam-to-carbon (S/C) ratio required to remove the heaviest hydrocarbons, while the study for the primary reformer addressed the effect of the S/C ratio on the conversion rate of methane. The S/C ratio used for the pre-reformer and the SMR was 0.3 and 3.0 respectively. Both case studies can be found in Appendix C.

The pre-reformer was modeled at 400 °C, while the SMR was set at 900 °C, heated by the furnace surrounding it.

Furnace

As shown in Figure 2.4 in Chapter 2, the SMR has an integrated furnace that surrounds the reformer tubes. For simulation purposes in Aspen Hysys, a reactor was added with fuel and excess air as inlet flows. Here, the combustion occurs and creates the heat which will be used in the SMR. The temperature in the flue gas exiting the furnace was limited to not exceed 1600 °C to ensure safe heating of the reformer tubes as described previously in Section 2.5. For heat recovery purposes, the waste heat from the furnace was used to heat up the reboiler in the carbon capture plant.

A case study was done to find the amount of air and fuel necessary to provide sufficient heating while reducing CO_2 emissions and avoiding other emissions such as CH_4 and CO. The case study investigated two variables: the AF and the inlet mass flow of fuel. The inlet mass flow of fuel includes the tail gas from the PSA. The AF used in this simulation was 20, while the mass of fuel was $3.2 \cdot 10^4$ kg/h. The amount of fuel was mainly determined from the heat requirement, to ensure that sufficient heating for the SMR was provided. The amount of air was found to ensure complete combustion of the fuels so that there are no CO emissions from the furnace. The case study can be found in Appendix C.

Simulations of a furnace at stoichiometric conditions were also conducted. At these stoichiometric conditions, the furnace was not limited by the outlet temperature and no excess air was added. This will be referred to as an ideal furnace. The stoichiometric amount of air dependent on the fuel and tail gas was calculated. The amount of natural gas as fuel was minimized while ensuring that the temperature of the flue gas was sufficient for heat transfer. The inlet flow of tail gas is, as known, constant. By minimizing the amount of fuel, the emissions were also minimized, and by only including the stoichiometric amount of air the temperature could be higher than it would with excess air, making it possible to use less fuel to reach higher temperatures.

The heat of combustion for the reactions based on the fuel consumption was used in the calculation of the efficiency, η, of the furnace. This efficiency refers to the heat loss after heat has been supplied to the SMR and the reboiler. A simulation like this, where the SMR requires temperatures of 900 °C while the reboiler is at around 120 °C, will always endure heat losses. The efficiency was calculated from the following equation:

$$\eta = \frac{\text{Energy used}}{\text{Energy input}} = \frac{Q_{SMR} + Q_{reboiler}}{Q}, \tag{3.1}$$

where the energy input, Q, was calculated from the heat of combustion. Q_{SMR} and $Q_{reboiler}$ denotes the heat requirement in the SMR and reboiler respectively. The enthalpy for each reaction, H_{rx}, was found from the heat of formation of the reactions. This was used to find the heat of combustion:

$$Q = \sum_i n_i H_{rx,i}, \tag{3.2}$$

where n is the molar flow and i denotes the different components.

Shift Reactors

Post SMR, the hydrogen and carbon monoxide that has been produced enters the shift reactors. As recommended for industrial applications, they were modeled as two shift reactors: the high temperature shift reactor (HTSR) and the low temperature shift reactor (LTSR). The HTSR was set at 320°C, while the LTSR was set at 190°C, and both were modeled as isotherm reactors. The temperatures were based on values from literature [33]. The reactors follow the WGS reaction (Reaction 2.5), where the carbon monoxide is converted to carbon dioxide. More information about the specifics of the shift reactors can be found in Table A.5 in Appendix A.

Carbon Capture Plant

To remove the CO_2 that was produced in the shift reactors, a carbon capture plant was implemented. An amine-based capture plant with a 95% capture rate was simulated. This amine-based carbon capture plant consists of an absorber, two flash drums, a cross heat exchanger, and a stripper.

The absorber was simulated with 12 stages; this number of stages was determined by a case study done for the autumn project. The pressure in the absorber was 22.5 bar from the outlet pressure from the LTSR, with an inlet temperature of 40°C. This temperature was chosen based on literature values [91]. The amine solvent was a blend of 35 wt% MDEA and 5 wt% PZ. After the absorber, two flash drums were introduced to reduce the pressure. In the first flash the pressure was set to 5 bar, while the pressure was 2 bar in the second flash. The gas flows from the top of both flash drums were mixed with the stripped CO_2-gas for transportation or utilization. This is shown in Figure 3.1.

The cross heat exchanger is the heat exchanger between the absorber and stripper, where the amine-rich stream is heated by the amine-lean stream. The heat exchanger was specified by setting the temperature difference on the hot side to 5°C. More on the specific temperatures from the Aspen Hysys simulation can be found in Appendix A.

The stripper, also known as the regenerator or desorber, was simulated with 10 stages, based on literature [91]. The specifications set for the stripper was to adjust the reboiler duty to capture 95% of the incoming CO_2. The condenser was set to 25°C. More specifications on the stripper can be found in Table A.10 in Appendix A.

A case study was done focusing on the solvent rate to find an optimal liquid-to-gas (L/G) ratio for the system. For this case study, the inlet mass flow of the solvent was considered in terms of how it affected the lean and rich loading and the reboiler duty.

PSA

To purify the hydrogen that comes from the top of the absorber, a PSA was used. The PSA was set to recover 90% of the hydrogen with a purity of 100%. It was modeled as a simple component splitter in Aspen Hysys. The tail gas that the hydrogen was separated from was sent into the furnace as fuel.

3.1.2 Electric SMR

The simulation of the case of electric SMR was based on the base case simulation, using all the same unit operations. As mentioned, Aspen Hysys does not have a specific equipment block for the SMR, and thus the furnace had already been modeled separately from the reformer. Therefore, in the simulation of electric SMR, the furnace was set to only supply heat to the reboiler in the carbon capture plant.

A similar case study to the one for conventional SMR was performed for electric SMR to calculate the amount of fuel and air needed in the furnace to ensure complete combustion and sufficient heating. This case study is also included in Appendix C. There is no option to choose the type of heat supply, such as electric heating, in Aspen Hysys, and hence the emissions from the electricity production and electric supply were found from literature. A print screen of the simulation can be found in Section A.1 in Appendix A, and an illustrative flow chart can be found in Figure 3.2. As mentioned in Section 2.6.1, there are some other differences between conventional and Electric SMR as well, such as the catalyst, the start-up time, and the size of the reactor. However, these features are not possible to include in the Aspen Hysys simulation for comparison, but they are discussed in Chapter 4.

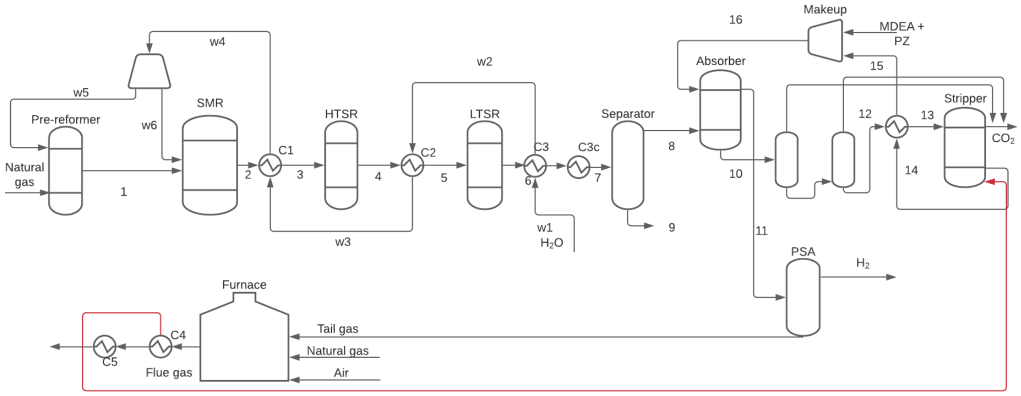
Makeup
16
MDEA +
PZ
w4
w2
Absorber
15
w5
SMR
Stripper
Pre-reformer
w6
HTSR
LTSR
Separator
12
13
CO$_2$
C1
C2
C3
C3c
8
Natural
gas
2
3
4
5
6
7
10
14
1
9
w3
w1
H$_2$O
11
PSA
H$_2$
Furnace
C4
Tail gas
C5
Natural gas
Flue gas
Air

FIGURE 3.2: Flow sheet diagram over the electric SMR process. The red line indicates a heat flow.

3.2 Cost Estimations

An important basis for comparison of industrial plants is the cost estimations of their implementation. The CAPEX estimates were calculated based on data from the Aspen Hysys simulation using general sizing and cost estimations protocols based on the textbooks from Sinnott et al (2013) and Turton et al (2009) [73][92]. Some costs for specific unit operations were also found from literature and scaled based on the equipment capacity. The OPEX estimates were based on costs from literature and values from the Aspen Hysys simulation. For the cost estimations, assumptions regarding lifetime and operating hours, as well as electricity efficiency were made and can be found in Table 3.3.

TABLE 3.3: Assumptions used for the OPEX calculations.

Lifetime	20 years
Operating hours	8000 hours annually
Electricity efficiency	100%

3.2.1 CAPEX

To estimate the CAPEX for the systems, the capital cost of each unit operation in the model was found. The internals of vessels were accounted for, as well as the cost of solvents used in the carbon capture plant.

A general formula was used to compute the purchase cost, C_p^0, of the equipment in the plant:

$$log_{10}\left(C_p^0\right) = k_1 + k_2 \cdot log_{10}\left(I\right) + k_3 \cdot \left[log_{10}\left(I\right)\right]^2, \tag{3.3}$$

where the k-values were found in Sinnott et al (2013), and I is the capacity or size parameter the equipment. For separators and vessels, I is the total volume of the vessel, while for heat exchangers, I is the total heat transfer area and the k-values are dependent on the type of heat exchanger chosen. All values for sizing and their respective k-values used can be found in Table B.5 in Appendix B.

The purchase cost, along with a bare module cost factor, F_{BM}, gives the bare module cost for the equipment, C_{BM}:

$$C_{BM} = C_p^0 \cdot F_{BM}, \tag{3.4}$$

which includes the direct and indirect costs for each unit [92]. The formulas, factors, and constants used to compute the bare module factor have been added to the appendix.

To convert between the bare module cost, C_{BM} to the total module cost, C_{TM}, which includes the contingency and contractor fees, a factor of 1.18 was used [93].

$$C_{TM} = 1.18 \cdot C_{BM} \tag{3.5}$$

CAPEX is given as C_{TM}, and was scaled to a 2020 basis based on the Chemical Engineering Plant Cost Index (CEPCI). The CEPCI for 2020 is 596.2. The cost was scaled using the following equation:

$$C_2 = C_1 \cdot \frac{\text{CEPCI}_1}{\text{CEPCI}_2}, \tag{3.6}$$

where C_1 and C_2 are the costs for two different years, with their respective CEPCI values.

A startup cost including the cost of the solvent chemicals, MDEA and PZ, was added as 10% of the fixed capital cost based on estimations from a rule of thumb found in literature [94].

Size Estimations of Vessels

As mentioned, the volume of the vessels was required to find a cost estimate. Two methods were used based on whether the vessel was a horizontal or vertical tank. Both types were estimated based on methods from Sinnott et al [73]. All the sizing calculations and cost estimates were done in Python and the specific size and cost of each vessel in the simulation can be found in Appendix C.

Vertical vessels are sized based on the settling velocity, v_s, and the volumetric flow rates of vapor, V_v, entering the column. This is used to find the minimum vessel diameter.

$$v_s = Ks \cdot \sqrt{\frac{\rho_l - \rho_v}{\rho_v}}, \tag{3.7}$$

where K_s was set to 0.07, ρ_v and ρ_l are the vapor and liquid densities respectively [73]. The settling velocity was multiplied with a factor of 0.15 for separators without a demister pad.

The diameter of the vessel, D_v, was found based on this settling velocity [73]:

$$D_v = \sqrt{\frac{4 \cdot V_v}{\pi \cdot v_s}}. \tag{3.8}$$

An estimation of the height of the vessel, H_v, was found by the following [73]:

$$H_v = \frac{3}{2} D_v + h_v, \tag{3.9}$$

where h_v is the height of the liquid in the vessel. The calculations including the height of the liquid are given in Appendix B.

For horizontal vessels, the sizing is more dependent on the length-to-diameter (L/D) ratio, which depends on the design pressure of the vessel, as given in Table 3.4.

TABLE 3.4: The length-to-diameter (L/D) ratio based on the pressure in the unit [73].

L/D	Pressure [bar]
3	0-20
4	20-35
5	35+

Horizontal vessels use the same starting point as the vertical vessels computing the settling velocity (Equation 3.7) which is used to calculate the vessel diameter based on an educated guess of the liquid height and a minimum liquid hold-up time. The full methodology applied in this section for the equipment sizing can be found in Appendix B.

SMR, PSA, and Pre-reformer

The cost of the primary reformer, the PSA, and the pre-reformer were based on literature and scaled to fit the system. Cost estimations of the SMR and the PSA were based on values from Turton et al [92], while the cost estimation of the pre-reformer was based on a cost estimate from [95]. The cost of the SMR includes the reformer tubes, the furnace surrounding the tubes, as well as the cost variables considering pressure, material factors, fees, and labor costs making up the total module cost.

The following equation was used for all three unit operations:

$$C_{TM} = C_O \left(\frac{F}{F_0} \right)^a, \tag{3.10}$$

where C_O is the base cost for a unit with capacity F_0, F is the capacity of the new system and a is a factor to adjust cost. The capacities can be based on different properties, based on the type of unit. The values for each unit that were used in the formula can be found in Table 3.5. These costs were also scaled based on the CEPCI as in Equation 3.6.

TABLE 3.5: Values used to compute the cost of the pre-reformer, SMR, and PSA in Equation 3.10 [92][95].

	Pre-ref	SMR	PSA
C_O [MUSD]	2.55	60.43	0.817
CEPCI (year)	390.6 (1999)	567.5 (2007)	567.5 (2007)
F (unit)	ton/day	kg/s (feed)	$Nm^3/h\ H_2$
F	$1.3{\cdot}10^3$	49.7	$17{\cdot}10^4$
F_0	$1.5{\cdot}10^3$	26.1	944
a	1	0.67	0.55

Absorption and Stripping Column

The diameter of the columns was found based on a method from the textbook by Sinnott (2013) [73]. The method is based on the capacity of the cross sectional area of the column while ensuring that the flooding is within the acceptable range of 60-80% [75]. Flooding is caused by excessive entrainment which occurs when the vapor in the column carries liquid from one tray upwards to the next [92]. This reduces the separation because liquids of different compositions mix. It is dependent on the cross sectional area because a small cross sectional area will increase the vapor velocity and the drag force from the vapor on the liquid will be higher than gravity, pulling liquid upwards [92].

It was assumed, based on statements from Perry's Chemical Engineers' Handbook (2000) as well as Meerman et al (2012) that the diameter of the absorber and stripper would be approximately the same [75] [96]. Hence the diameter of the stripper was set equal to the calculated diameter for the absorption column. As for the height estimations, it is standard practice to base the height estimate on existing plants for amine systems [48]. The complete method and calculations can be found in Appendix B.

The amount of packing was based on the volume of the columns. Packing was decided to be Pall Rings (3.5 in) based on pressure and column types [73]. To ensure that the packing is structurally supported throughout the tower, and ensure good distributions of the liquid throughout the column, both the need for packing support and liquid redistributors were assessed. Liquid redistributors are typically necessary every 6-7 meters to avoid poor distribution of the liquid and to hinder the liquid from migrating towards the column wall [97]. Packing support is a physical support to ensure that the packing on the bottom of the column is not crushed from the packing on top of it. It also allows free passage for gas and liquid throughout the column [97].

As the packing height was found from literature [96], the total height of the column was found through the following equation accounting for the additional height of liquid distributors and packing support [98]:

$$H_t = H_p + 2 + (0.25 \cdot D_c), \tag{3.11}$$

where H_t is the total height of the column, H_p is the height of the packing, and D_c is the diameter of the column.

Shift Reactors

The shift reactors were modeled as plug-flow reactors (PFR) for the size and cost estimations. Firstly, the reaction rate based on the reactant CO, r_{CO}, was calculated for each, from the following equation [92]:

$$-r_{CO} = k_0 \cdot exp\left[\frac{-E_0}{RT}\right]\left(y_{CO}y_{H_2O} - \frac{y_{CO_2}y_{H2}}{K_{eq}}\right), \tag{3.12}$$

where k_0 is the rate constant and E_0 is the activation energy, which can both be found in Table B.1 in Appendix B. R is the gas constant, T is the temperature, and y_i denotes the mole fraction of component i. The equation for the equilibrium constant, K_{eq}, can also be found in Appendix B in the same table. Both the equations for k_0 and K_{eq} was based on the catalyst of choice. From literature it was found that the most common catalyst for the shift reaction is Fe_2O_3-MgO [37].

The rate equation was used in the model to size the WGS reactors, using the mole balance:

$$V\frac{dc}{dt} = \phi_v c_{in} - \phi_v c_{out} - (-r_{CO})V, \tag{3.13}$$

where V is the volume, c is concentration, t is time, ϕ_v is volumetric flow. A model in MATLAB was made based on these equations and by trial and error, the length of the catalytic bed was adjusted to reach the same conversion found in the Aspen Hysys simulation. A L/D ratio of 3 was assumed. The complete method can be found in Appendix B. The conversion of the shift reactors were found to be 88.7% and 87.1% for HTSR and LTSR, respectively, from the simulation. This was used as the basis for the size calculations. The size of the reactor was estimated to be approximately the same size as the catalytic bed, and the reactor was sized accordingly. It was proven that altering the size of the WGS reactors would not make a significant impact on the total CAPEX estimate, and hence it was not deemed necessary to adjust the volume. This is because the cost of the WGS reactors is relatively small compared to the costs of for example the SMR.

Heat Exchangers

It was assumed that all heat exchangers would be of the same configuration. The heat exchanger configuration was chosen based on the TEMA standard, and a fixed tube heat exchanger was used for all heat exchangers. All heat exchangers, except the cross heat exchanger in the capture plant, were determined to use carbon steel in its configuration. The cross heat exchanger was determined to use stainless steel (SS). As carbon steel (CS) does not handle toxic chemicals well, and PZ is toxic, it was determined a better choice to go with SS. CS is a generally cheaper option, which should be opted for when it is safe to do so.

A complete overview of the process to find the type of heat exchanger can be found in Appendix B. The size estimations were found by the following equation:

$$A = \frac{Q}{U\Delta T_{LM}}, \tag{3.14}$$

where A is the total heat transfer area, Q is the heat transferred, U is the overall heat transfer coefficient, and ΔT_{LM} is the logarithmic mean temperature difference between the hot and cold side of the exchanger. The cost of the heat exchanger is dependent on the type of heat exchanger as well as the area. The type of heat exchanger determines the k-values in Equation 3.3, while the area is used for the specific value, I. The general methodology as given previously was used to find the total module cost. Information on the type of heat exchanger and the k-values, as well as the cost estimations can be found in Appendix B and C.

Electric SMR

The CAPEX estimation of the electric SMR was based on the CAPEX for conventional SMR. The cost of all unit operations other than the primary reformer is the same for electrical and conventional SMR, as the production of hydrogen is kept constant. With regards to the primary reformer, the biggest difference costwise between the technologies is that in electric SMR there is no furnace surrounding the reformer to supply heat. To find an estimate for the cost of the primary reformer in electric SMR, an approximate cost for the furnace was found that could be deducted from the cost of the primary reformer in the base case. The cost of the furnace was found from Equations 3.3- 3.5, where Equation 3.3 would be based on the heat, Q, supplied from the furnace,

$$log_{10}\left(C_p^0\right) = k_1 + k_2 \cdot log_{10}\left(Q\right) + k_2 \cdot \left[log_{10}\left(Q\right)\right]^2,$$

the k-values can be found in Appendix B. Even though there is no furnace to supply heat to the reformer, the electric SMR plant still utilizes a furnace to supply heat to the reboiler in the carbon capture plant. This cost was estimated from the same equations as the furnace in the conventional SMR (shown above), only with a lower heat supply.

To get an estimate for the CAPEX of electric SMR, the CAPEX for all unit operations excluding the primary reformer and its incorporated furnace were added together. The smaller furnace was also added along with an estimate of the primary reformer from conventional SMR without the furnace. This estimate was multiplied with a factor F_{SMR} that was varied between 1 and 10. The F_{SMR} was added because of the assumption that the internals of the primary reformer, hence the reformer without the furnace, would be more expensive for electric SMR based on the additional material such as the copper sockets, the new type of catalyst and the labor costs necessary. The CAPEX estimate would then look like this,

$$\text{CAPEX}_{elSMR} = \text{CAPEX - SMR (incl. furnace) + Furnace for el SMR + SMR (excl. furnace)} \cdot \text{F}_{SMR}\ ,$$

where CAPEX is the CAPEX for conventional SMR found previously.

3.2.2 OPEX

For the OPEX calculations, the focus was especially on the raw materials needed and the resources required for heat supply to the primary reformer. All costs were found in literature, and the costs along with their respective source can be found in Table 3.6.

TABLE 3.6: Variables considered in the OPEX calculations.

Variable	Cost	Source
Natural gas	0.16 USD/Sm^3	[99]
Electricity	0.18 kr/kWh	[100]
Cooling water (CW)	0.01 €/ton	[101]
CW treatment chemicals	0.0025 €/ton	[101]
Boiler feedwater	0.1 €/ton	[101]
O&M costs	4% of CAPEX	[96]
Carbon tax	588 kr/ton CO_2	[102]
Electrical power tax	0.17 kr/kWh	[72]

These costs were used for both conventional and electric SMR. The O&M costs were used as 4% of CAPEX of the base case for both conventional and electric SMR, due to uncertainties in the CAPEX for the electric SMR and to have a solid basis for comparison. Hence it is assumed that the operation and maintenance costs for the electric SMR would be similar to the conventional SMR. However, a report from McKinsey (2020) suggested that electrically driven equipment often has lower maintenance costs than the conventional option [88].

The cost of natural gas was found from the average of the internal gas prices reported for each quarter in 2019 from Equinor [99]. 2020 was a unique year and affected the industry greatly, including natural gas prices. Figure 3.3 shows the variation of the internal gas price from 2015 to the first quarter of 2021, derived from the average of quarterly prices reported. The price from 2019 was used as the basis for the calculations, as the dip in the price in 2020 might not be representative of the current price.

To provide a more thorough analysis, more scenarios were considered based on the two technologies. For the conventional SMR, an ideal SMR was calculated based on an ideal furnace as described in Section 3.1.1. As the ideal furnace emits less CO_2 and uses less fuel, the cost of conventional SMR with an ideal furnace is slightly lower than with a furnace simulated in Aspen Hysys. This scenario is referred to as "Ideal SMR".

Based on the electric SMR two additional scenarios were created, the "El SMR reduced tax" and the "Ideal el. SMR". The first scenario was based on the electrical power tax. Based on information from the Norwegian Tax Administration, it is likely that the electric SMR plant could receive a reduced tax, as mentioned in Section 2.7.1 [72]. The second scenario, the "Ideal el. SMR", created for the electric SMR includes the reduced electrical power tax as well as an ideal furnace, which was calculated by the same method as for conventional SMR. The setup in Aspen Hysys and additional calculations for each scenario can be found in Section A.5 in Appendix B.

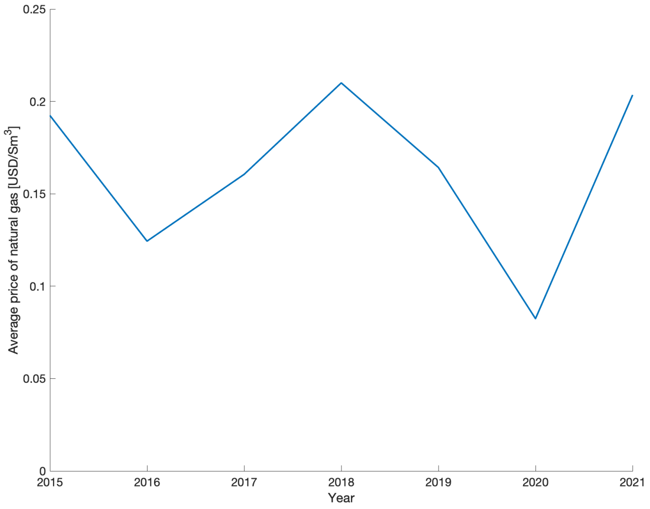

FIGURE 3.3: Average prices of natural gas from the internal gas price at Equinor from 2015 to the first quarter of 2021 [99].

The motivation behind these additional scenarios was to compare ideal situations for both plants so that the efficiency of the furnace would not be a limiting factor for the cost of conventional SMR. For the electric SMR, a limiting factor might be the electrical power tax. Motivated by a statement in the annual climate report from the Norwegian government that the carbon tax would be increased to 2000 kr/ton CO_2 by 2030, the OPEX was predicted for the different scenarios from 2021 to 2030 [103]. This prediction assumes that the cost of natural gas, electricity, and the carbon tax will change, while other OPEX such as cooling water, operational and maintenance costs, and the electrical power tax will remain constant. Predictions for the price of natural gas were found from Equinor's quarterly finance reports, and the electricity price was predicted by Statistics Norway. The results can be found in Figure 4.6 in the next chapter.

A more in-depth prediction for the OPEX in 2030 was also included for conventional and electric SMR. This was done to understand how the OPEX comparison may be expected to evolve as electric SMR might become a more mature technology. Table 3.7 shows the updated costs used in the OPEX prediction for 2030 along with their respective sources.

Some variables were not accounted for in the OPEX calculations, such as the loss of MDEA and PZ. In the simulation model, these losses were negligible, equating to around 620 kg/h (0.00003% of the total flow). Taxes other than the carbon tax or electrical power tax were not included specifically. The factor of 1.18 to account for contingency fees and other building costs were included, however, no insurance costs were accounted for. Labor costs were not specifically added but are included as a part of the 4% of the capital cost for operation and maintenance costs.

A sensitivity analysis was performed for both conventional and electric SMR to explore the impact of a change in costs of natural gas, electricity, electrical power tax, and carbon tax on the OPEX calculations. These sensitivity analyses were carried

TABLE 3.7: Variables considered in the OPEX calculations for the 2030 estimate.

Variable	Cost	Source
Natural gas	0.27 USD/Sm^3	[104]
Electricity	0.98 kr/kWh	[87]
Cooling water (CW)	0.01 €/ton	[101]
CW treatment chemicals	0.0025 €/ton	[101]
Boiler feedwater	0.1 €/ton	[101]
O&M costs	4% of CAPEX	[96]
Carbon tax	2000 kr/ton CO_2	[103]
Electrical power tax	0.17 kr/kWh	[72]

out by increasing and decreasing the cost of each variable by 20% and observing the impact on total operating costs. The sensitivity analyses were performed for the 2021 estimate as well as the 2030 prediction.

3.2.3 LCOH

The levelized cost of hydrogen (LCOH) is used to compare technologies based on the cost per kg hydrogen it produces. The LCOH was found based on a method from Viktorsson (2017) [105] using the annual life cycle costs (LCC). First, the CAPEX was annualized by using the capital recovery factor (CRF):

$$CRF = \frac{i(1+i)^n}{(1+i)^n - 1}, \tag{3.15}$$

where n is the assumed lifetime and i is the nominal discount rate. The nominal discount rate was set at 6% [105]. By multiplying the CRF with the CAPEX, an annualized investment cost can be found:

$$CAPEX_{annual} = CRF \cdot CAPEX. \tag{3.16}$$

The annualized LCC is represented by the annualized capital cost and the annual operating cost, which is used to find the LCOH,

$$LCC = CAPEX_{annual} + OPEX \tag{3.17}$$

$$LCOH = \frac{LCC}{E_{H_2}}, \tag{3.18}$$

where E_{H_2} is the mass of hydrogen produced annually.

3.3 Analyses of CO_2 Emissions

In recent times, the carbon dioxide equivalent emissions when evaluating industrial plants have become increasingly important. For electric SMR to be a superior alternative to conventional SMR, the CO_2 emissions from the plant should be lower. Therefore, both technologies were investigated in terms of their direct emissions. During production in a conventional SMR with carbon capture, the most significant emission from the plant is the combustion of fuels in the furnace. For electric SMR, the emissions will also depend on the production source of electricity, which is why an investigation into the implications of the emissions connected to different sources was conducted. Data was collected from a comprehensive international study, as well as the average emissions from electricity production in the United States [82][80]. Both life-cycle emissions and direct emissions were investigated. By collecting data on the emissions of electricity productions, a best and a worst case scenario in terms of direct emissions for the electric SMR could be found. The direct emissions for the electric SMR were found by,

$$\text{Emissions} = \text{Direct emissions from furnace} + \text{direct emissions from electricity source.}$$

The goal of comparing emissions from the base case of conventional SMR to electric SMR with various sources of electricity was to discover if the source of electricity was important for determining whether electric SMR was more sustainable than conventional SMR.

Chapter 4

Results and Discussion

In this chapter, the results from the simulations of the base case and the electric SMR are presented. First, the results focus on ensuring that the simulation results are in line with literature values. Then cost estimations, for both CAPEX and OPEX were calculated, and sensitivity analyses were performed for the OPEX estimates. Another important aspect of the evaluation and comparison of the two cases is the emissions from each technology. The emissions from SMR are well documented in the literature, both with and without carbon capture. The research on electric SMR is limited, so the section on emissions and comparison investigates the implications and possibilities for electric SMR in terms of environmental impact.

4.1 Process Simulations

The process simulations were compared to literature values and trends. The evaluation on parts other than the primary reformer is the same for the base case as well as the electric case, and can be found in the base case evaluation below.

4.1.1 Simulation of Base Case

All compositions, temperatures, and pressures for flows entering and exiting the large unit operations in the simulation, as well as the energy consumption/production for unit operations are given in Table 4.2 at the end of this section. Table 4.3 includes temperature, pressure, mass flow, and loadings for the absorber and stripper in the carbon capture plant.

As mentioned in Table 3.1, $4.1 \cdot 10^4$ kg/h natural gas was used to produce $1.5 \cdot 10^4$ kg/h H_2. The main energy consumption is the primary reformer, requiring $2.1 \cdot 10^2$ MW at 900 °C. After supplying heat to the SMR, the temperature of the flue gas was found to be 935°C, which could be used to supply heat to the reboiler in the carbon capture plant (further discussed in the next section). The total amount of heat produced from the furnace was $5.1 \cdot 10^5$ MW, when cooled back down to 25 °C.

Some specific values in the simulation were compared with values from literature to validate the results. This can be seen in Table 4.1 and was based on values from a technical review by the IEA Greenhouse Gas R&D Programme (IEAGHG) on reference data and supporting literature reviews [25]. The data is based on the syngas, which is the synthesis gas from the primary reformer.

TABLE 4.1: Comparison of literature values and simulation results from Aspen Hysys. Literature values were collected from the IEAGHG Technical Review (2017) and are based on an SMR plant with CCS [25].

	Literature	This work
Pressure in SMR [bar]	15-40	20
Temperature in SMR [°C]	750-950	900
S/C ratio [mole/mole]	1.8-3.0	3.0
H_2 in syngas [mole%] (dry basis)	68-73	73.5
H_2/CO in syngas [mole/mole]	3.5-5.5	4.7
CO_2 in syngas [mole%] (dry basis)	7-10	8.3
CO_2 in syngas shift outlet [mole%] (dry basis)	15-20	20.5
CH_4 in syngas [mole%] (dry basis)	2-6	2.6

Table 4.1 shows that the results from the simulation seem to fit well within the range of the technical review by the IEAGHG [25]. This provides a good basis for further analyses.

The case study for the furnace in the base case of conventional SMR resulted in $3.21 \cdot 10^4$ kg of natural gas as fuel, and 16% excess air. It is typical to use around 15% excess air in an industrially fired furnace [106]. The efficiency was calculated from Equation 3.1, and was found to be very low, at 56%. A modern industrially fired furnace is usually around 80-90% efficient [73]. Efficiencies of around 50% are more typical for cold-air burners, where there is no combustion pre-heating included [107]. Furnaces are complex, and there are several types with different efficiencies [107]. A simple furnace without internal preheating of combustion air and fuel and optimized heat recovery was simulated. The heat in the SMR is required to be 900 °C, and since not all available heat below this temperature is possible to use in the process, the efficiency is reduced. The low efficiency also affects emissions from the furnace, as these emissions are dependent on the amount of fuel required in the furnace.

Even though a generally low overall capture rate of 60% is the maximum from an SMR plant with amine-based carbon capture, a low efficiency furnace can decrease the overall capture rate further. For the whole process in the base case, the overall CO_2 capture efficiency was found to be 44%, while the CO_2 capture efficiency in the carbon capture plant was 95%. This might have been improved by including CCS after the furnace.

Because of this, emissions are higher than expected. An ideal furnace was not modeled, but a calculation was done to find how much natural gas an ideal furnace would need as fuel. With an ideal furnace, the overall capture rate was increased to 68%.

The complete calculation of the efficiencies can be found in Appendix B.

Carbon Capture Performance

The reboiler duty was examined as a function of the L/G ratio, the results can be found in Figure 4.1. This plot was made by altering the L/G ratio and examining the effect on the reboiler duty, while the capture rate was kept constant.

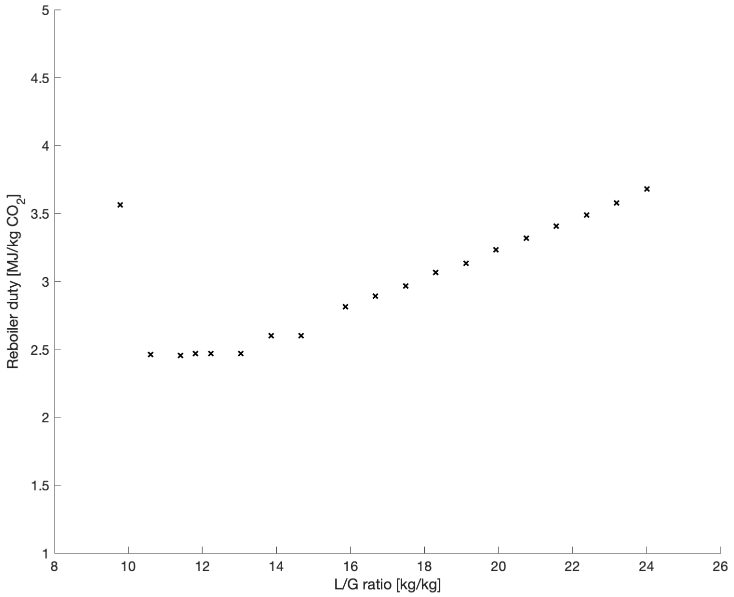

FIGURE 4.1: Reboiler duty as a function of the L/G ratio with a constant capture rate.

The optimum L/G ratio is found at the point where the energy requirement is at its lowest. For L/G ratios lower than this optimum, it can be shown that the reboiler duty is high before it drops rapidly. At the optimum, there is just enough liquid solvent to strip off the CO_2 relatively easily, and there is not a lot of excess solvent that increases the need for heating from the reboiler. Figure 4.1 also shows that the reboiler duty increases with increasing L/G ratio after the optimum since more solvent goes through the system and requires heating in the stripper [108]. The optimal L/G was found to be 12 for this simulation.

A similar trend has been obtained by Giorgetti et al (2017) and Agbonghae et al (2014) [108] [109]. Similar results for the reboiler duty for MDEA/PZ systems can be found from Zhao et al (2017) and Khan et al (2020) [110][111].

The results on specific reboiler duties can be further discussed by examining the rich and lean loading, as shown in Figure 4.2.

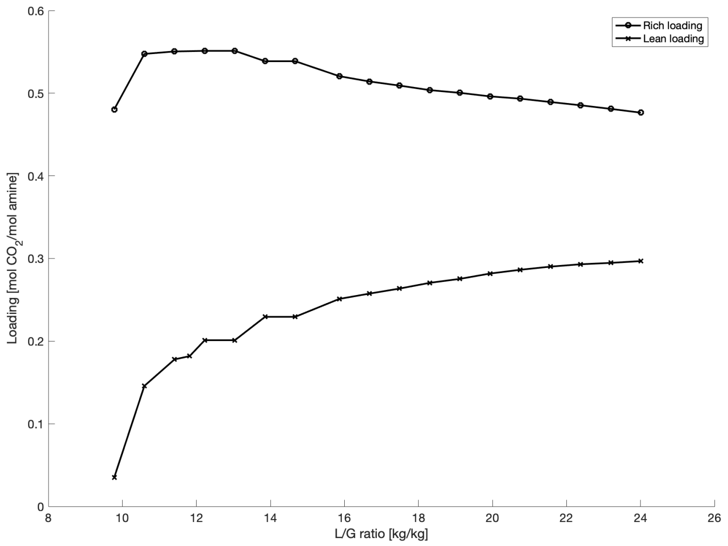

FIGURE 4.2: Rich and lean loading as a function of the L/G ratio with a constant capture rate.

Increasing the L/G ratio means that more solvent enters the system. This decreases the rich loading, because the moles of solvent increases, while the moles of CO_2 remain constant. At the lowest L/G ratios, around 10, the rich loading is relatively low. The temperatures of the rich solvent at the bottom of the absorber and lean solvent in the reboiler as a function of the L/G ratio is shown in Figure 4.3. By examining the temperature in Figure 4.3 the relatively low loading can be explained by the high temperatures for the lowest L/G ratio compared to the temperatures for the rest of the L/G ratios. As can be seen from this figure, the temperature is significantly higher throughout the system for the lowest L/G ratio. This high temperature makes the equilibrium loading, which is the maximum rich loading, unfavorable, resulting in a lower rich loading.

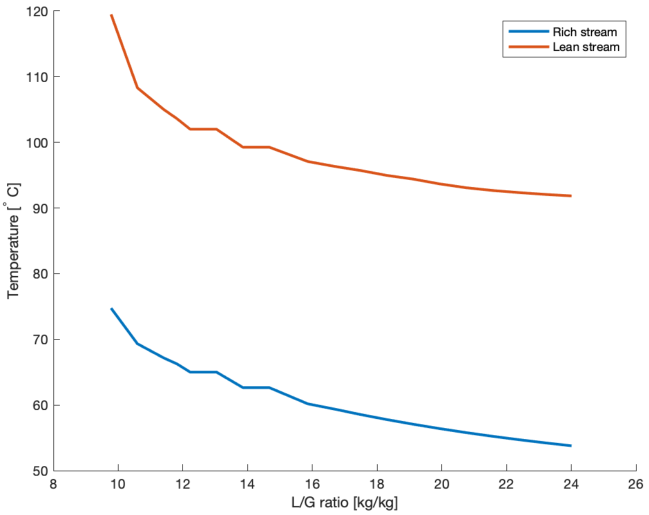

FIGURE 4.3: Temperature in the amine-rich (blue) and amine-lean (red) flows in the system as a function of the L/G ratio.

As shown in Figure 4.2, the lean loading increases with increasing L/G which agrees with work of Agbonghae et al (2014) [109]. For this work, an L/G at around 15 was used as it was close to the optimum while allowing the simulation to converge more easily. This gave a reboiler duty of $7.4 \cdot 10^1$ MW. The reboiler requires heating at around 130 °C. Based on this, it can be seen that the SMR requires almost 3 times as much heat as the reboiler, and at a much higher temperature.

4.1.2 Simulation of Electric SMR

Unlike conventional SMR, there is little research on electric SMR. But since the simulation of electric SMR is very similar to the simulation of conventional SMR, many of the results from the base case simulation are still applicable. Because the furnace and reformer were simulated separately in conventional SMR, a simple adjustment of removing the connection from the furnace to the SMR was performed. Hence, the same amount of feedstock was used to produce the same amount of hydrogen as in the base case. The SMR also requires the same amount of heat of $2.1 \cdot 10^2$ MW at 900 °C, supplied by electricity. The furnace case study carried out to find the amount of fuel necessary and the optimal AF, may be found in Appendix A. From this case study, it was determined to use 2400 kg of natural gas along with the tail gas as fuel, with 16% excess air. This is a reduction of 92%, and as this is only a reduction of natural gas used as fuel, not including feedstock, this is a significant decrease.

As there are no changes to the chemical process in the simulation, all compositions, temperatures, and pressures are the same for the pre-reformer, SMR, shift reactors, carbon capture plant, and the PSA will be unchanged from Table 4.2 for conventional SMR. However, the furnace is different as it does not supply heat to the SMR, hence less fuel and air are required. A complete table of the simulation values for electric SMR can be found in Table A.1 in Appendix A. The overall CO_2 capture in the electric SMR was found to be 78%, assuming that the electricity is supplied from a renewable source. The consequences and emissions based on the source of electricity are further discussed in Section 4.4.

This calculation assumes that the electric power is 100% efficient, as might be the case for the conversion of electrical energy to useful heat [75]. However, the conversion of fuels, such as coal, oil, or gas generators, to electric energy is approximately just 30% efficient [112]. This is important to consider when calculating efficiencies of electric SMR plants in subsequent research.

As the focus of this thesis was to estimate costs and emissions, these calculations were carried out using Python and Matlab due to limitations with the Aspen Hysys software. These results are included in later parts of this chapter.

4.2 Comparison of Conventional and Electric SMR

In the simulation, electric SMR differentiates itself from conventional SMR by the source of heating. There are other differences as well such as start-up time and catalyst optimization, which will be discussed further in Section 4.5.

From the simulations, the greatest difference can be found in the CO_2 capture efficiency, which was vastly improved for electric SMR. Clearly, this stems from greatly reduced furnace emissions for electric SMR. Another point of comparison is the hydrogen plant efficiency, which was found from the following formula,

$$\frac{\text{Energy in product hydrogen}}{\text{Natural gas energy} + \text{electricity}}, \tag{4.1}$$

from National Renewable Energy Laboratory (NREL) where all units are given in kJ/h based on the higher heating value [113]. This formula can be used for this application, although because of the difference in value between electricity and natural gas, one should in general be careful of adding those together uncritically. Replacing electricity with heat seems like an easy swap, but it should be noted that while electricity can always be converted to heat, conversion of heat to electricity is not as efficient. Electricity is considered more valuable than heat.

Although it is possible to include steam export and steam consumption in the plant and the formula, this is not included in this plant. The hydrogen plant efficiency for conventional SMR was found to be 67%, while the efficiency for electric SMR was found to be 80%. As mentioned previously, the inclusion of would increase the efficiency of both plants. Still, the hydrogen plant efficiency is in favor of electric SMR, which is a promising result for this new technology.

Table 4.2: Values from the Aspen Hysys simulation of conventional SMR. The flows are numbered according to Figure 3.1, compositions are given as mole%. A negative sign in front of the energy indicates energy demand, while a positive sign indicates energy produced. The table does not include heat exchangers, pumps or flash drums throughout the simulation (see Appendix A).

	Pre-reformer		**SMR**		**HTSR**		**LTSR**		**Furnace**			
Energy [MW]	0		207		-14		-1.5		213			
S/C ratio	0.3		3.0		-		-		-			
Flow name →	Feed	Natural gas	1	2	3	4	5	6	Tail gas	NG (fuel)	Air	H_2
T [°C]	50	400	400	900	320	320	190	190	25	25	25	25
P [bar]	50	25.25	24.75	24.25	24.00	23.50	23.25	22.75	2.5	1.00	1.00	20.00
M [kg/h]	$4.142\cdot 10^4$	$4.142\cdot 10^4$	$5.517\cdot 10^4$	$1.835\cdot 10^5$	$1.835\cdot 10^5$	$1.835\cdot 10^5$	$1.835\cdot 10^5$	$1.835\cdot 10^5$	$1.130\cdot 10^4$	$3.210\cdot 10^4$	$8.025\cdot 10^5$	$1.546\cdot 10^4$
Composition												
Methane	85.30	85.30	75.38	1.71	1.71	1.71	1.71	1.71	19.83	85.30	0	0
Ethane	7.05	7.05	0.01	0	0	0	0	0	0	7.05	0	0
CO_2	2.21	2.21	5.65	5.53	5.53	14.76	14.76	15.71	8.43	2.21	0	0
Propane	2.73	2.73	0	0	0	0	0	0	0	2.73	0	0
i-Butane	0.55	0.55	0	0	0	0	0	0	0	0.55	0	0
n-Butane	0.94	0.94	0	0	0	0	0	0	0	0.94	0	0
i-Pentane	0.27	0.27	0	0	0	0	0	0	0	0.27	0	0
n-Pentane	0.27	0.27	0	0	0	0	0	0	0	0.27	0	0
n-Hexane	0.18	0.18	0	0	0	0	0	0	0	0.18	0	0
n-Heptane	0.13	0.13	0	0	0	0	0	0	0	0.13	0	0
n-Octane	0.04	0.04	0	0	0	0	0	0	0	0.04	0	0
Nitrogen	0.33	0.33	0.22	0.05	0.05	0.05	0.05	0.05	0.56	0.33	79.00	0
Hydrogen	0	0	2.73	48.72	48.72	57.94	57.94	58.90	68.44	0	0	100.00
H_2O	0	0	15.93	33.68	33.68	24.46	24.46	23.50	1.19	0	0	0
Oxygen	0	0	0	0	0	0	0	0	0	0	21.00	0
CO	0	0	0.08	10.31	10.31	1.09	1.09	0.13	1.55	0	0	0

TABLE 4.3: Results from the absorber and stripper in the Aspen Hysys simulation. Flow names are given in accordance with Figure 3.1. More information on the specifics of the absorber and stripper in the simulation can be found in Appendix A.

	Absorber			
Flow name	16	8	11	10
T[°C]	40	40	40	56
P [bar]	22.25	22.25	20.00	20.00
M [kg/h]	$2.490 \cdot 10^6$	$1.227 \cdot 10^5$	$2.365 \cdot 10^4$	$2.589 \cdot 10^6$
α				0.55
	Stripper			
Flow name	13		CO_2	14
T [°C]	77		25	102
P [bar]	2.00		2.00	2.00
M [kg/h]	$2.585 \cdot 10^6$		$9.598 \cdot 10^4$	$2.489 \cdot 10^6$
α				0.20

4.3 Cost Estimations

This chapter includes a section on CAPEX and OPEX. The cost estimations are preliminary and more research is needed, especially with regards to the CAPEX. For the OPEX estimations, cost developments for the technologies were predicted from 2021 to 2030. A more thorough breakdown of the OPEX predictions for 2030 was also included. The levelized cost of hydrogen was found and compared for both conventional and electric SMR.

4.3.1 CAPEX

The CAPEX was estimated based on the unit operations in the SMR plant. As mentioned in the Methodology, each unit operation was sized separately and cost estimated. The CAPEX is often split into the fixed capital investment and the variable investment cost. In this thesis, the fixed capital investment includes all the unit operations such as vessels and heat exchangers. Meanwhile, the variable CAPEX consists of the chemicals required in the plant as well as the start-up cost (estimated as 10% of fixed capital investment). The main results for the CAPEX for conventional SMR can be found in Table 4.4.

Literature values for the CAPEX of SMR plants vary a great deal and are in the range 15 - 72 USD/MWh [3] [114]. While the CAPEX found for this system was 30 USD/MWh (1.17 USD/kg H_2) based on the production capacity of one year. The total costs vary a great deal depending on the size and capacity of the plant. A

TABLE 4.4: CAPEX for the base case (conventional SMR).

Fixed capital investment	131 MUSD
Total CAPEX	144 MUSD
Total CAPEX	1.17 USD/kg H_2 annually

breakdown based on the unit operations for the CAPEX in the base case can be found in Table 4.5. A complete breakdown of the costs of each unit operation can be found in the tables in Appendix C, where costs and sizing dimensions of each unit operation are included. The primary reformer was by far the main cost, accounting for 68% of the CAPEX. It was also found that the cost of the pre-reformer is rather significant for the total CAPEX. In Table 4.5, separators and vessels include the vessels for all columns, including the flash columns, separators, the stripper and absorber columns, and the shift reactor vessels.

TABLE 4.5: Overview of the CAPEX breakdown.

Units	Cost [MUSD]
Heat exchangers	0.6
Separators/Vessels	3.5
Pre-ref	13.4
SMR	97.8
PSA	15.0
Packing	1.30
Start up and solvents	13.1

Both the absorber and stripper in the carbon capture plant were found to be very large, with a diameter of 3.5 m for both, and volumes of 124 m^3 and 75 m^3 respectively. The SMR was not sized, but is generally a very large piece of equipment in conventional SMR.

Since electric SMR is a novel technology, it is difficult to get a good estimate for the capital cost of the plant. Still, it is possible to provide some insights into some of the most important factors that are likely to influence the CAPEX estimations.

Labor costs are often the most difficult variable in cost estimations, as they are dependent on the skill and competence necessary for the workers as well as the time it takes to complete the project. It is often based on historical plants of the same type, which is why it is challenging to estimate for the electric SMR, as it has not been built before. [115]

Another important point is that conventional SMR uses a nickel catalyst on alumina pellets, while electric SMR uses a nickel catalyst on top of a zirconia washcoat. In a study by Wismann (2019), only a single lab-scale tube was used, and hence the catalyst washcoat was only placed along the walls [16]. For a large SMR, a monolithic structure with the washcoat catalyst might be more reasonable. A monolithic catalyst structure increases the mass transfer effectiveness, which could result reduced operating costs due to its high mechanical strength, minimizing risks of shutdown due to breakage [77].

The additional copper that needs to be placed on each end of the tubes might require some extra labor costs. As mentioned, there are generally over 100 tubes in one reformer. And even though the furnace is not necessary for heating the electric SMR, there is still the need for electric heating. Setup and installation of either an electric production plant, or for export of electricity is a factor of uncertainty this far in the research, and needs to be evaluated in terms of plant location with respect to availability and production. The electricity source also needs to be evaluated in terms of costs and emissions.

The installation costs of the electric reformer are also very uncertain as no research has been conducted on the topic of cost before. More research is therefore necessary to get a better idea of the feasibility of the CAPEX of an electric SMR plant. However, it may be assumed that this will be more expensive, due to the additional required materials such as copper sockets, the new type of catalyst, and the necessary labor costs.

The total CAPEX for conventional SMR was found to be 144 MUSD, where the cost of the primary reformer accounts for 68%. The fact that the most expensive part of the plant is the primary reformer is well-established [116]. The cost estimate for the furnace surrounding the reformer in conventional SMR was found to be 45 MUSD. As the furnace in the electric SMR plant is separated from the primary reformer, the cost was added to the CAPEX for electric SMR. As expected, the cost of the furnace is significantly lower for the electric SMR compared to the conventional SMR, at 10 MUSD.

A simple analysis was performed to examine how the cost of the primary reformer would affect the CAPEX of electric SMR, based on the cost of conventional SMR (equation in Section 3.2.1). Because the cost of the surrounding equipment such as the heat exchangers, shift reactors, capture plant, etc. was assumed to be unchanged, their cost clearly remain unchanged as well. Hence, the only changes in costs were those of the primary reformer and the furnace. The CAPEX estimate examined how expensive the primary reformer in the electric SMR could be, while not exceeding the CAPEX for conventional SMR. An overview of this situation is shown in Table 4.6.

TABLE 4.6: Variation of the F_{SMR} to evaluate the total CAPEX for electric SMR. The CAPEX per kg H_2 is for a years worth of hydrogen production.

F_{SMR}	Total CAPEX	
-	[MUSD]	[USD/kg H_2]
1	109	0.88
1.5	135	1.09
2	161	1.30
3	213	1.72

The values from Table 4.6 show that if the cost of the primary reformer (excluding the furnace) is twice as expensive for the electric SMR compared to the conventional SMR, the total CAPEX would be 12% higher. If the CAPEX of electric SMR is equal to the CAPEX of conventional SMR, the F_{SMR} factor would be 1.67, meaning that the primary reformer could be up to 67% more expensive for electric SMR when excluding the furnace. This is because the furnace is not connected to the reformer and cheaper in electric SMR, the internals in the reformer (tubes, copper sockets, catalyst, etc.) can therefore afford to be more expensive.

However, when the furnace is included in the total cost of the reformer, the results look slightly different. The total cost of the conventional reformer is 97 MUSD, and since the furnace in the electric SMR plant costs 10 MUSD, the cost of the electric reformer would have to be less than 87 MUSD.

4.3.2 OPEX

As mentioned previously, the OPEX estimations for both the conventional and electric SMR were based on costs from literature and taxes from governmental web pages. Table 3.6 in Chapter 3 shows an overview of the expenses accounted for in the OPEX calculations. The same variables were accounted for in both the conventional and electric case in order to provide a good basis for comparison.

In the following section, all small costs such as the cooling water, and its treatment chemicals, as well as the O&M costs and boiler feedwater, were included as one cost, referred to as "Other O&M costs". The carbon tax and electrical power tax are both given as the official Norwegian rates as of 2021. It should be possible to apply for a reduction of the electrical power tax based on the fact that this electricity is used for production of an energy product. This gives an electrical power tax of 0.00546 kr/kWh [72], reduced from the 0.1669 kr/kWh used in this thesis.

The breakdown of the costs for both conventional and electric SMR can be found in Figure 4.4. The complete total breakdown of absolute costs of the OPEX of conventional and electric SMR can be found in Table C.1 in Appendix C.

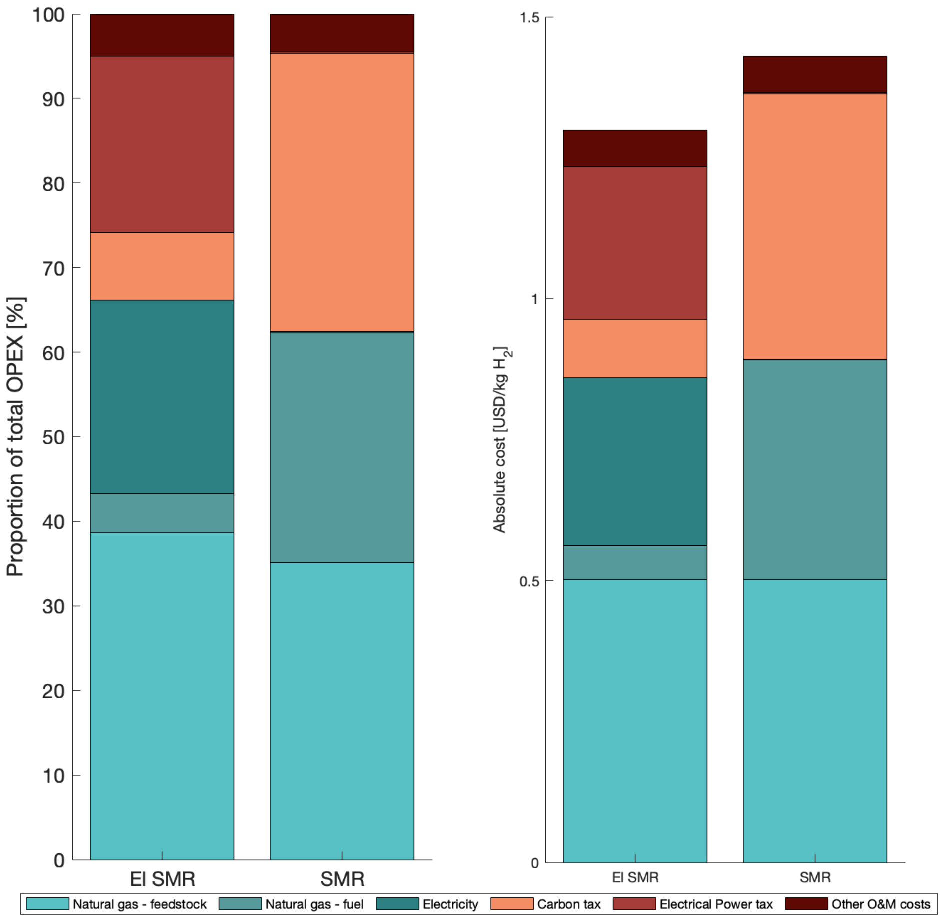

FIGURE 4.4: Breakdown of OPEX for both conventional and electric SMR, in terms of the proportional costs and absolute costs.

The most notable result is that the OPEX for conventional and electric SMR are similar to one another even though electric SMR is cheaper. The OPEX for conventional SMR was found to be 1.43 USD/kg H_2, compared to 1.30 USD/kg H_2 for electric SMR. The greatest proportional cost for both technologies is natural gas, accounting for 62% for conventional SMR and 42% for electric SMR. However, the total cost of feedstock and heat supply, either as fuel in the furnace or as electricity is very similar for both reformers. As the electricity to heat conversion was assumed to be 100% efficient while the furnace was calculated to be 54% efficient, including a more efficient furnace may shift the cost difference in favor of the conventional SMR. This will be discussed further in a later section.

Most studies on the possibilities of electrification claim that the cost of electricity is the main issue [86][4]. However, this simulation and study show that this would not be the main drawback for electric SMR in Norway as of 2021. Even though this was an unexpected result, Wismann (2019) suggested that this would be the case for Nordic countries based on the cost of natural gas and electricity [16].

Another interesting result is that from the left-hand of the plot in Figure 4.4 one can see that the percentage of taxes and raw feed materials are approximately the same for both plants. Although taxes are fairly similar for conventional and electric SMR, it is important to note that conventional SMR is more affected by the carbon tax. This is of course due to the reduced emissions during operation of electric SMR.

For electric SMR, the electrical power tax constitutes a greater proportion of costs than does the carbon tax. The electrical power tax is a larger proportion of the electric SMR than the carbon tax. This implies that taxation is an effective policy for political leaders to sway the relative feasibility of these two technologies. Reducing the general electrical power tax or granting the tax deduction would mean a great deal for the electric SMR. Even though subsequent studies will most likely show that there are changes and differences in the absolute costs, this thesis shows that electric SMR is a competitive technology that could very well replace conventional SMR with respect to operational expenditures. This is a highly positive result for a new technology this early on.

Several different scenarios for the OPEX were investigated, prompted by the uncertainties with the furnace and the possible electrical power tax deduction. The base costs (as in Figure 4.4) were included as a reference for both conventional and electric SMR. The other cases include "Ideal SMR", "El SMR reduced tax" and "Ideal el. SMR". The "Ideal SMR" case presents conventional SMR with an ideal furnace. This scenario presents a theoretical optimal SMR, minimizing costs by reducing both CO_2 emissions and fuel requirements.

As mentioned previously, it should be possible in Norway to receive a tax deduction on the electrical power tax because the plant is used to produce energy products. This was applied in the case of "El SMR reduced tax". An extension of this case was the scenario of an ideal electric SMR ("Ideal el. SMR"). This scenario includes the reduced electrical power tax as well as an ideal furnace, based on the same premises as the ideal SMR.

OPEX for the different scenarios can be seen in Figure 4.5. The case studies and calculations for the different scenarios can be found in Appendix B.

The different scenarios in Figure 4.5 show that the OPEX for conventional SMR is reduced from 1.43 USD/kg H_2 to 1.23 USD/kg H_2 from the base case to the ideal case. For electric SMR, the potential to reduce costs appears to be even greater. Reducing the electrical power tax alone leads to a decrease in the OPEX from 1.30 USD/kg H_2 to 1.04 USD/kg H_2. Because the furnace costs of electric SMR are significantly smaller than those of conventional SMR, going from a non-ideal furnace to an ideal furnace in electric SMR is less impactful. The cost for this ideal electric SMR with reduced power tax is 0.99 USD/kg H_2.

Finally Figure 4.5 shows that by comparing electrical and conventional SMR it can be seen that the latter has a generally higher OPEX for both the non-ideal cases and ideal cases. For the development of SMR technologies, this shows that electric SMR is the best prospective option as of now.

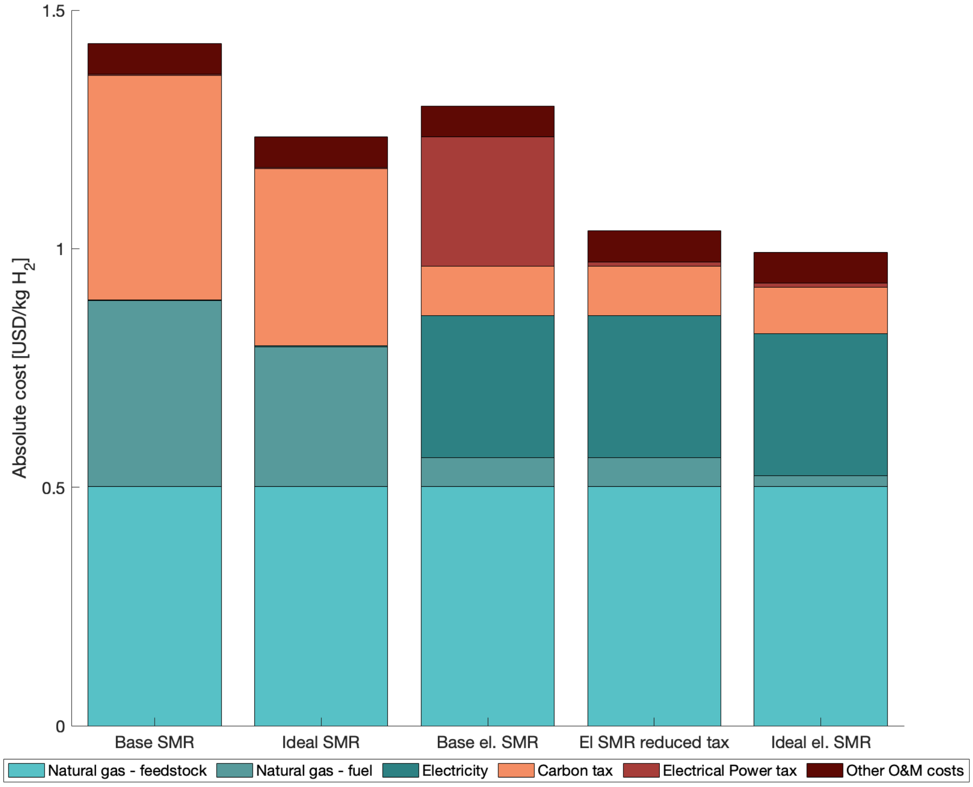

FIGURE 4.5: OPEX estimates for the different scenarios including the base cases for both conventional SMR and electric SMR as well as an "Ideal SMR" based on an ideal furnace, the "El SMR reduced tax" which uses a lower electrical power tax and the "Ideal el. SMR" which uses both the reduced tax as well as an ideal furnace.

4.3.3 OPEX Prediction 2021-2030

Due to the ongoing energy transition, it is difficult to predict how the terrain of energy demand, consumption, and costs will evolve. However, companies are always trying to predict the future to make the most economically viable choices and maximize profit. Therefore, discussing the current operating costs of a plant that is not readily available is of limited usefulness. As the technologies discussed in this thesis have estimated lifetimes of 20 years and will most likely be functional beyond that, they should be both economically and environmentally sustainable over a long time frame. The operating costs were predicted based on the changing costs of natural gas, electricity, and carbon tax. Some of these predictions are easier than others, like the carbon tax. The Norwegian government's annual climate report clearly states their plan to increase carbon tax to 2000 kr/ton CO_2 by 2030. Other costs, especially those affected by supply and demand are harder to predict. Both electricity and natural gas fall under this category.

The cost of natural gas is affected by the production volume, economic growth, and availability (and hence cost) of other fuels [117]. The cost of natural gas has decreased in recent years, and this is due to a combination of factors. Natural gas is increasingly a global market resource, with new international participants such as the US now producing more liquefied natural gas (LNG) than before. This has lead to a reduction in the cost of European gas production. However, despite the recent increase in production, it is expected that the overall gas production will decrease in the long term [104] [118]. When gas production decreases, the cost is expected to increase [104]. The prediction for the natural gas price was found from Equinor's Quarterly Report [104]. Because the predictions were only for the natural gas price from Equinor for the years 2025 and 2030, the prices were interpolated through 2021 to 2025 and from 2025 to 2030. The natural gas prices will of course deviate from this, but these predictions were deemed sufficient to examine the trends in the price of natural gas.

As for the price of electricity, the cost is of course dependent on the production method, as shown in Figure 2.7 in the Background chapter. This is one of the key factors affecting the electricity price, along with the power plant costs, the transmission and distribution system, weather conditions, as well as governmental regulations [119]. The electricity price predictions for 2022-2030 were based on a study by Statistics Norway. The study estimated an increase in the electricity price due to new electricity interconnector cables between Norway, the UK, and Germany, which are estimated to be operational by 2022 in addition to an increase in the prices of CO_2-quotas [87].

The carbon tax was assumed to increase linearly to the 2030 value of 2000 kr/ton CO_2 based on a statement from the annual climate report that it would increase gradually [103].

The development of operating costs from 2021 to 2030 for each scenario described previously, was plotted to get an idea of the increase for each case. The plot is shown in Figure 4.6.

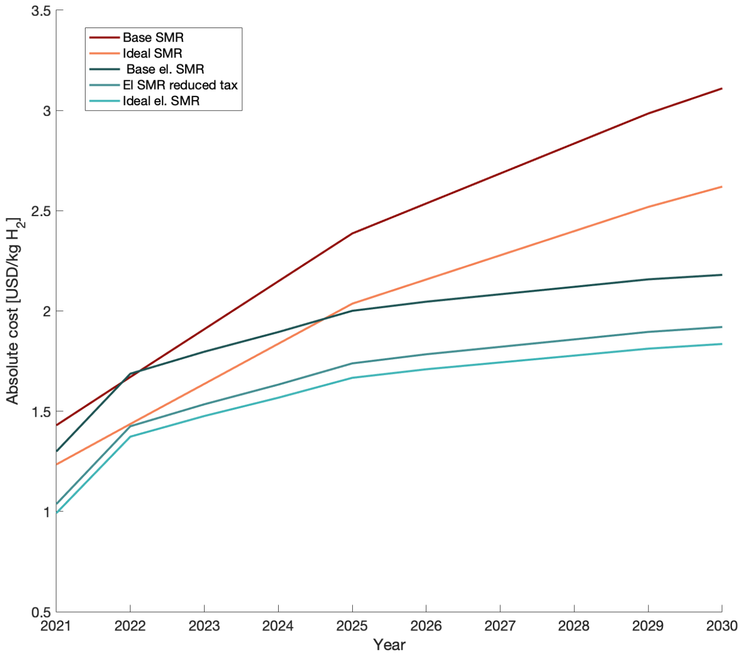

FIGURE 4.6: Change in the predicted OPEX for different scenarios of conventional and electric SMR for the years of 2021 - 2030 based on changes in cost of natural gas, electricity and an increased carbon tax.

As both the cost of natural gas and electricity are predicted to rise from 2021 to 2030 and coupled with an increase in the carbon tax, it is natural that the costs of all scenarios will increase. However, the relative rates of their increase is interesting. As Figure 4.6 shows, conventional SMR has an almost linear increase in costs leading up to 2030. This increase is very steep, indicating that the costs will increase significantly in the next few years. This is of course due to the linear increase in carbon tax, and a steady increase in the price of natural gas.

For electric SMR (all three scenarios) the trend is a bit different. The jump in the OPEX in 2022 is due to an increased electricity cost caused by the new interconnector cables as described. After this escalation, the electricity price is predicted to stabilize and only slightly increase towards 2030 [87]. Because of this stable electricity price, the costs of the three scenarios of electric SMR are relatively flat throughout the rest of the time frame. Compared to conventional SMR, the electric SMR is not as affected by the price of natural gas nor the carbon tax. Assuming that these predictions of natural gas and electricity prices are correct, the OPEX of electric SMR will increase significantly less than that of conventional SMR. It also indicates that the cost difference between the conventional and electric SMR will increase as time goes on.

4.3.4 OPEX Prediction for 2030

Based on the changes in the cost of natural gas, electricity, and the carbon tax, it is interesting to investigate the breakdown of the OPEX prediction for 2030 for both base cases. This provides an opportunity to look at what creates the biggest difference between the costs. Based on cost predictions for natural gas, electricity, and an increased carbon tax, the proportional and absolute costs for conventional and electric SMR were investigated. The results can be seen in Figure 4.7. The natural gas price uses the European estimate for 2030 according to Equinor's Quarterly Report [104], with similar estimations also found in other sources [120]. The electricity price was predicted by Statistics Norway [87], while the carbon tax was given by the annual climate report from the Norwegian government [103].

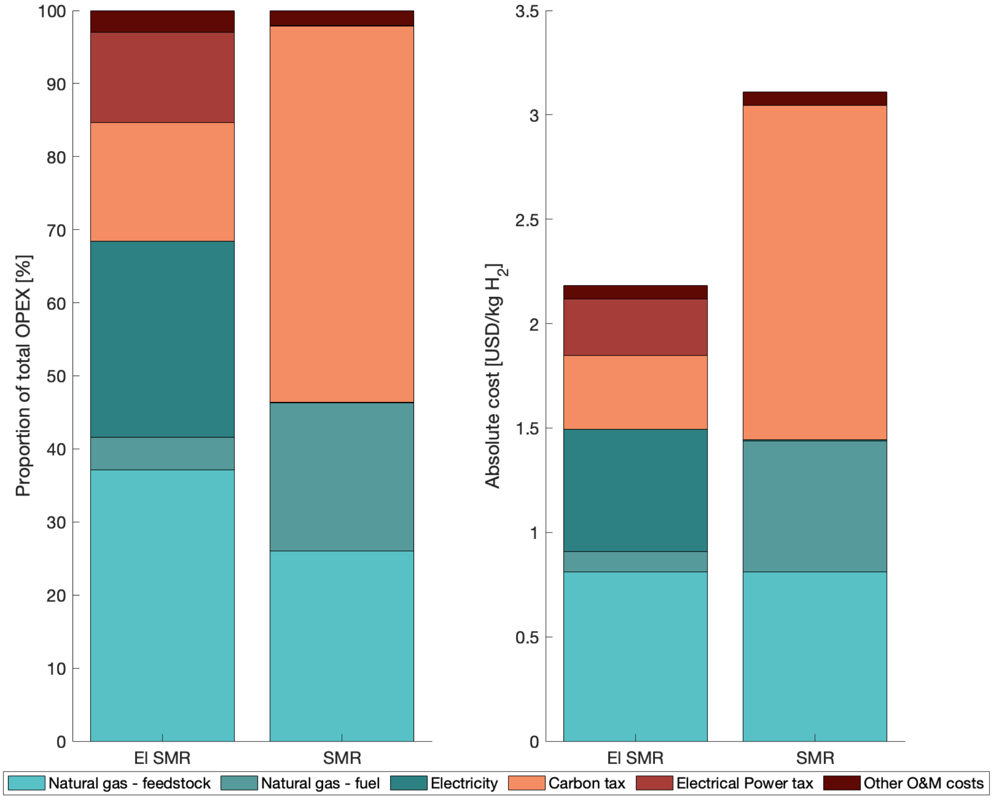

FIGURE 4.7: Breakdown of estimated OPEX for both conventional and electric SMR, in terms of the proportional costs and absolute costs in 2030.

An obvious result is the increased cost difference between the two technologies. From the absolute costs in Figure 4.7, there is a strong argument that the electric SMR will be the more economically feasible technology in the long run. Looking at the conventional SMR, the carbon tax accounts for almost half of the operating costs. It seems that the increase in carbon tax will make the biggest impact on the difference between conventional and electric SMR. No change was included in the electrical power tax, due to a lack of information. However, even though there might be a change in the electrical power tax, it is not expected to be as great as the leap in carbon tax. This indicates that the electric SMR is a much more future-proof technology.

Figure 4.8 shows the same scenarios as in the original OPEX calculations recreated for the 2030 price estimates.

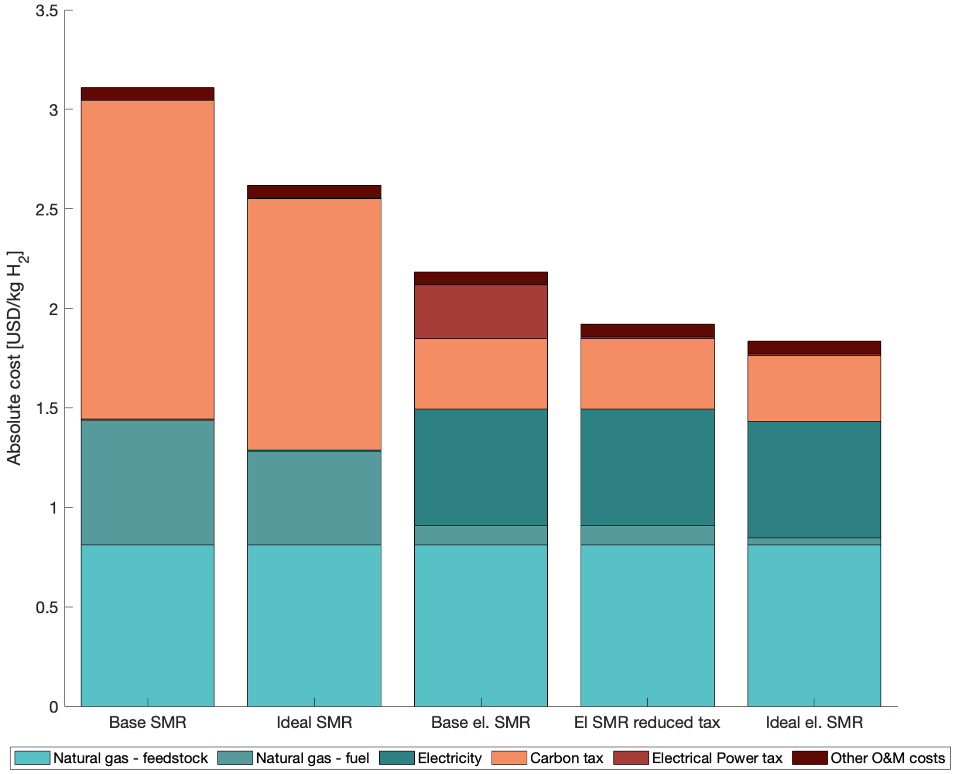

FIGURE 4.8: OPEX estimates for the different scenarios predicted for 2030 including the base cases for both conventional SMR and electric SMR as well as an "Ideal SMR" based on an ideal furnace, the "El SMR reduced tax" which uses a lower electrical power tax and the "Ideal el. SMR" which uses both the reduced tax as well as an ideal furnace.

As it can be seen in Figure 4.6 as well as Figure 4.8, the costs for each scenario increases from the 2021 estimate. The conventional SMR cases more than double in costs, while the base case of electric SMR, the electric SMR with reduced electrical tax and the ideal SMR has increase 68%, 86%, and 85% respectively.

The 2030 OPEX predictions also show that the cost of the ideal conventional SMR case is higher than for the base electric SMR case, with a difference of 0.5 USD/kg H_2. From the ideal scenario for conventional SMR, it can be seen that the carbon tax is still a very large portion of the OPEX despite the fact that this ideal furnace utilizes the least amount of natural gas possible. The carbon tax affects the electric SMR as well, although less than it does conventional SMR. Naturally, the carbon tax is a relatively high cost for both technologies when it is 2000 kr/ton CO_2. This prompts the question on whether the furnace in electric SMR can be removed entirely, thus decreasing emissions even further. Using renewable electricity-to-heat up the reboiler may remove most of the direct emissions from the plant, and hence get an even lower operating cost for the electric SMR. This might also be possible to retrofit, when suitable, so that the plant is optimized in terms of costs throughout its lifetime.

Further examining the electric SMR scenarios it can be seen that both the 2030 prediction and the 2021 estimate benefit significantly from a reduced electrical power tax. The OPEX for an electric SMR with reduced power tax is 12% lower than for the base case of electric SMR.

Comparing the 2030 cost prediction for the ideal cases of conventional and electric SMR shows that the lowest possible cost for conventional SMR is 2.62 USD/kg H_2 compared to 1.84 USD/kg H_2 for the electric SMR. This is significantly lower, and a promising result for electrical SMR.

4.3.5 Sensitivity Analyses

Sensitivity analyses were conducted for both the conventional and the electric SMR based on the OPEX estimates for 2021 and 2030. This was done to get an idea of the factors that most affect the cost of the plants, given changes in the cost of natural gas, electricity, and the carbon tax, all of which are very likely. Each factor was increased and decreased by 20% at a time while keeping other factors constant, although it is possible that all of them will vary by the time electric SMR is a ready-to-use industrial technology.

SMR

The sensitivity analysis for conventional SMR using the 2021 estimate can be seen in Figure 4.9(A), while the sensitivity analysis for the 2030 prediction is in Figure 4.9(B). As can be seen from this plot, the OPEX of the conventional SMR is most affected by the cost of natural gas. This makes sense considering how large of a proportion this was of the total OPEX (Figure 4.4).

Neither the cost of electricity, nor the electrical power tax affects the OPEX at all because the only electricity requirements come from two small pumps in the simulation. A change in the carbon tax is more significant, though it is worth noting that the carbon tax is highly dependent on the country and current government, as it was mentioned in Chapter 2.

If the cost of natural gas were to decrease by 20% the OPEX for conventional SMR would drop to 1.25 USD/kg H_2, which is rather significant. However, that also implies that the cost of the conventional SMR would increase significantly to 1.61 USD/kg H_2 if the cost of natural gas were to increase as predicted previously. By 2030 it can be seen that the factor that affects the cost of conventional SMR most is the carbon tax, surpassing the effect of natural gas.

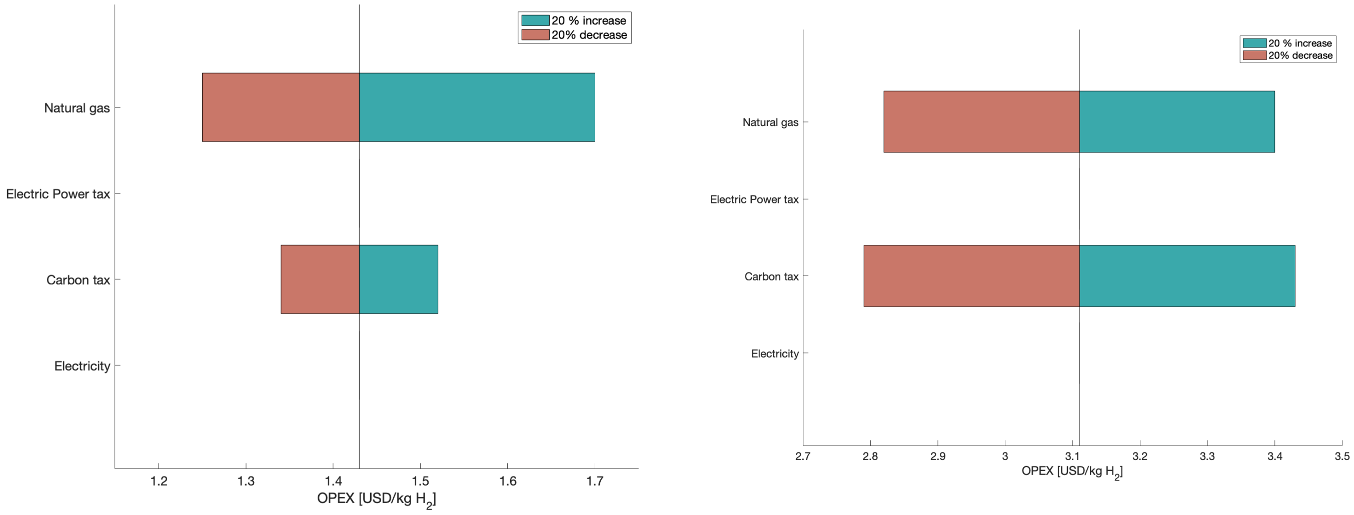

(A)

(B)

FIGURE 4.9: Sensitivity analyses for the OPEX estimates for conventional SMR for 2021 (A) and 2030 (B).

Electric SMR

The sensitivity analyses for electric SMR using the 2021 estimate and 2030 prediction can be seen in Figure 4.10(A) and 4.10(B) respectively. Starting with the 2021 case, the operating cost of electric SMR is highly dependent on the cost of natural gas because of the amount used for feedstock. The operating cost of electric SMR is of course also dependent on the cost of electricity and the electrical power tax. This was based on the full electrical power tax, not the reduced tax for which electric SMR would be a likely candidate. Based on the full electric power tax, it seems that an increase in the tax would almost impact the cost as much as the electricity price would. The carbon tax affects cost the least, since electric SMR does not emit much CO_2, when using renewable electricity. The importance of the electricity production source is discussed a bit later in this chapter.

As can be seen from the sensitivity analysis for the 2030 prediction, the cost of natural gas still influences the OPEX the most. However, because of the drastic increase in the carbon tax, it can now be seen that changes within the carbon tax would change the OPEX more than changes in the electrical power tax. The cost of electricity is also significant, although not as significant as the cost of natural gas.

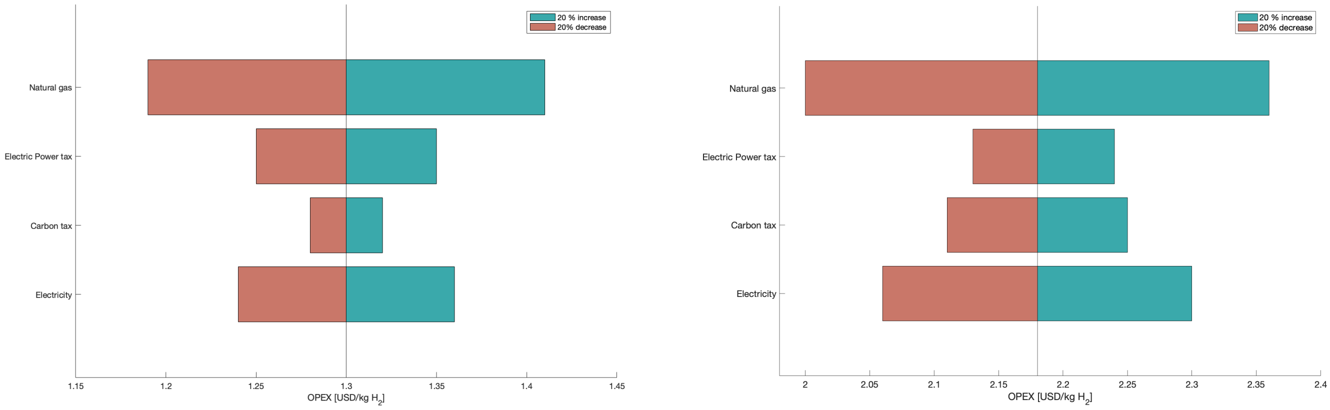

(A) (B)

FIGURE 4.10: Sensitivity analyses for the OPEX estimates for electric SMR for 2021 (A) and 2030 (B).

Comparing Sensitivity Analyses

Better visualization for comparison of the sensitivity analyses are shown in Figure 4.11 and Figure 4.12 for the two sensitivity analyses for conventional and electric SMR. The graphs show how a 20% increase in costs would increase the OPEX percentage-wise. Because the sensitivity analysis plots (Figure 4.9 and Figure 4.10) have a different baseline, it was determined that the best way to compare the analysis would be by their percentage effect.

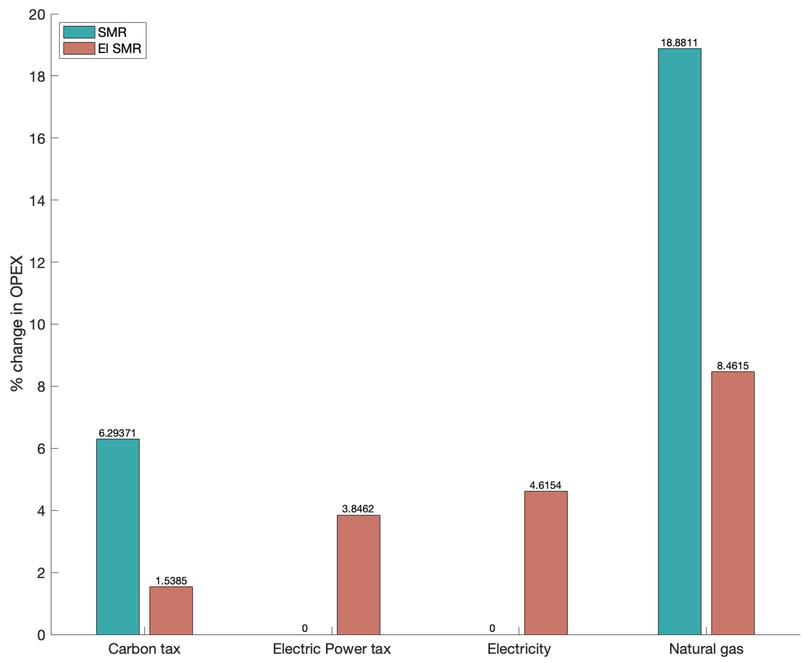

FIGURE 4.11: A comparison of how a 20% increase in the cost of carbon tax, electric power tax, electricity and natural gas would affect the cost of each technology, given as a percentage of the total OPEX for the 2021 estimate.

The price of natural gas has the largest effect on both technologies, as expected from the sensitivity analyses. It affects the conventional SMR more than the electric SMR because the conventional technology needs more natural gas since it is also used as fuel. Another important finding is that electric SMR, which emits less CO_2 than conventional SMR is less impacted by a change in the carbon tax. This is the most certain change that will occur, and should be taken into consideration when deciding between the two technologies.

It may also be of interest that the cost of electric SMR is dependent on more factors than the conventional SMR, which could be both positive and negative depending on the cost development. A positive outcome would be if the costs even each other out. For example, if the electricity price were to increase due to higher demand because of the energy transition, while the electrical power tax were to decrease as a result of policy shifts, this could ensure that the cost of electric SMR could stay relatively constant. The worst-case scenario would of course be that all costs increase.

For the 2030 prediction, the effect of an increased carbon tax has increased greatly because it now accounts for such a large part of the OPEX for conventional SMR. As before, only the electric SMR is affected by changes within the electricity price and electrical power tax. As was seen from the sensitivity analyses, carbon tax has a large effect on the OPEX for conventional SMR. A 20% increase in the price of natural gas would still increase the OPEX by about 8% for the electric SMR, but, the percentage effect is reduced from 18% to 9% for conventional SMR. This is because the carbon tax has become such a large expenditure for the plant. It should be remembered that the overall costs have increased for both technologies.

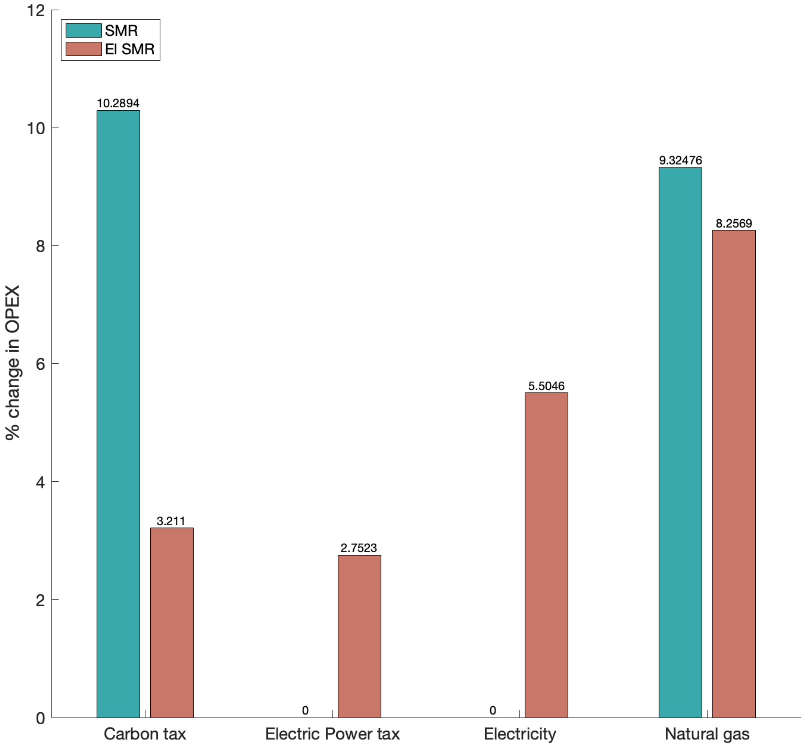

FIGURE 4.12: A comparison of how a 20% increase in the cost of carbon tax, electric power tax, electricity and natural gas would affect the cost of each technology, given as a percentage of the total OPEX for the 2030 prediction.

4.3.6 Comparison of the LCOH

For the conventional SMR, the levelized cost of hydrogen (LCOH) was found to be 1.53 USD/year. As the LCOH depends on the capital investment of the plant it is not possible to determine an absolute LCOH for the electric SMR. However, it is possible to conduct a simple analysis of how CAPEX affects the LCOH. The same factor, F_{SMR} as used previously to calculate the CAPEX for electric SMR was used, with results shown in Table 4.7.

TABLE 4.7: The levelized cost of hydrogen (LCOH) for conventional and electric SMR. The F_{SMR} denotes the factor the CAPEX for conventional SMR was multiplied with to get a CAPEX for electric SMR.

Technology	Factor	LCOH [USD/yr]
SMR	-	1.53
El SMR	1	1.38
	3	1.45
	5	1.53
	10	1.71

This calculation of LCOH assumes that the OPEX is correct and constant throughout the lifetime of the plant. This estimates the approximate lifetime investments of the technologies. The factor F_{SMR} indicates how expensive the primary reformer in an electric SMR plant can be compared to the cost of the primary reformer excluding the furnace of a conventional plant. If F_{SMR} is equal to 1, meaning that the cost of the internals of the primary reformer of a conventional and electric SMR are equal, the LCOH would be cheaper for an electric SMR plant. It was found that the F_{SMR} could maximally be 5.23 before the LCOH for electric SMR reaches the LCOH for conventional SMR without the furnace. When including the furnace, this value is reduced. Comparing the total costs of the reformers still indicate that the cost of the electrical reformer can be significantly higher than the conventional reformer while still providing an equal LCOH. With a F_{SMR} at 5.23, the total cost of the electrical reformer is 273 MUSD, compared to the total for conventional SMR at 97 MUSD.

This indicates that there is some leeway for the cost of the electrical reformer. However, this assumes that the operational costs stay constant although it is known that for example, the carbon tax will increase. As previously seen, increasing the carbon tax will affect the conventional SMR more than the electric SMR, indicating that this factor might be somewhat higher.

Neither storage nor transport of the hydrogen is included in this calculation, which might have increased the factor even further. The fact that this factor is significantly higher for the LCOH than for the CAPEX estimations in section 4.3.1 is due to the inclusion of OPEX, which is higher for the conventional SMR. This also divides the CAPEX into annual costs, making it a smaller cost altogether.

4.4 CO_2 Emissions

As the motivation for the thesis was to explore the challenges and opportunities for the electric SMR to replace a conventional SMR, an analysis of CO_2 emissions was deemed of high importance. Even though the hydrogen produced from both technologies is categorized as blue hydrogen, there are some differences in the CO_2 emissions. This is where the hydrogen cleanness index (HCI) comes in handy, allowing quantification of how much cleaner the electric SMR is or can be compared to conventional SMR. Additionally, this could be used to better differentiate between electric SMR using different sources of electricity.

Currently, one of the limitations of steam methane reforming is CO_2 emissions. The most common method of reducing CO_2 emissions from the plant is carbon capture, which was included in the simulation made in Aspen Hysys. However, it would not be feasible to connect the flue gas to the existing absorber as the concentrations of CO_2 in the gas are relatively low. This results in a lower overall capture rate for the plant than what it was set to be in the carbon capture part. This was also discussed in the evaluation of the simulation in Section 4.1.1.

CO_2 emissions may either be categorized as direct emissions or life cycle emissions. Direct emissions are the emissions from the use of fuel, while the life-cycle emissions are the emissions from the entire process, including feedstock production and transportation, fuel production and distribution, and the final usage of the fuel [121]. Direct emissions were considered, when comparing the two technologies.

4.4.1 Direct Emissions

For the conventional SMR, the main direct emissions are from the furnace, which is well-documented in the literature [122][123]. The direct emissions for the conventional SMR were found to be 6.67 kg CO_2/kg H_2. For the electric SMR, the furnace used to cover the heat requirement for the reboiler also accounts for the main direct emissions. However, the source of electricity also affects the emissions, and the following sections highlight some results concerning this. There are several studies on the emissions of different sources of electricity, and with some variations found between the studies. A comprehensive study based on international values and findings completed as a contribution to the Intergovernmental Panel on Climate Change (IPCC) from 2014 was used in all calculations to ensure that the comparative basis would be as correct as possible [82]. Information from the U.S. Energy Information Administration (EIA) was also used [80].

The comparison of conventional SMR and electric SMR with different production sources of electricity can be found in Figure 4.13. All emissions are direct emissions. For the electric SMR, emissions were found based on emissions from the simulation in addition to emissions from the electricity required for the reformer. A renewable option was added for the electricity as well, which only includes the direct emissions from the furnace in the simulation. As the electricity production in Norway is around 99% renewable, this is more relevant for other countries where this is not the case. One such country is the U.S., where emissions from electricity production are a lot higher than in Norway.

As seen from Figure 4.13, the direct emissions from electric SMR vary greatly depending on the source of electricity. Highest emissions are achieved by electric SMR where the electricity is produced from coal, right above electricity produced by petroleum in the United States. The international average emissions from electricity produced by coal are slightly lower although still significantly higher than the base case of conventional SMR. The electricity produced from coal does not include carbon capture, which could reduce emissions significantly. For the cases of electricity produced from gas, both the international average and US production result in emissions fairly similar to those of the base case. These findings are highly relevant

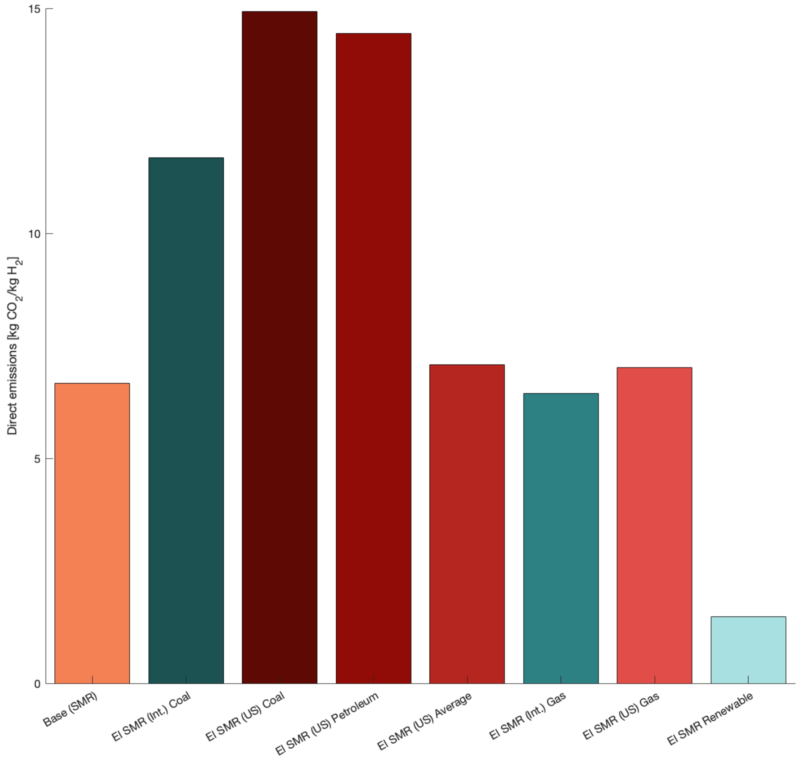

FIGURE 4.13: Comparison of the direct emissions from electric SMR (El SMR) with different production methods of electricity, both renewable and non-renewable, and compared to the base case of conventional SMR. Values for international (Int.) emissions are from [82]. Values for the U.S emissions are from [80]. These have been added together with emissions found from the simulation.

because it illustrates the importance of electricity source when considering the sustainability of the plants. Looking at the grid and possibilities to produce renewable electricity either now or in the future is crucial for electric SMR to be a sustainable option to conventional SMR.

From the Global Energy Review by the IEA, it has been assessed that in 2021, renewables might provide half of the increase in electricity supply [2]. Slowly switching over to more renewable sources may be a realistic possibility. By doing so, there is no need to wait for a completely renewable electricity source before building an electric SMR plant. Another possibility is fuel switching for electricity production, but this will not be discussed any further in this thesis.

4.4.2 Life Cycle Emissions

This thesis has shown that electric SMR should use renewably produced electricity to be more environmentally friendly than the conventional SMR. However, even though renewable electricity production does not have any direct emissions their environmental impact can be measured through life cycle emissions. The life cycle

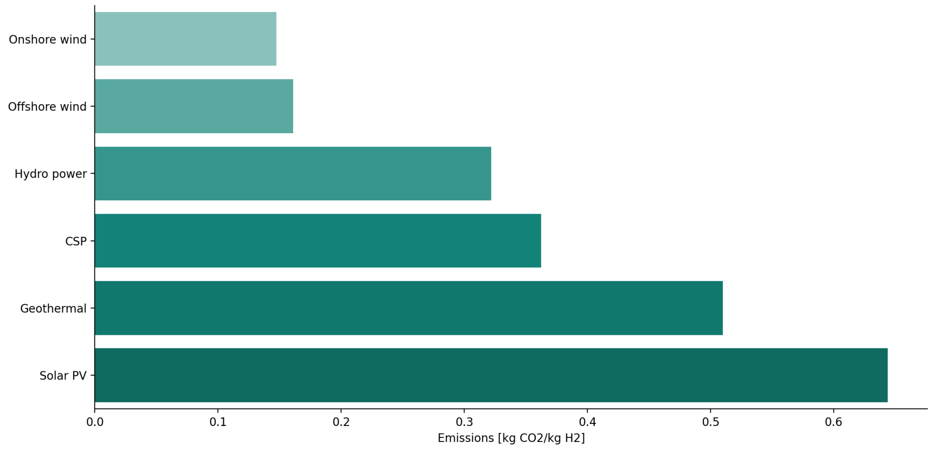

FIGURE 4.14: Lifecycle emissions (including the albedo effect) for the case of electric SMR based on the source of electricity.

emissions were found from the same source as the direct emissions [82]. The life cycle emissions were added to the emissions previously estimated for the entire electric SMR plant. There is of course a range of maximum and minimum emissions, and for this study, the international median was used (as shown in Figure 2.7).

Based on Figure 4.14, the life cycle emissions range from 0.15 kg CO_2/kg H_2 to 0.64 kg CO_2/kg H_2, where onshore wind seems to be the most environmentally friendly option based on the international median emissions. This shows that no matter which renewable option is chosen, the electric SMR would still be highly sustainable. The emissions should also be further investigated with regards to plant location, as the international median is not a representative value for all countries. For example, in Norway, the hydro power used to generate electricity has life cycle emissions of about 3.3 g CO_2/kWh as opposed to the international median of 24 g CO_2/kWh (as shown in Figure 2.7). This would mean that the life cycle emissions for an electric SMR using hydro power to generate electricity would emit 0.04 kg CO_2/kg H_2 from the electricity generation in Norway. The total emissions for the electric SMR was found to be 1.48 kg CO_2/kg H_2, and hence 0.04 CO_2/kg H_2 would be a small addition to that.

4.5 Benefits and Challenges with Electric SMR

Switching from fossil fuels to renewable sources to cover energy supply is the basis of the energy transition. Transitioning from the combustion of natural gas for heating to electricity is part of this energy transition. It has been shown that transitioning to a new technology that provides increased efficiency is the main source of economic growth [124]. There have been past energy transitions; large ones, such as the Industrial Revolution, but also small energy transitions that consistently improve technologies in energy production to the benefit of profit, the environment, and status. These past energy transitions can teach us about the current one. Successful transitions between energy sources and technologies have often been recognized by either (i) that new technology was cheaper than the incumbent or (ii) that this new technology might be more expensive but in turn provided some enhanced characteristic such as increased flexibility, exclusivity, etc. that made it worth the extra cost to a consumer. [125]. However, in absence of public policies, the markets are unlikely to provide a proper incentive for such development [126].

Although electricity is generally more expensive than natural gas, the increased flexibility of the start-up time, in addition to the improved catalyst utilization that electric SMR provides, is appealing. Even for countries where electricity taxes are higher and the cost of natural gas is lower than in Norway, this enhanced characteristic, coupled with the environmental aspect of this technology may be sufficient to tip the scales in favor of electric SMR.

There are several other benefits mentioned by Wismann that were not simulated in this thesis, including start-up time, catalyst utilization, and reactor size [16]. Wismann's preliminary experiments and simulations indicate that the start-up time for an industrial reformer could be 3 minutes [16], as opposed to up to a week, which is a great improvement. This could also decrease the start-up cost which consisted of 10% of the total CAPEX found. This 10% includes loss of income while the plant is shut down or operating at partial capacity [94]. Failures with the reformer tubes accounts for consequential downtime [77]. Because Wismann's claim was based on preliminary studies, the start-up time might not be this low immediately, but, going from a week in start-up time to minutes, or even hours, will be a remarkable improvement. It might also be possible that the start-up time will be reduced as time goes on as more knowledge is acquired on plant maintenance, and the possibility of partial shutdowns.

As mentioned previously regarding catalyst utilization for conventional and electric SMR, better catalyst utilization might be experienced when switching to a washcoat catalyst. The characteristic timescale for internal diffusion has been shown to be a limiting factor for optimal catalyst utilization in conventional SMR which is why the washcoat catalyst has been investigated. Studies conducted by Wismann (2019) on the catalyst thickness concluded that there is an optimal catalyst thickness based on the methane conversion and activity loss. A catalyst layer thicker than optimal might cause sintering or poisoning of the catalyst [16]. Sintering is defined as a thermal process that causes powders to lump together in a solid mass with high temperatures or pressures [127]. The choice of using a wall-coated catalyst instead of catalyst pellets is based on the temperature gradient [16]. The heat transfer from the heating medium to reaction system is the most critical step in the steam methane reforming process, and a packed bed often suffers from limited heat transfer because of suboptimal utilization of the catalyst [77]. It has been proved that optimization of the process would be dependent on the catalyst structure, and catalyst pellets lead to increased heat resistance due to poor utilization of the catalyst volume [128]. A reason for this poor utilization is because the catalyst pellets located near the walls receive heat significantly more efficiently than the pellets towards the middle of the tube, due to conduction difficulties through the tube [77].

By changing the catalyst structure to a monolithic structure, it seems as though the tubes themselves could be thinner because the catalyst will take up less space in the reformer [16][77]. When the catalyst tubes are thinner, the thermal difference is further decreased through the tubes [16]. Smaller tubes might make the reformer smaller, but it will most likely not make as big an impact as removing the furnace. In the literature, it has been estimated that an electric SMR plant with a capacity of 100,000 Nm^3/h H_2 could be 99.89% smaller than a conventional SMR plant of the same capacity. This was assumed without inclusion of wiring, power supply, etc. [16]. Including wiring and a power supply would increase total volume. As there are no opposing views or other literature on the subject, it is difficult to provide a better estimate, and further research is definitely needed.

Chapter 5

Conclusions and Future Work

With concerns growing regarding the effects of climate change, more papers on renewable energy sources are published than ever before. This research has lead to significant improvements in capacity and a reduction in costs for energy production methods. In this thesis, an improvement of steam methane reforming was assessed. By substituting combustion of natural gas as heating for the primary reformer with resistance based electric heating, the CO_2 emissions can be decreased by 77 %. This was shown through simulations in Aspen Hysys as well as calculations based on existing research.

CAPEX and OPEX were estimated for both conventional and electric SMR. Despite challenges in obtaining a reliable estimate for CAPEX and LCOH, the total cost of the primary reformer was investigated. From the CAPEX, it was found that the total cost of the primary reformer would have to be 11% cheaper for electric SMR to achieve the same CAPEX as for conventional SMR. Based on the LCOH estimate on the other hand, electric SMR was proven to be a better investment even if the total primary reformer was up to 2.8 times more expensive than conventional SMR.

The operating costs were also assessed, and based on different scenarios it was discovered that the base case of electric SMR was slightly cheaper than conventional SMR. By introducing an ideal furnace for the conventional SMR, the cost could be reduced below the cost of the base case electric SMR. However, the lowest operating cost was found for an ideal electric SMR, just below the electric SMR with a reduced electrical power tax. Based on predictions of the evolving cost of natural gas, carbon tax, and electricity, it was estimated that in 2030 electric SMR would be cheaper than conventional SMR, and thus offers a better alternative as a more promising, future-oriented technology.

As this is a preliminary study and there is little published literature on the subject, more research is necessary to obtain a better understanding of the mechanics and implications of electric SMR. Future work should focus on how an electric SMR plant may be built on a large-scale to complement the lab-scale tests that have been conducted so far. Additionally, further research on how daily operations of the plant, such as maintenance and the possibility of partial shutdowns could increase plant reliability. It would be beneficial to build the electric SMR in a modular fashion, so that it is possible to remove one (or more) reformer tube at a time if maintenance is required or in case of tube failure. Being able to manage and minimize downtime would be an important improvement from conventional SMR. The consequences of using intermittent electricity sources or the possibilities of using fuel switching should also be considered. With this in mind, the existing studies in addition to this thesis demonstrate that electric SMR is a promising technology that could very well be considered a more sustainable option to conventional SMR.

Bibliography

[1] IEA. "Net Zero by 2050 - A Roadmap for the Global Energy Sector". In: (2021), p. 222.

[2] International Energy Agency. "Global Energy Review 2020". In: *Global Energy Review 2020* (2020).

[3] International Energy Agency. *The Future of Hydrogen*. Report, 2019.

[4] Theo Bosma, Marcel Eijgelaar, and Rob van Gerwen. *Sector coupling*. Tech. rep. DNV GL, 2020.

[5] International Energy Agency. *Key World Energy Statistics*. Tech. rep. IEA, 2017.

[6] NOAA National Centers for Environmental Information. "State of the Climate: Global Climate Report for Annual 2020". In: (Jan. 2020). URL: `https://www.ncdc.noaa.gov/sotc/global/202013` (visited on 05/05/2021).

[7] NASA's Goddard Institute for Space Studies (GISS). "Global Temperature". In: (2020). URL: `https://climate.nasa.gov/vital-signs/global-temperature/` (visited on 05/05/2021).

[8] M.A. Habib et al. *Experimental and numerical analysis of oxy-fuel combustion in a porous plate reactor*. Int. J. Energy Res. 2015; 39:1229–1240. Wiley, 2015.

[9] Sam Fankhauser and Frank Jotzo. "Economic growth and development with low-carbon energy". In: *Wiley Interdisciplinary Reviews: Climate Change* 9.1 (Jan. 2018).

[10] Chunshan Song. "Global challenges and strategies for control, conversion and utilization of CO2 for sustainable development involving energy, catalysis, adsorption and chemical processing". In: *Catalysis Today* 115 (1-4 2006).

[11] IRENA. *Global Renewables Outlook: Energy transformation 2050*. 2020, p. 292.

[12] Hydrogen Europe. *Hydrogen Production*. `https://hydrogeneurope.eu/hydrogen-production-0` (visited December 11, 2020). 2017.

[13] J O Abe et al. "Hydrogen energy, economy and storage: Review and recommendation". In: *International Journal of Hydrogen Energy* 44.29 (2019), pp. 15072–15086.

[14] Kasper T. Møller et al. *Hydrogen - A sustainable energy carrier*. p. 34-40. Progress in Natural Science: Materials International vol.27, 2017.

[15] Méziane Boudellal. *Power-to-Gas: Renewable Hydrogen Economy for the Energy Transition*. Walter de Gruyter GmbH, Feb. 2018, pp. 1–211.

[16] Sebastian Thor Wismann. *Electrically heated steam methane reforming*. Technical University of Denmark, 2019.

[17] E. Shoko et al. *Hydrogen from coal: Production and utilisation technologies*. Vol 65, Issues 3–4, Pages 213-222. International Journal of Coal Geology, 2006.

[18] N. Van Hulst. *The clean hydrogen future has already begun*. International Energy Agency, 2019.

[19] Jørgen Aarnes, Marcel Eijgelaar, and Erik A. Hektor. “Hydrogen as an energy carrier. An evaluation of emerging hydrogen value chains. Group Technology & Research - Position Paper 2018”. In: *DNV GL* (2018).

[20] Furat Dawood, Martin Anda, and G. M. Shafiullah. *Hydrogen production for energy: An overview*. 2020.

[21] Thomas Rostrup-Nielsen. *Manufacture of Hydrogen*. p.293-296. Catalysis today 106, 2005.

[22] IEA Greenhouse Gas R&D Programme. *IEAGHG Technical Review Techno-Economics of Deploying CCS in a SMR Based Hydrogen Production using NG as Feedstock/Fuel*. 2017.

[23] Daniel Jakobsen and Vegar Åtland. *Concepts for Large Scale Hydrogen Production*. Master of science in Mechanical Engineering. Norwegian University of Science and Technology, 2016.

[24] K. Amo et al. *Low-Quality Natural Gas Sulfur Removal/Recovery*. Membrane Technology and Research, Inc., 1998.

[25] IEA Greenhouse Gas R&D Programme. *IEAGHG Technical Review Reference data and Supporting Literature Reviews for SMR Based Hydrogen Production with CCS*. 2017.

[26] L. Chen et al. *Catalytic Hydrogen Production from Methane: A Review on Recent Progress and Prospect*. Catalysts 10, 2020.

[27] R. Elshout. *Hydrogen Production By Steam Reforming*. pp.34-38. Chemical Engineering, 117(5), 2010.

[28] Lu Zhou et al. *Investigation of a novel porous anodic alumina plate for methane steam reforming: Hydrothermal stability, electrical heating possibility and reforming reactivity*. p.844-858. International Journal of Hydrogen Energy 34, 2009.

[29] Rais Hanizam et al. “Effect of Steam to Carbon Ratio (S : C) on Steam Methane Reforming ’ s yield over Coated Nickel Aluminide (Ni 3 Al) Catalyst in Micro Reactor”. In: 32.4 (2020), pp. 657–662.

[30] M. Wang et al. “Process Modeling and Energy Efficiency Analysis of Natural Gas Hydrate Production by CH4-CO2/H2 Replacement Coupling Steam Methane Reforming”. In: *Computer Aided Chemical Engineering*. Vol. 47. Elsevier B.V., Jan. 2019, pp. 131–136.

[31] C. Lee & C.G. Jou. *Enhancing Furnace Thermal Efficiency by Adjusting Fuel Temperature*. Vol. 3, No. 2. Energy and Environment Research, 2013.

[32] H Idriss, H Scott, and V Subramani. “Introduction to hydrogen and itsproperties”. In: *Compendium of Hydrogen Energy*. 2015.

[33] W.H Chen et al. *Modeling and simulation of high-temperature and low-temperature water gas shift reactions*. International Journal of Hydrogen Energy 33, 2008.

[34] Vitor P. Paixão, Luís F.M. Franco, and José Vicente H. D’Angelo. “Simulation and Design of a Water-Gas Shift Catalytic Multitubular Reactor with Integrated Heat Exchange”. In: *Industrial and Engineering Chemistry Research* (2020).

[35] E.V. Rebrov. *Advances in water-gas shift technology: modern catalysts and improved reactor concepts*. pp. 387-412. Advances in Clean Hydrocarbon Fuel Processing, 2011.

[36] F. Rosner et al. *Water gas shift reactor modelling and new dimensionless numberfor thermal management/design of isothermal reactors*. Applied Thermal Engineering 173, 2020.

[37] R. Bouarab et al. “Hydrogen Production from the Water-Gas Shift Reaction on Iron Oxide Catalysts”. In: *Journal of Catalysts* 2014 (2014), pp. 1–6.

[38] S. Kwon et al. *CO2 Sorption*. pp. 293-339. Coal Gasification and Its Applications, 2011.

[39] P. Biswas S. Agrawal and S. Sinha. *Modeling and Simulation for Pressure Swing Adsorption System for Hydrogen Purification*. pp. 409–414. Chemical and Biochemical Engineering Quarterly, 2010.

[40] J. A.Arran Gibson et al. “Adsorption Materials and Processes for Carbon Capture from Gas-Fired Power Plants: AMPGas”. In: *Industrial and Engineering Chemistry Research* 55.13 (Apr. 2016), pp. 3840–3851.

[41] R. Ben-Mansour et al. *Carbon capture by physical adsorption: Materials, experimental investigations and numerical modeling and simulations – A review*. Elsevier, 2016.

[42] K. Thambimuthu et al. *Capture of* CO_2. IPCC Special Report on Carbon dioxide Capture and Storage, 2018.

[43] M. Wang et al. “Post-combustion CO2 capture with chemical absorption: A state-of-the-art review”. In: *Chemical Engineering Research and Design* 89.9 (Nov. 2011), pp. 1609–1624.

[44] T.A. Saleh & V.K. Gupta. *An Overview of Membrane Science and Technology*. Elsevier, 2016.

[45] M.A Nemitallah et al. *Oxyfuel Combustion for Clean Energy Applications*. Springer, 2019.

[46] G. Ji & M. Zhao. *Membrane Separation TEchnolgy in Carbon Capture*. doi:10.5772/65723. IntechOpen, 2017.

[47] T. Wilberforce et al. *Outlook of carbon capture technology and challenges*. pp. 56-72. Science of the Total Environment, 2019.

[48] Arthur L. Kohl and Richard B. Nielsen. “Alkanolamines for Hydrogen Sulfide and Carbon Dioxide Removal”. In: *Gas Purification* (1997), pp. 40–186.

[49] S. Roussanaly, R.Anantharam, and C. Fu. “Low-Carbon Footprint Hydrogen Production from Natural Gas: A Techno-Economic Analysis of Carbon Capture and Storage from Steam-Methane Reforming”. In: *Chemical Engineering Transactions* 81 (Apr. 2020).

[50] B. Dutcher et al. *Amine-Based CO2 Capture Technology Development from the Beginning of 2013 - A Review*. ACS, 2015.

[51] E. Oko et al. *Current status and future development of solvent-based catbon capture*. International Journal of Coal Science & Technology, 2017.

[52] J. Gibbins & H. Chalmers. *Carbon capture and storage*. Volume 36, Issue 12. Energy Policy, 2008.

[53] Michael Dent. “Innovation in Carbon Capture Technology”. In: *IDTechEx* (2021).

[54] Ida M. Bernhardsen and Hanna K. Knuutila. “A Review of potential amine solvents for CO2 absorption process: Absorption capacity, cyclic capacity and pKa”. In: *Department of Chemical Engineering, Norwegian University of Science and Technology (NTNU)* (2017).

[55] G.T. Rochelle. *Conventional amine scrubbing for CO_2 capture*. Elsevier, 2016.

[56] J.I. Huertas et al. *CO2 Absorbing Capacity of MEA*. Journal of Chemistry, 2015.

[57] Firoz Alam Chowdhury et al. “CO2 capture by tertiary amine absorbents: A performance comparison study”. In: *Industrial and Engineering Chemistry Research* 52.24 (2013), pp. 8323–8331.

[58] F. Closmann. *MDEA/Piperazine as a solvent for CO2 capture*. 1351-1357. Energy Procedia, 2009.

[59] G.Puxty & M. Maeder. *The fundamentals of post-combustion capture*. pp.14-31. Elsevier, 2016.

[60] S. Mokhatab & W.A. Poe. *Handbook of Natural Gas Transmission and Processing (Second Edition)*. pp. 253-290. Elsevier, 2012.

[61] L.V. Van der Ham et al. *Absorption-Based Post-combustion Capture of Carbon Dioxide*. pp. 103-119. Woodhead Publishing, 2016.

[62] N.E. Flø. *Assessment of Material Selection for the CO2 Absorption Process with Aqueous MEA Solution based on Results from Corrosion Monitoring at Technology Centre Mongstad*. 14th International Conference on Greenhouse Gas Control Technologies, GHGT-14, 2018.

[63] R. Shirmohammadi. *CO2 Utilization via Integration of an Industrial Post-Combustion Capture Process with a Urea Plant: Process Modelling and Sensitivity Analysis*. processes, MDPI, 2020.

[64] M H V A N D E Voorde and Material Division. “High-temperature materials and industrial applications”. In: *Butlletí de les Societats Catalanes de Física, Química, Matemàtiques i Tecnologia* XI (1991), pp. 199–226–226.

[65] Eugenio Meloni, Marco Martino, and Vincenzo Palma. “A short review on ni based catalysts and related engineering issues for methane steam reforming”. In: *Catalysts* 10.3 (2020).

[66] François Ropital and Frédéric Bonnet. “Mechanism of catalytic coke formation and some means to limit it in refinery processes”. In: *Materials Science Forum* 595-598 PART 2 (2008), pp. 681–688.

[67] Sebastian T. Wismann et al. *Electrified methane reforming: A compact approach to greener industrial hydrogen production*. pp. 756-759. Science 364, 2019.

[68] M.A. Almind et al. *Improving performance of induction-heated steam methane reforming*. pp. 13-20. Catalysis Today 342, 2020.

[69] Regjeringen.no. *CO2-avgiften*. 2020. URL: `https://www.regjeringen.no/no/tema/okonomi-og-budsjett/skatter-og-avgifter/veibruksavgift-pa-drivstoff/co2-avgiften/id2603484/` (visited on 04/18/2021).

[70] Bengt Johansson. “Economic instruments in practice 1: Carbon tax in Sweden”. In: *OECD workshop on innovation and the environment* (2000), pp. 1–12.

[71] CBO. “Effects of a carbon tax on the economy and the environment”. In: *Taxes in the United States: Developments, Analysis, and Research* 4532.May (2013), pp. 17–50.

[72] *Avgift på elektrisk kraft*. 2021. (Visited on 05/21/0003).

[73] R. K. Sinnott and Gavin Towler. *Chemical Engineering Design*. 2013.

[74] Ghanim Putrus and Edward and Bentley. “Integration of distributed renewable energy systems into the smart grid”. In: *Electric Renewable Energy Systems*. Elsevier, 2016, pp. 487–518.

[75] S Perry et al. *Perry’s chemical engineers’ handbook*. Vol. 38. 02. 2000, pp. 38–0966–38–0966.

[76] Hyun Seog Roh et al. “Natural gas steam reforming for hydrogen production over metal monolith catalyst with efficient heat-transfer”. In: *International Journal of Hydrogen Energy* 35.4 (2010), pp. 1613–1619.

[77] Luqmanulhakim Baharudin and Matthew James Watson. “Monolithic substrate support catalyst design considerations for steam methane reforming operation”. In: *Reviews in Chemical Engineering* 34.4 (2018), pp. 481–501.

[78] Magne Holstad, Ingvild R. Ruen, and Tom Jonas Billit. *Elektrisitet*. 2021. URL: `https://www.ssb.no/elektrisitet` (visited on 04/18/2021).

[79] EIA. *What is U.S. electricity generation by energy source?* 2021. URL: `https://www.eia.gov/tools/faqs/faq.php?id=427&t=3` (visited on 04/21/2021).

[80] EIA. *How much carbon dioxide is produced per kilowatthour of U.S. electricity generation?* 2020. URL: `https://www.eia.gov/tools/faqs/faq.php?id=74&t=11` (visited on 05/21/0005).

[81] Anton Eliston and Astrid Stavseng. *Strømforbruk i Norge har lavt klimagassutslipp*. 2020. URL: `https://www.nve.no/nytt-fra-nve/nyheter-energi/stromforbruk-i-norge-har-lavt-klimagassutslipp/` (visited on 04/20/2021).

[82] Intergovernmental Panel on Climate Change. "Technology-specific Cost and Performance Parameters". In: *Climate Change 2014 Mitigation of Climate Change* (2015), pp. 1329–1356.

[83] IRENA. *Renewable Power Generation Costs in 2014*. 2014.

[84] *How Norway produces hydropower with a minimal carbon footprint - The Explorer*. URL: `https://www.theexplorer.no/stories/energy/how-norway-produces-hydropower-with-a-minimal-carbon-footprint/` (visited on 05/20/2021).

[85] Rob van Gerwen, Marcel Eijgelaar, and Theo Bosma. "Hydrogen in the Electricity Value Chain". In: (2019), p. 62.

[86] Max Wei, Colin A. McMillan, and Stephane de la Rue du Can. "Electrification of Industry: Potential, Challenges and Outlook". In: *Current Sustainable/Renewable Energy Reports* 6.4 (2019).

[87] Kevin R Kaushal, Lars Lindholt, and Hidemichi Yonezawa. *Effects of changes in electricity prices on the power-intensive industries and other sectors in Norway towards 2030*. Statistisk sentralbyrå • Statistics Norway, 2019.

[88] O Roelofsen et al. "Plugging in: What electrification can do for industry". In: *McKinsey & Company* May (2020), pp. 1–12.

[89] John C. Molburg and Richard D. Doctor. "Hydrogen from Steam-Methane Reforming with CO2 Capture". In: *20th Annual International Pittsburgh Coal Conference*. ACADEMIA, 2003.

[90] X. D. Peng. "Analysis of the thermal efficiency limit of the steam methane reforming process". In: *Industrial and Engineering Chemistry Research* 51.50 (Dec. 2012), pp. 16385–16392.

[91] Lars Erik Øi. "Aspen HYSYS Simulation of CO 2 Removal by Amine Absorption from a Gas Based Power Plant". In: *SIMS2007 Conference* (2007), pp. 73–81.

[92] Richard Turton et al. *Analysis, Synthesis, and Design of Chemical Processes*. 3rd. editi. Pearson Education, 2009.

[93] Ying Feng and Gade P. Rangaiah. *EVALUATING CAPITAL COST ESTIMATION PROGRAMS*. `https://www.chemengonline.com/evaluating-capital-cost-estimation-programs-2/?printmode=1` (visited April 04, 2021). 2011.

[94] Max S. Peters, Klaus D. Timmerhaus, and Ronald E. West. *Plant Design and Economics for Chemical Engineers 5th Edition*. Vol. 369. 1. 2003, pp. 1–1006. arXiv: `arXiv:1011.1669v3`.

[95] "Directory of Energy Conservation Technology in Japan - Section 3: Chemical Indstry". In: *New Energy and Industrial Technology Development Orgnization and the Energy Conservation Center* (1999).

[96] J. C. Meerman et al. “Techno-economic assessment of CO 2 capture at steam methane reforming facilities using commercially available technology”. In: *International Journal of Greenhouse Gas Control* 9 (2012), pp. 160–171.

[97] James R. Fair and Henry Z. Kister. “Absorption (Chemical Engineering)”. In: *Encyclopedia of Physical Science and Technology (Third Edition)*. 2003.

[98] Robert Y Purcell et al. *Evaluation of control technologies for hazardous air pollutants*. Research Triangle Park, NC, 1986.

[99] Equinor. *Internal gas price*. 2021. URL: `https://www.equinor.com/no/investors.html` (visited on 03/05/2021).

[100] Magne Holstad, Robert Skotvold, and Thomas Aanensen. *Elektrisitetspriser*. 2021. URL: `https://www.ssb.no/energi-og-industri/statistikker/elkraftpris/kvartal`.

[101] Ana Maria Cormos et al. “Economic assessments of hydrogen production processes based on natural gas reforming with carbon capture”. In: *Chemical Engineering Transactions* 70 (2018).

[102] Regjeringen.no. *Statsbudsjettet 2021: Endringer i klimaavgiftene*. 2020. URL: `https://www.regjeringen.no/no/statsbudsjett/2021/statsbudsjettet-2021-skatter-og-avgifter/statsbudsjettet-2021-endringer-i-klimaavgiftene/id2767839/` (visited on 04/18/2021).

[103] *Meld. St. 13 - Klimaplan for 2021-2030*. Tech. rep. Klima- og miljødepartementet, 2021.

[104] Equinor. “First quarter 2020 - Financial statements and review”. In: (2020).

[105] Ludvik Viktorsson et al. “A step towards the hydrogen economy - A life cycle cost analysis of a hydrogen refueling station”. In: *Energies* 10.6 (2017), pp. 1–15.

[106] E. Platvoet. *When excess air becomes too much*. XRG Technologies, 2020.

[107] Steven R Mickey. *Efficient Gas Heating of Industrial Furnaces*. 2017. URL: `https://thermalprocessing.com/efficient-gas-heating-of-industrial-furnaces/` (visited on 05/05/2021).

[108] Simone Giorgetti et al. “Carbon Capture on a Micro Gas Turbine: Assessment of the Performance”. In: *Energy Procedia*. Vol. 105. 2017, pp. 4046–4052.

[109] Elvis O. Agbonghae et al. “Experimental and process modelling study of integration of a micro-turbine with an amine plant”. In: *Energy Procedia*. Vol. 63. 2014, pp. 1064–1073.

[110] Bin Zhao et al. “Enhancing the energetic efficiency of MDEA/PZ-based CO2 capture technology for a 650 MW power plant: Process improvement”. In: *Applied Energy* 185 (2017), pp. 362–375.

[111] B.A. Khan et al. *Energy Minimization in Piperazine Promoted MDEA-Based CO2 Capture Process*. sustainability, MDPI, 2020.

[112] *Electric Resistance Heating*. URL: `https://www.energy.gov/energysaver/home-heating-systems/electric-resistance-heating` (visited on 03/03/2021).

[113] Pamela L. Spath and Margaret K. Mann. *Life Cycle Assessment of Hydrogen Production via Natural Gas Steam Reforming*. Tech. rep. National Renewable Energy Laboratory, 2001.

[114] B Gaudernack and S Lynum. "Hydrogen from natural gas without release of CO2 to the atmosphere". In: *International Journal of Hydrogen Energy* 23 (1998), pp. 1087–1093.

[115] Carl R. Branan. *Rules of Thumb for Chemical Engineers*. 2005.

[116] *Steam-methane reformer (SMR) for hydrogen production | Linde Engineering*. URL: https://www.linde-engineering.com/en/process-plants/furnaces_fired_heaters_incinerators_and_t-thermal/steam_reformer_furnaces/steam_reformer_for_hydrogen_production/index.html (visited on 05/24/2021).

[117] Eia. *Natural gas explained*. 2020.

[118] Kjetil Malkenes Hovland. *Equinor rammet av lave priser: Gass-smell for Sætre*. Feb. 2020. URL: https://e24.no/olje-og-energi/i/zGPa0b/equinor-rammet-av-lave-priser-gass-smell-for-saetre (visited on 04/18/2021).

[119] Eia. *Electricity explained - Factors affecting electricity prices*. 2021. URL: https://www.eia.gov/energyexplained/electricity/prices-and-factors-affecting-prices.php (visited on 04/18/2021).

[120] N Sönnichsen. *U.S. and European natural gas commodity prices 1980-2030*. 2021. URL: https://www.statista.com/statistics/252791/natural-gas-prices/ (visited on 07/05/2021).

[121] EPA. *Renewable Fuel Standard Program*. 2020. URL: https://www.epa.gov/renewable-fuel-standard-program/lifecycle-analysis-greenhouse-gas-emissions-under-renewable-fuel (visited on 05/09/2021).

[122] R Soltani, M A Rosen, and I and Dincer. "Assessment of CO2 capture options from various points in steam methane reforming for hydrogen production". In: *International Journal of Hydrogen Energy* 39.35 (2014), pp. 20266–20275.

[123] Andrea Bassani et al. "Mitigating carbon dioxide impact of industrial steam methane reformers by acid gas to syngas technology: Technical and environmental feasibility". In: *Journal of Sustainable Development of Energy, Water and Environment Systems* 8.1 (2020), pp. 71–87.

[124] Glen Norcliffe. "Technological Change". In: *International Encyclopedia of Human Geography*. Elsevier, Jan. 2020, pp. 187–192.

[125] Roger Fouquet and Peter J G and Pearson. "Past and prospective energy transitions: Insights from history". In: *Energy Policy* 50 (2012), pp. 1–7.

[126] David Popp, Richard G Newell, and Adam B Jaffe. *Energy, the Environment, and Technological Change*. Vol. 2. Handbook of the Economics of Innovation, Volume 2. Amsterdam: North Holland, 2010, pp. 873–937.

[127] L Lu and O Ishiyama. "Iron ore sintering". In: *Iron Ore*. Mineralogy, Processing and Environmental Sustainability, 2015. Chap. 14, pp. 395–433.

[128] Antonio Ricca et al. “Innovative catalyst design for methane steam reforming intensification”. In: *Fuel* 198 (2017), pp. 175–182.

Appendix A

Simulation

A.1 Conventional SMR (Hysys figure)

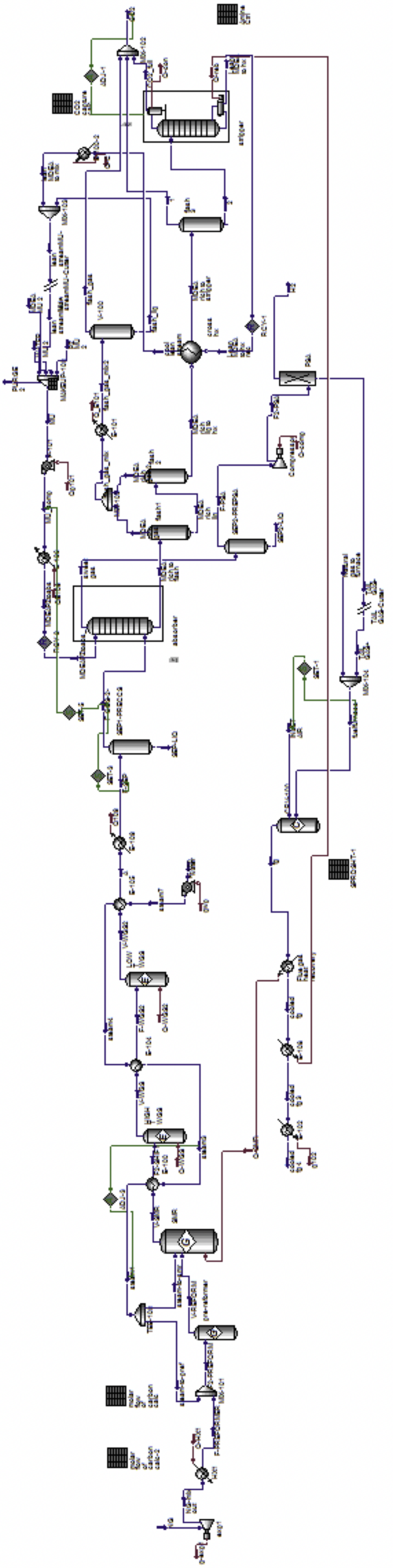

A.2 Electric SMR (Hysys figure)

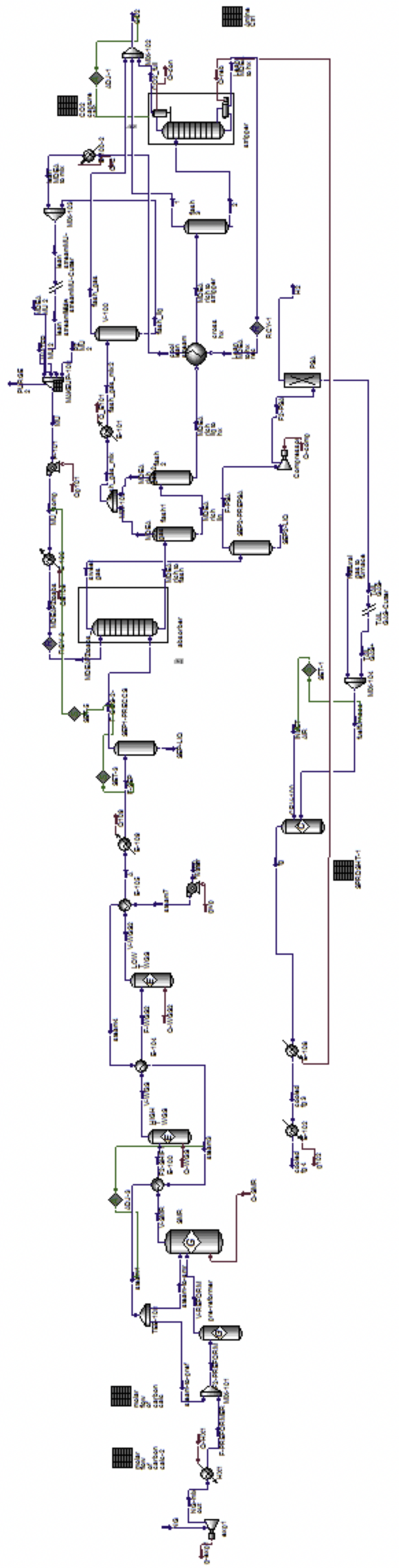

A.3 Simulation values (El. SMR)

TABLE A.1: Values from the Hysys simulation of conventional SMR. The flows are numbered according to Figure 3.1, compositions are given as mole%. A negative sign in front of the energy indicates energy demand, while a positive sign indicates energy produced. The table does not include heat exchangers, pumps or flash drums throughout the simulation (see Appendix A)

	Pre-reformer		**SMR**		**HTSR**		**LTSR**		**Furnace**			
Energy [MW]	0		207		-14		-1.5		213			
S/C ratio	0.3		3.0		-		-		-			
Flow name	Feed	Natural gas	1	2	3	4	5	6	Tail gas	Natural gas	Air	H_2
T [°C]	50	400	400	900	320	320	190	190	25	25	25	25
P [bar]	50	25.25	24.75	24.25	24.00	23.50	23.25	22.75	2.5	1.00	1.00	20.00
M [kg/h]	$4.142\cdot 10^4$	$4.142\cdot 10^4$	$5.517\cdot 10^4$	$1.835\cdot 10^5$	$1.835\cdot 10^5$	$1.835\cdot 10^5$	$1.835\cdot 10^5$	$1.835\cdot 10^5$	$1.130\cdot 10^4$	2400	$2.70\cdot 10^5$	$1.546\cdot 10^4$
Composition												
Methane	85.30	85.30	75.38	1.71	1.71	1.71	1.71	1.71	19.83	85.30	0	0
Ethane	7.05	7.05	0.01	0	0	0	0	0	0	7.05	0	0
CO2	2.21	2.21	5.65	5.53	5.53	14.76	14.76	15.71	8.43	2.21	0	0
Propane	2.73	2.73	0	0	0	0	0	0	0	2.73	0	0
i-Butane	0.55	0.55	0	0	0	0	0	0	0	0.55	0	0
n-Butane	0.94	0.94	0	0	0	0	0	0	0	0.94	0	0
i-Pentane	0.27	0.27	0	0	0	0	0	0	0	0.27	0	0
n-Pentane	0.27	0.27	0	0	0	0	0	0	0	0.27	0	0
n-Hexane	0.18	0.18	0	0	0	0	0	0	0	0.18	0	0
n-Heptane	0.13	0.13	0	0	0	0	0	0	0	0.13	0	0
n-Octane	0.04	0.04	0	0	0	0	0	0	0	0.04	0	0
Nitrogen	0.33	0.33	0.22	0.05	0.05	0.05	0.05	0.05	0.56	0.33	79.00	0
Hydrogen	0	0	2.73	48.72	48.72	57.94	57.94	58.90	68.44	0	0	100.00
H2O	0	0	15.93	33.68	33.68	24.46	24.46	23.50	1.19	0	0	0
Oxygen	0	0	0	0	0	0	0	0	0	0	21.00	0
CO	0	0	0.08	10.31	10.31	1.09	1.09	0.13	1.55	0	0	0

A.4 Specifics of each unit operation

A.4.1 Pre-reformer

The specifics for the pre-reformer in the Hysys simulation can be found in Table A.2.

TABLE A.2: Specifications of the pre-reformer in the simulation.

Reactor type	Gibbs reactor
Reaction types	Specified equilibrium reactions
Vessel temperature	400°C
Vessel pressure	24.75 bar
Specification	Adiabatic
Reactions	$CO + H_2O \longrightarrow CO_2 + H_2$ $CH_4 + H_2O \longrightarrow CO + 3H_2$ $C_2H_6 + 2H_2O \longrightarrow 2CO + 5H_2$ $C_3H_8 + 3H_2O \longrightarrow 3CO + 7H_2$ $iC_4H_{10} + 4H_2O \longrightarrow 4CO + 9H_2$ $nC_4H_{10} + 4H_2O \longrightarrow 4CO + 9H_2$ $iC_5H_{12} + 5H_2O \longrightarrow 5CO + 11H_2$ $nC_5H_{12} + 5H_2O \longrightarrow 5CO + 11H_2$ $nC_6H_{14} + 6H_2O \longrightarrow 6CO + 13H_2$ $nC_7H_{16} + 7H_2O \longrightarrow 7CO + 15H_2$ $nC_8H_{18} + 8H_2O \longrightarrow 8CO + 17H_2.$

A.4.2 SMR

TABLE A.3: Specifications of the SMR in the simulation.

Reactor type	Gibbs reactor
Vessel temperature	950°C
Vessel pressure	24.25 bar
Reactions	$CO + H_2O \longrightarrow CO_2 + H_2$ $CH_4 + H_2O \longrightarrow CO + 3H_2$ $C_2H_6 + 2H_2O \longrightarrow 2CO + 5H_2$ $C_3H_8 + 3H_2O \longrightarrow 3CO + 7H_2$ $iC_4H_{10} + 4H_2O \longrightarrow 4CO + 9H_2$ $nC_4H_{10} + 4H_2O \longrightarrow 4CO + 9H_2$ $iC_5H_{12} + 5H_2O \longrightarrow 5CO + 11H_2$ $nC_5H_{12} + 5H_2O \longrightarrow 5CO + 11H_2$ $nC_6H_{14} + 6H_2O \longrightarrow 6CO + 13H_2$ $nC_7H_{16} + 7H_2O \longrightarrow 7CO + 15H_2$ $nC_8H_{18} + 8H_2O \longrightarrow 8CO + 17H_2.$

Furnace

For the simulation of conventional SMR, the specifications for the furnace is given in Table A.4.

TABLE A.4: Specifications of the furnace used to heat the SMR reactor in the simulation.

Reactor type	Conversion reactor
Inlet temperature	25°C
Vessel temperature	1876 °C
Vessel pressure	1 bar
AF	20
Fuel rate	$2.5 \cdot 10^4$ kg/h
Reactions	$CO + 0.5\,O_2 \longrightarrow CO_2$ $CH_4 + 1.5\,O_2 \longrightarrow CO + 2\,H_2O$ $C_2H_6 + 2.5\,O_2 \longrightarrow 2\,CO + 3\,H_2O$ $C_3H_8 + 3.5\,O_2 \longrightarrow 3\,CO + 4\,H_2O$ $iC_4H_{10} + 4.5\,O_2 \longrightarrow 4\,CO + 5\,H_2O$ $nC_4H_{10} + 4.5\,O_2 \longrightarrow 4\,CO + 5\,H_2O$ $iC_5H_{12} + 5.5\,O_2 \longrightarrow 5\,CO + 6\,H_2O$ $nC_5H_{12} + 5.5\,O_2 \longrightarrow 5\,CO + 6\,H_2O$ $nC_6H_{14} + 6.5\,O_2 \longrightarrow 6\,CO + 7\,H_2O$ $nC_7H_{16} + 7.5\,O_2 \longrightarrow 7\,CO + 8\,H_2O$ $nC_8H_{18} + 8.5\,O_2 \longrightarrow 8\,CO + 9\,H_2O.$

For the simulation of electric SMR, where the furnace is solely used to heat the reboiler in the stripper, the specifications for the furnace is given in Table A.4.

A.4.3 Shift reactors

TABLE A.5: Specifications of the HTSR and LTSR in the simulation.

	HTSR	LTSR
Reactor type	Equilibrium reactor	Equilibrium reactor
Vessel temperature	320°C	190°C
Inlet pressure	2375 kPa	2300 kPa
Pressure drop	50 kPa	50 kPa
Specification	Isothermal	Isothermal
Reaction	$CO + H_2O \longrightarrow CO_2 + H_2$	$CO + H_2O \longrightarrow CO_2 + H_2$

A.4.4 Heat exchangers before capture plant

TABLE A.6: Specifications of the heat exchangers before the capture plant.

	C1	
Stream	Stream number in model	Temperature
Hot inlet	2	900.0 °C
Hot outlet	3	320.0 °C
Cold inlet	w4	184.7 °C
Cold outlet	w5	246.9 °C
Logarithmic mean temperature difference		307 °C
Ft correction factor		0.933
	C2	
Stream	Stream number in model	Temperature
Hot inlet	4	320.0 °C
Hot outlet	5	190.0 °C
Cold inlet	w3	85.4 °C
Cold outlet	w4	184.7 °C
Logarithmic mean temperature difference		98.2 °C
Ft correction factor		0.823
	C3	
Stream	Stream number in model	Temperature
Hot inlet	6	190.0 °C
Hot outlet	7	147.4 °C
Cold inlet	w2	25.2 °C
Cold outlet	w3	85.4 °C
Logarithmic mean temperature difference		109.3 °C
Ft correction factor		0.966

A.4.5 Carbon capture plant

Absorber

TABLE A.7: Specifications of the absorber in the capture plant.

Inlet temperature	40°C
Absorbent	35 wt% MDEA, 5 wt% PZ
Pressure	20 bar
Inlet liquid flow	$1.946 \cdot 10^6$ kg/h
Inlet gas flow	$1.227 \cdot 10^6$ kg/h
L/G	15.8
Stages	12

A.4.6 Flash drums in capture plant

All flash drums in the simulation were simulated as separators in Aspen Hysys, the flash drums in the order they appear in the simulation (and n Figure 3.1) and their respective pressures can be found in Table A.8.

TABLE A.8: Specifications of the flash drums in the capture plant.

Flash	Pressure
1	5 bar
2	2 bar
3	2 bar

A.4.7 Cross heat exchanger

The specifications for the cross heat exchanger in the carbon capture plant can be found in Tale A.9.

TABLE A.9: Specifications of the cross heat exchanger in the capture plant.

Stream	Stream number in model	Temperature
Hot inlet	14	101.8 °C
Hot outlet	15	82.1 °C
Cold inlet	12	56.7 °C
Cold outlet	13	77.1 °C
Logarithmic mean temperature difference		22.1 °C
Ft correction factor		0.882

A.4.8 Stripper

TABLE A.10: Specifications of the stripper in the capture plant.

Pressure	2 bar
Stages	10
Condenser	Full reflux
Condenser temperature	25 °C
Reboiler duty	$7.4 \cdot 10^4$ kW
Capture rate	95%

A.4.9 PSA

TABLE A.11: Specifications of the PSA in the simulation.

Equipment type	Component splitter
Hydrogen recovery	90%
Hydrogen purity	100%

A.5 Scenarios

A.5.1 Ideal SMR

The case of the "Ideal SMR" was found by calculating an ideal furnace as described in the Methodology. The simulation in Aspen Hysys was done by using a spreadsheet to calculate the stoichiometric amount of air dependent on the inlet flow of the fuels. An adjust block was used to minimize the flow of natural gas while ensuring that the temperature was high enough.

From the simulations, the minimum amount of fuel for a furnace at stoichiometric conditions with no upper temperature limit, the amount of fuel was $2.4 \cdot 10^4$ kg/h. From stoichiometric conditions the amount of air becomes $4.8 \cdot 10^5$ kg/h. The temperature of the flue gas reached 1882 °C. The emissions were found to be 5.26 kg CO_2/kg H_2.

A.5.2 Electric SMR with reduced tax

This scenario was simply made by replacing the electrical power tax that was used for the base case (in Table 3.6) with the reduced tax of 0.00546 kr/kWh.

A.5.3 Ideal electrical SMR

This scenario was made using the reduced tax as described previously as well as calculating an ideal furnace. The simulation was executed the same was as for ideal conventional SMR. From the simulations, the minimum amount of fuel for a furnace at stoichiometric conditions with no upper temperature limit, the amount of fuel was $1.8 \cdot 10^3$ kg/h. From stoichiometric conditions the amount of air becomes $1.5 \cdot 10^5$ kg/h. The temperature of the flue gas reached 1292 °C. The emissions were found to be 1.37 kg CO_2/kg H_2.

Appendix B

Calculations

B.1 Sizing calculations

B.1.1 Height of vertical vessels

The liquid volume in the vessel, $V_{l,invessel}$ is found by

$$V_{l,invessel} = V_l \cdot t_{holdup}, \tag{B.1}$$

where V_l is the liquid volumetric flow rate, and t_{holdup} is the liquid hold up time, which is often assumed to be 10 minutes [73]. From this the liquid height is found, as the liquid fills the bottom of the vessel,

$$h_l = \frac{V_{l,invessel}}{\frac{\pi \cdot D_v^2}{4}} \tag{B.2}$$

B.1.2 Sizing of horizontal vessels

From the settling velocity in Equation 3.7 and the volumetric vapor flow rate, the minimum diameter required can be solved based on the L/D found from the pressure in the plant (as shown in Table 3.4).

All flash drums were designed as horizontal vessels, and due to the large amount of liquid, it was assumed that the liquid would account for 80% of the total area in the vessel. It was also assumed that a liquid hold up time of half a minute would be sufficient.

The Python script to solve the sizing can be found in Appendix D.

B.1.3 Diameter of the absorber

As mentioned, the diameter of the absorber was found by using the approach given in Sinnott et al (2013) [73]. A pressure drop of 20 mmH_2O per metre packing was assumed [73]. The diameter was based on the flooding, which was found through constants in Sinnott et al (2013) [73]:

$$\text{Percentage flooding} = \frac{K_4}{K_{4(flooding)}}, \tag{B.3}$$

where K_4 and $K_{4(flooding)}$ was found from Sinnott et al. Then the gas mass flow rate per unit column cross sectional area, V_W^* was found:

$$V_W^* = \left[\frac{K_4\rho_v(\rho_L - \rho_v)}{13.1F_p(\mu_L/\rho_L)^{0.1}}\right]^{\frac{1}{2}}, \tag{B.4}$$

where F_p is a constant found from Sinnott et al (2013) as well. the V_W^* was used to solve for the column area:

$$A = \frac{V_v}{V_W^*}, \tag{B.5}$$

which in turn was used to solve for the diameter:

$$D = \sqrt{\frac{\pi}{4} \cdot A}. \tag{B.6}$$

B.1.4 Shift reactors

The values for calculation of the reaction rate for both the low temperature and high temperature shift reactors can be found in Table B.1.

TABLE B.1: Specific values for the size estimations in the model for the shift reactors.

Value	Unit	HTSR	LTSR	Source
k_0	kmole/(kg cat · s)	0.2986	0.2986	[92]
E_0	kJ/kmole	40.739	40.739	[92]
K_{eq}	-	$exp\left(-4.33 + \frac{4577.9}{T}\right)$	$exp\left(-4.72 + \frac{4800}{T}\right)$	[92]

To find the length of the catalytic bed, Equation 3.13 was rewritten as such, assuming steady state:

$$0 = \phi_v c_{in} - \phi_v c_{out} - (-r_{CO})S \cdot dz$$

$$0 = \frac{\phi_v c_{in} - \phi_v c_{out}}{dz} - (-r_{CO})S$$

$$0 = \frac{\phi_v c_{in} - \phi_v c_{out}}{dz} - (-r_{CO})S$$

$$\frac{dc}{dz} = (-r_{CO})\frac{S}{\phi_v}$$

z is the length of the catalytic bed, S is the surface area. This was solved as a nonstiff differential equation in Matlab by trial and error of the length of the catalytic bed. The conversion was calculated from Equation 3.12

TABLE B.2: Currency conversions used in the thesis.

1 EUR	1.18 USD
1 NOK	0.12 USD

B.1.5 Heat exchangers

Choice of heat exchanger type

The heat exchanger type was based on the TEMA-standard. From Brogan (2011) it was found that there are essentially three main combinations of heat exchangers, we have fixed tubesheet exchangers, U-tube exchangers and Floating head exchangers. The fixed tube sheet (L, M, or N) are geerally the simplest and most economic. It has easy cleaning, which can be done both mechanically or chemically (also stated that L, M or N can be used as long as there is no need for mechanical cleaning). Usually the other two main types would be used if there is a possibility of a large temperature difference between the tube and shell.

For the shell selection, one pass shells, E-type, is the most common, and would be suitable for this application.

For front header selection, A is chosen for dirty tubeside fluids, while B is chosen for clean tubeside fluids. However if the tubeside fluids are hazardous, then C- or N-types might be considered. D-type front ends should only be considered in high-pressure applications.

Based on this discussion a fixed tube was chosen (which can be both AEL and CEL in the TEMA standard). The cost estimate did not differ based on the front header selection, and hence it was not necessary to differentiate on whether AEL or CEL was chosen.

B.2 Currency conversions

The conversions between currencies used is given in Table B.2.

B.3 Equations and calculations

The bare module factor, F_{BM} was found as a function of a pressure factor,F_P a material factor, F_M, and two constants, B_1 and B_2:

$$F_{BM} = B_1 + B_2 F_P F_M. \tag{B.7}$$

When finding the material factor for vessels, F_M is 1 for CS and 3.1 for SS. The F_P for vessels can be based on the pressure in the unit,

$$F_{P,vessel} = \frac{\frac{(P+1)\cdot D}{2\cdot[S\cdot E-0.6(P+1)]}+CA}{t_{min}}, \tag{B.8}$$

where P is the operating pressure, D is the diameter, S is the maximum allowable working pressure. E is the weld efficiency, CA is the corrosion allowance and t_{min} is the minimum wall thickness to withstand the radial stress. [92] All of these values can be found in Table B.3 on assumptions from Turton et al (2009) for vessels [92].

TABLE B.3: Assumptions used in the computation of the pressure factor for vessels, $F_{P,vessel}$ [92].

S	944 bar
E	0.9
CA	0.00315 m
t_{min}	0.0063 m

For heat exchangers, the pressure factor, $F_{p,HX}$ is given in terms of constants dependent on the type of heat exchanger as well as the pressure which provides the constants: C_1, C_2, and C_3. These are used in Equation B.9:

$$log(F_{p,HX}) = C_1 + C_2 \cdot log_{10}(P) + C_3 \cdot [log_{10}(P)]^2, \tag{B.9}$$

where P is the operating pressure of the heat exchanger. The constants C_1, C_2, and C_3 are 0 for pressures between 0 and 5 bar, for pressures above 5 bar (and up to 140 bar) they are 0.0388, -0.1127, and 0.0818 respectively.

The material factor for heat exchangers depend on the shell and tube materials, the values can be found in Table B.4.

TABLE B.4: Overview of the material factor, F_M based on the materials for the tubes and shells in a heat exchanger [92].

Material		
Tube	Shell	F_M
CS	CS	1
SS	SS	1.8

The cost estimates for the heat exchangers are dependent on the type of heat exchangers. The k-values used in Equation 3.3 for a fixed tube heat exchanger can be found in Table B.5. The values for the B_1 and B_2 for different unit operations can be found in Table B.5.

TABLE B.5: The factors used for the different units to compute the bare module factor, F_{BM} [92].

Unit	B_1	B_2	k_1	k_2	k_3
Vertical vessel	2.25	1.82	3.4974	0.4485	0.1074
Horizontal vessel	1.49	1.52 3.5565	0.3776	0.0905	
Fixed tube heat exchanger	1.63	1.66	4.3247	-0.303	0.1634
Furnace	-	-	3.0680	0.6597	0.0194

Appendix C

Supplementary results/Case studies

C.1 Case studies

C.1.1 Steam requirements

The result from the case study to determine the S/C ratio for the SMR is given in Figure C.1. The case study was done by changing the S/C ratio while monitoring the conversion rate of natural gas, mainly methane to hydrogen.

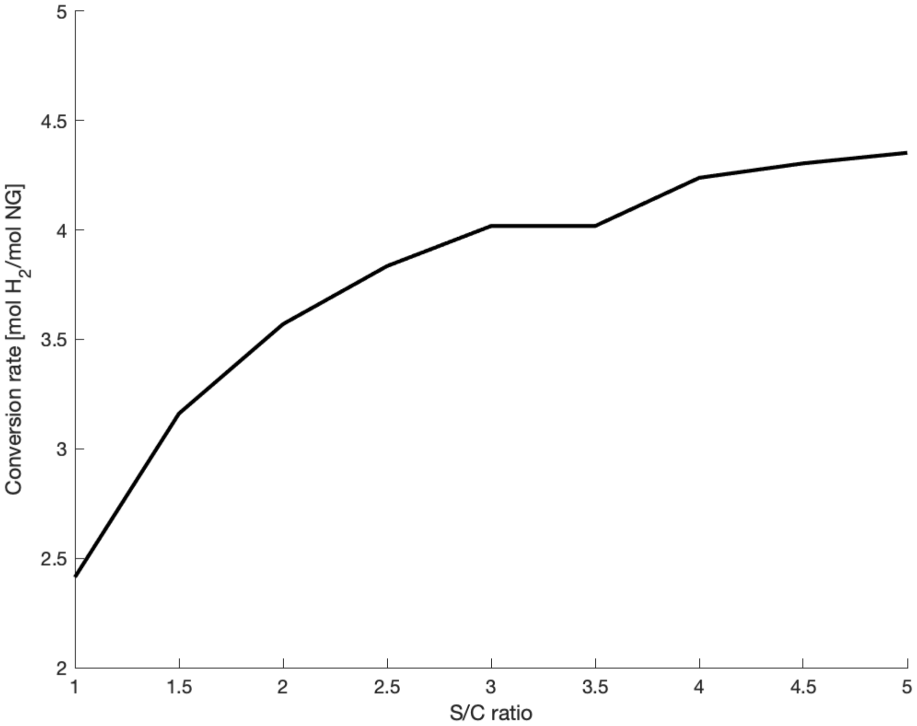

FIGURE C.1: Conversion of hydrogen as a function of the S/C ratio.

The case study for the pre-reformer was based on the amount of steam required in order for the heavier (than methane) hydrocarbons to be removed so that there is only methane in the primary reformer. This is shown in Figure C.2.

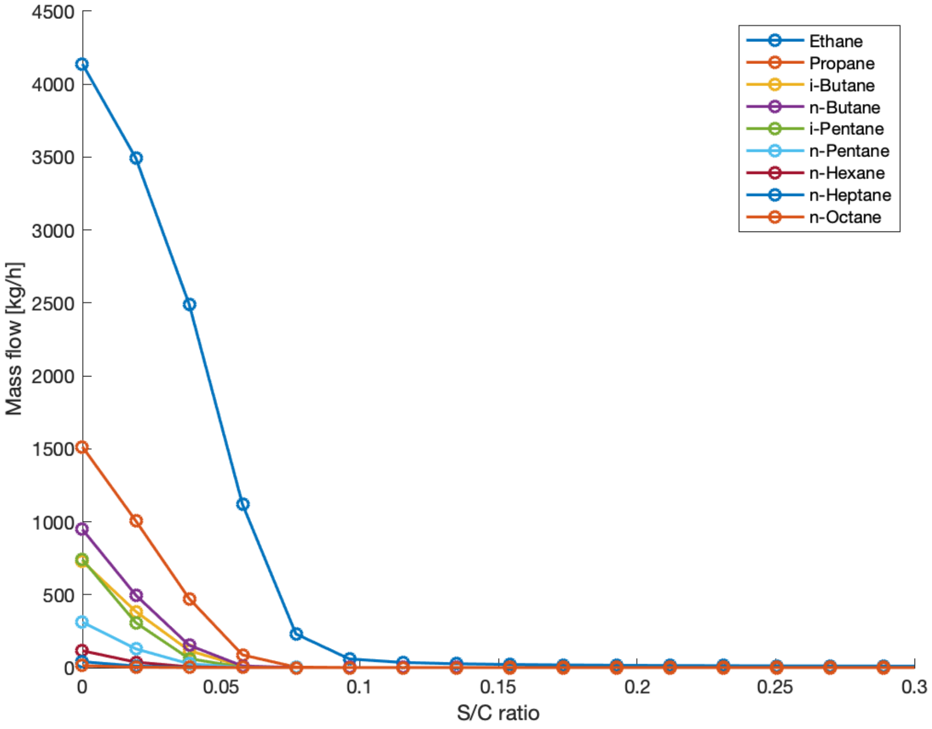

FIGURE C.2: Mass flow of the heavier hydrocarbons exiting the pre-reformer as a function of the S/C carbon.

C.1.2 Furnace case studies

Conventional SMR

For the conventional SMR, the requirements is that the furnace combusts sufficient amounts of natural gas with excess air to ensure high enough heat transfer for both the SMR and the reboiler. This was done as mentioned by adjusting the amount of natural gas as well as the amount of air. The variables looked into for the case study, with these adjusting variables, were the carbon monoxide emissions, the temperature after the SMR heater and the temperature after the reboiler. Aspen Hysys does not provide a limitation when temperature is transferred from a place of lower temperature to a place of higher temperature, hence this must be consciously taken into account manually.

From the two figures (Figure C.3 and Figure C.4) below, the criteria of the case study are taken into consideration.

The temperature after supplying heat to the reboiler was also checked for the case chosen to be sufficiently high.

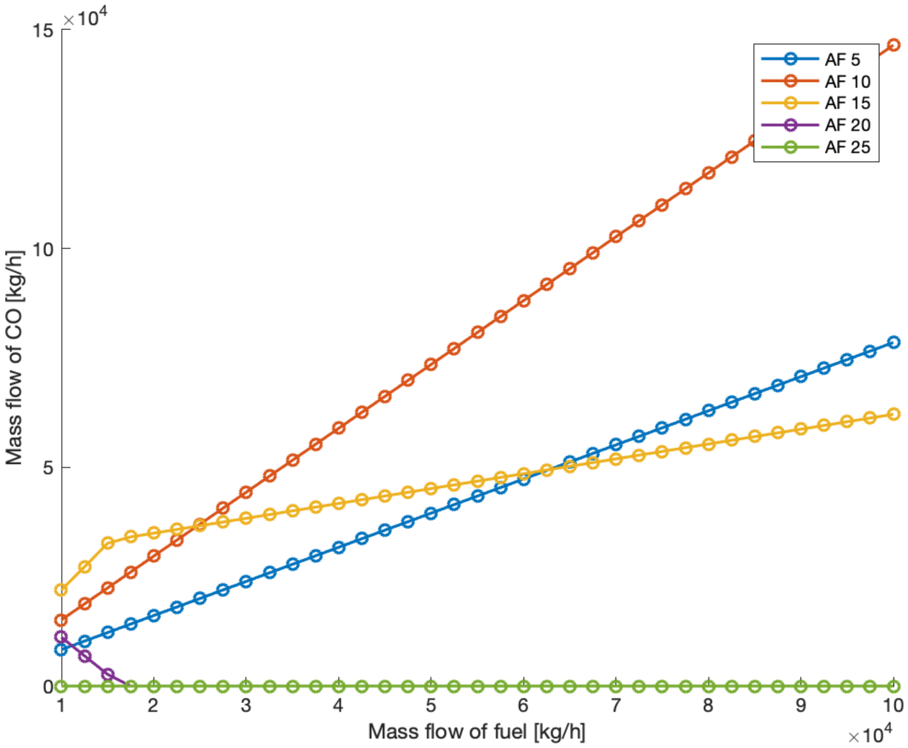

FIGURE C.3: The mass flow of CO as a function of the inlet mass flow of fuel into the furnace varying with the air factor.

Electrical SMR

The same case study as for the conventional SMR was executed for the furnace in the simulation of electrical SMR. As the simulation of electrical SMR does not require heating sufficient for the SMR, only the reboiler, this was only considered. The temperature after the reboiler as a function of the inlet mass flow of fuel into the furnace varying with the air factor. This is shown in Figure C.5

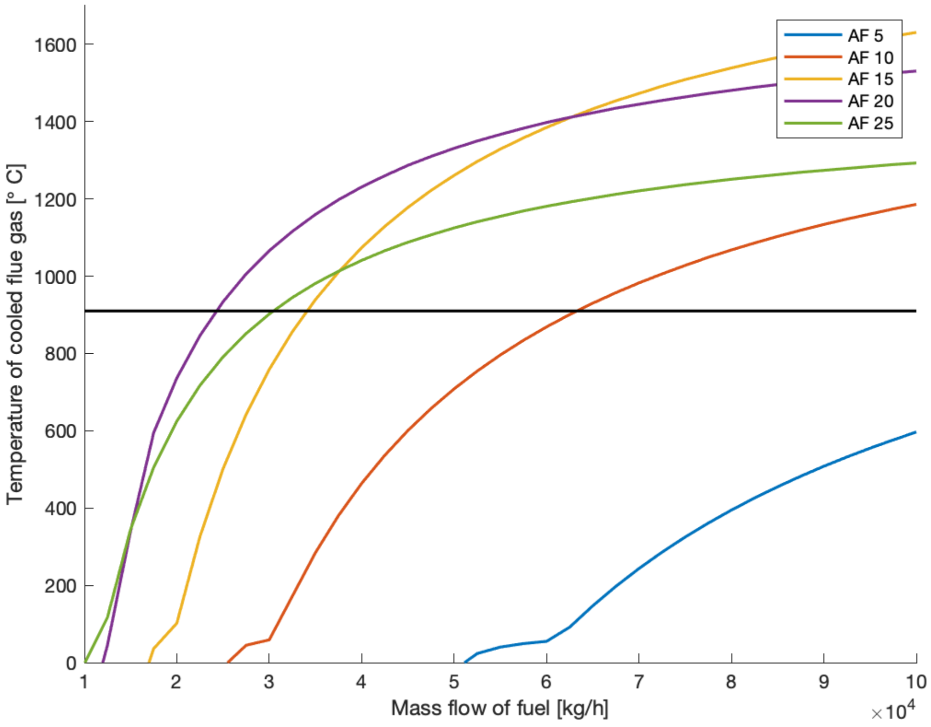

FIGURE C.4: The temperature of the cooled flue gas after supplying heat to the SMR as a function of the inlet mass flow of fuel into the furnace varying with the air factor.

C.2 OPEX

Table C.1 shows the breakdown of all costs included in the OPEX estimate, as used in Figure 4.4.

TABLE C.1: Comparison of OPEX costs for the base case (SMR) and the case of electric SMR (el SMR). All costs are given in USD/kg H_2.

Variable	SMR	El SMR
Natural gas (feedstock)	0.50192	0.50192
Natural gas (fuel)	0.38899	0.06059
Cooling water (CW)	0.00172	0.00172
CW treatment chemicals	0.00043	0.00043
Boiler feedwater	0.01118	0.01118
O&M costs	0.04665	0.04665
Carbon tax	0. 0.47062	0.10416
Electricity	0.00210	0.29712
Electrical power tax	0.00191	0.27098

Table C.2 shows the breakdown of all costs included in the OPEX estimate, as used in Figure 4.7.

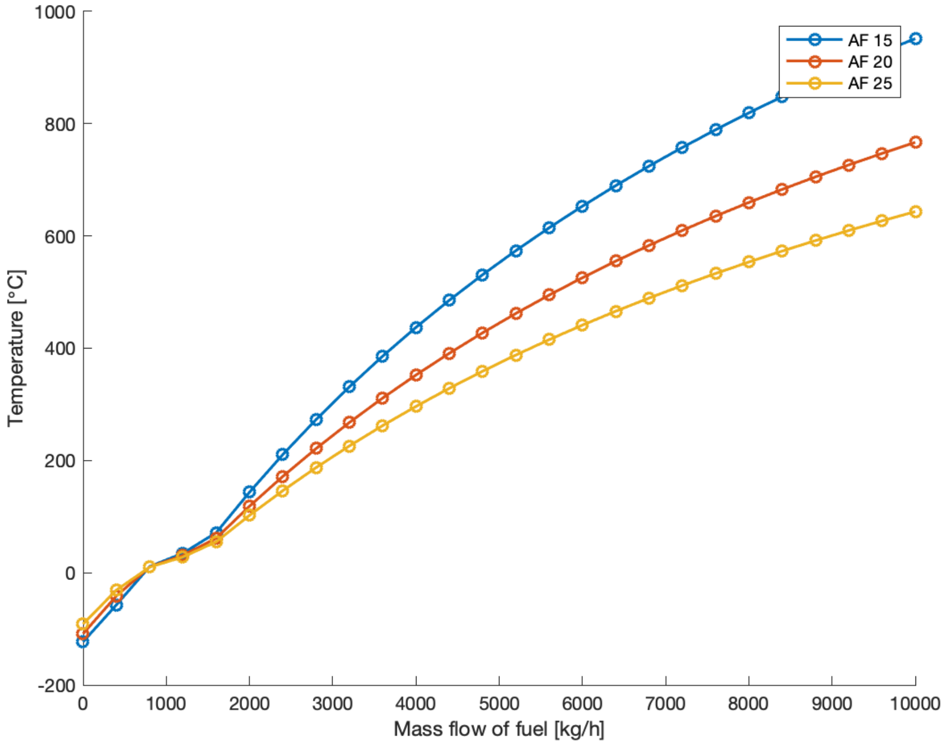

FIGURE C.5: Temperature of the flue gas exiting the furnace as a function of the mass flow of fuel and AF.

TABLE C.2: Comparison of OPEX costs for the base case (SMR) and the case of electric SMR (el SMR). All costs are given in USD/kg H_2.

Variable	SMR	El SMR
Natural gas (feedstock)	0.81065	0.81065
Natural gas (fuel)	0.62824	0.09786
Cooling water (CW)	0.00172	0.00172
CW treatment chemicals	0.00043	0.00043
Boiler feedwater	0.01118	0.01118
O&M costs	0.04665	0.04665
Carbon tax	1.60073	0.35429
Electricity	0.00413	0.58450
Electrical power tax	0.00191	0.27098

C.3 CAPEX

C.3.1 Breakdown of capital costs for each unit in the simulation

In the tables below (Table C.3 and Table C.4) you can find the breakdown of the costs making up the capital cost for the conventional SMR.

TABLE C.3: Cost and size estimation of each heat exchanger in the simulation. The pressure is the operating pressure of the heat exchanger.

Equipment	Type	Area $[m^2]$	Shell	Tube	Pressure [bar]	CBM [USD]	FBM [-]	Fp [-]	Cp0 [USD]
Cross hx	Fixed tube	60.320	SS	SS	2	119094.999	5.925	1	20100.422
HX1	Fixed tube	60.308	CS	CS	25.5	69298.967	3.448	1.102	20099.312
Cooler E-100-2	Fixed tube	60.320	CS	CS	2.0	66130.388	3.290	1	20100.422
Cooler E-101	Fixed tube	60.320	CS	CS	2.0	66130.388	3.290	1	20100.422
Cooler E-109	Fixed tube	60.320	CS	CS	22.5	68820.848	3.424	1.086	20100.422
Heater E-100	Fixed tube	60.308	CS	CS	24	69060.079	3.436	1.094	20099.349
Heater E-104	Fixed tube	60.297	CS	CS	23.5	68975.930	3.432	1.092	20098.296
Heater E-105	Fixed tube	60.321	CS	CS	22.5	68821.212	3.424	1.086	20100.528

Heat exchangers

Vessels

TABLE C.4: Cost and size estimates of each vessel in the simulation.

Equipment	Diameter [m]	Height [m]	Volume $[m^3]$	CBM [USD]	FBM [-]	Fp [-]	Cp0 [USD]
F-SEP	6.543	9.818	330.147	1658444.131	5.388	1.724	203410.786
F-SEP PrePSA	4.094	6.141	80.825	1629876.303	19.432	9.441	55428.765
Flash1	2.160	3.590	23.733	113644.088	4.252	1.817	17661.118
Flash2	2.122	3.539	22.500	83136.407	3.216	1.136	17082.741
Flash3	2.147	3.579	23.317	85312.035	3.228	1.143	17467.031
Absorber vessel	3.505	12.876	124.236	2298794.188	18.789	9.087	80855.932
Stripper vessel	3.505	7.876	75.994	403498.219	5.071	1.550	52581.920
HTSR vessel	0.667	2	0.698	25769.566	6.327	2.240	2691.669
LTSR vessel	0.833	2.500	1.364	38642.628	7.038	2.631	3628.658

Packing

The cost of packing used in the absorber and stripper was found from Sinnott et al (2013), and the cost used was 7700 USD/m^3. This provides the cost as shown in Table C.5.

TABLE C.5: Packing costs for the absorber and the stripper, based on cost estimates from Turton et al 2009 [92].

Unit	Packing volume [m^3]	Packing cost [USD]
Absorber	96.5	869,151.29
Stripper	48.2	434,125.31

Appendix D

Python and Matlab scripts

D.1 Sizing of horizontal vessels

```
    def L_D(D_p): # Length/Diameter ratio general guide
    if D_p <= 20 and D_p > 0:
        L_D = 3
    elif D_p <= 35 and D_p > 20:
        L_D = 4
    elif D_p > 35:
        L_D = 5
    else:
        print("The operating pressure is invalid. Error occured")
    return L_D

def simpleTerminalVelocity(rho_p, rho_f, demister):
    vt = Ks*((rho_f-rho_p)/rho_p)**(1/2)
    if demister == False:
        vt*=0.15 #safety measure if the sep does not have a demister
    return vt

def VapVolFlowRate(VapMassFlowRate, rho_p):
    Vv = VapMassFlowRate/(3600*rho_p)
    return Vv


def Dv(hv_Dv, Lv_Dv, simpleTerminalVelocity, VapVolFlowRate):
    Dv = symbols(’Dv’)
    #first calculate the cross sectional area for vapor flow
    Av = np.pi*hv_Dv/4*Dv**2
    # calculate the uv
    uv = VapVolFlowRate/(Av)
    #hv/us
    hv_us = hv_Dv*Dv/(simpleTerminalVelocity)
    #Lv/uv
    Lv_uv = Lv_Dv*Dv/(uv)
    expr = hv_us - Lv_uv
    sol = solve(expr)
    return sol

def LiqVolFlowRate(LiqMassFlowRate, rho_f):
    Vl = LiqMassFlowRate/(3600*rho_f)
    return Vl

def LiquidArea(Dv):
    Al = np.pi*Dv**2/(4)*0.8 #assuming liquid area is 80% of total area
    return Al


## from vertical
def HoldUpTime(Lv_Dv, Dv, Al, LiqVolFlowRate):
    Lv = Lv_Dv*Dv
    V_holdup = Al*Lv #Al = liquid area
    t_holdup_s = V_holdup/LiqVolFlowRate #liquid hold up time in seconds
    t_holdup = t_holdup_s/60 #converting liquid hold up time to minutes
    return t_holdup

def VolumeInVessel(liqVolFlowRate, liqholdup): #liquid volume
    Vl_inVessel = liqVolFlowRate*liqholdup
    return Vl_inVessel

def liqDepth(VolumeInVessel, minVesselDiameter):
    hv = VolumeInVessel/(np.pi*minVesselDiameter**2/4)
    return hv

def requiredHeight(minVesselDiameter, liqDepth):
    Dv = minVesselDiameter
    hv = liqDepth
    H = Dv/2+ Dv + hv
    return H

def VolumeTotal(minVesselDiameter, L_D):  #volume of total separator
    V = (np.pi*minVesselDiameter**2)/4*(L_D*minVesselDiameter)
    return V

t_holdup_demand = 0.5 #minutes

while t_holdup < t_holdup_demand:
    Dv+=0.05
    Al = LiquidArea(Dv)
    t_holdup = HoldUpTime(Lv_Dv, Dv, Al, Vl)
    Vl_invessel = VolumeInVessel(Vl, Dv)
    hv = liqDepth(Vl_invessel, Dv)
    H = requiredHeight(Dv, hv)
```

```
V = VolumeTotal(Dv, Lv_Dv)
t_holdup = HoldUpTime(Lv_Dv, Dv, Al, Vl)
print("Dv ",Dv)
print("t ", t_holdup)
```

Ida Synnøve Bukkholm

Electric steam methane reforming

NTNU
Kunnskap for en bedre verden